A TWO-DIMENSIONAL REPRESENTATION OF THE CROSSWIND FOR THE JET INTERFERENCE PROBLEM

Approved:

Chairman

Date approved by Chairman: May 28, 1970

A TWO-DIMENSIONAL REPRESENTATION OF THE CROSSWIND FOR THE JET INTERFERENCE PROBLEM

A THESIS

Presented to

The Faculty of the Graduate Division

by

Mary Anne Wright

In Partial Fulfillment

of the Requirements for the Degree

Doctor of Philosophy in the School of Aerospace Engineering

Georgia Institute of Technology

May, 1970

In presenting the dissertation as a partial fulfillment of the requirements for an advanced degree from the Georgia Institute of Technology, I agree that the Library of the Institute shall make it available for inspection and circulation in accordance with its regulations governing materials of this type. I agree that permission to copy from, or to publish from, this dissertation may be granted by the professor under whose direction it was written, or, in his absence, by the Dean of the Graduate Division when such copying or publication is solely for scholarly purposes and does not involve potential financial gain. It is understood that any copying from, or publication of, this dissertation which involves potential financial gain will not be allowed without written permission.

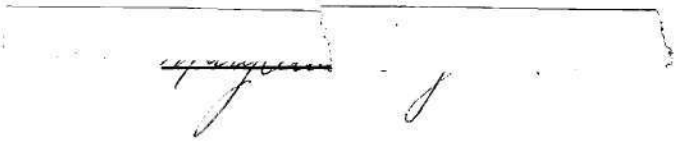

7/25/68

ACKNOWLEDGMENTS

I would like to express my great appreciation to my thesis advisor, Dr. James C. Wu, and to the other members of my committee, Dr. Howard M. McMahon and Professor James E. Hubbartt, for their guidance and advice during the course of this investigation.

I especially want to thank my husband, Dr. Terry Wright, for his many helpful suggestions concerning programming and data presentation, and for his patience and encouragement. I also thank Mr. David K. Mosher and Mr. John Palfery for the use of their experimental data and their many helpful discussions of their experimental observations.

The financial assistance of the National Science Foundation, Zonta International, and the Georgia Institute of Technology are gratefully acknowledged. Also the support of the United States Army through Project THEMIS is deeply appreciated.

I want to thank my mother-in-law, Mrs. Karolyn P. Wright, for always listening to my comments on this work with an air of understanding and for never once criticizing my housekeeping during the course of this work.

The efforts of Mrs. Jan Boyce in typing this thesis, above and beyond the call of duty, are most deeply appreciated.

Finally, I want to thank my parents, Mr. and Mrs. Claude Jackson, for their encouragement of my academic pursuits through the years and the great sacrifices they made for my education.

TABLE OF CONTENTS

LIST OF TABLES

LIST OF FIGURES

NOMENCLATURE

a	radius of a circular jet exit
a_e	equivalent jet radius: radius of a circle having the same area as the jet exit under consideration
$a_\zeta = \frac{1}{2}(A + B)$	radius of a circle, equation (18)
A	semi-major axis of elliptic jet exits
B	semi-minor axis of elliptic jet exits
C_d	drag coefficient
C_F	force distribution coefficient, defined by equation (13)
C_p	plate pressure coefficient, defined in equation (1)
C_s	integrated interference force coefficient, defined by equation (4) or (14)
C_{s_e}	integrated interference force coefficient calculated from experimental data
C_{s_o}	reference values of integrated interference force coefficient used in the parametric study
D	distance between the source and sink in the Rankine oval
E	entrainment parameter, equation (39)
$\mathcal{E}$	mass entrained per unit length of jet per unit time
F	empirical parameter, equation (40)
G	empirical factor, equations (6) and (7)
K	dimensionless entrainment coefficient, defined in equation (3)
K_j	dimensionless entrainment parameter calculated at the point x_j

K_o	reference values of dimensionless entrainment coefficient used in the parametric study
ℓ	length of the exit in the free-stream direction
ℓ_a	half-length of the Rankine oval
m	entrainment sink strength
p	static pressure on the plate
p_∞	free-stream static pressure
r, β	polar coordinates of the plate
R	radial upper limit of integration, equations (4) and (13)
R_o	radial lower limit of integration, equation (13)
S	strength of the source-sink pair in the Rankine oval
u, v	velocity components in the x- and y-directions, respectively, non-dimensionalized by V_∞
u_b, v_b	non-dimensionalized velocity components due to the uniform stream and blockage
u_s, v_s	non-dimensionalized velocity components due to the sink
u_t	non-dimensionalized test velocity along the line $\beta = 0$
V_j	jet velocity
V_∞	free-stream velocity
w	width of the jet exit
w_a	half-width of the Rankine oval
w_{a_o}	reference values of the Rankine oval half-width used in the parametric study

x, y, z	Cartesian coordinates, non-dimensionalized by a_e
x_i, y_i	Cartesian coordinates of the afterbody-jet exit intersection points, non-dimensionalized by a_e
x_j	discrete points along the $\beta = 0$ where theoretical and experimental pressure coefficients are matched
x_s	entainment sink location
$Z = x + \lambda y$	complex number describing the plate plane
β_w	angular coordinate of the afterbody-jet exit intersection for the circular jet exit
β_{w_o}	reference values of β_w used in parametric study
β_o	angular upper limit of integration, equations (4) and (14)
γ, δ, ϵ	exponents used in dimensional analysis
ΔC_s	difference between calculated integrated interference force coefficient and the reference value, equation (41)
$\Delta C_{s_{wake}}$	integrated interference force coefficient for the wake region, calculated from experimental data
$\Delta\beta_j$	angular increments used in numerical procedures, Appendix B
$\zeta = \xi + \lambda\eta$ $\zeta' = \xi' + \lambda\eta'$	complex numbers
θ	momentum thickness of the plate boundary layer
μ	fluid viscosity
ν	kinematic viscosity
$\Pi_1, \Pi_2, \Pi_3,$ $\Pi_4, \Pi_4', \Pi_5,$ $\Pi_5', \Pi_6, \Pi_7, \Pi_7'$	dimensionless Π products

ρ_j	jet density
ρ_∞	free-stream density
ξ_1'	location of the source in the Rankine oval
ξ_2'	location of the sink in the Rankine oval
ξ_3'	upstream stagnation point of the Rankine oval
ω	non-dimensionalized complex potential function

SUMMARY

The problem of a jet exhausting normally from an infinite flat plate into a crosswind is studied analytically, primarily in terms of the resulting interference pressures on the plate. Three jet exit shapes are considered: a circle; an ellipse with the major axis aligned with the crosswind, called the streamwise exit; and an ellipse with the major axis perpendicular to the crosswind, called the blunt exit. It is shown that a two-dimensional steady potential flow model for the crosswind in planes parallel to the plate may be used, provided the jet-to-crosswind speed ratio is sufficiently large and the wake region is excluded. It is also shown that the effects of entrainment must be represented in the model. A two-dimensional blockage-sink model is developed. The blockage elements in this model represent both the blockage due to the jet plume and that due to the presence of the wake. It is found that there is entrainment into the wake as well as directly into the jet plume; hence entrainment is represented by a sink located aft of the jet exit. Ten sets of blockage and entrainment parameters are found so that the model provides good agreement with ten sets of experimental data. An example of application of the model to cases of other jet exit shapes and speed ratios is given. The blockage and entrainment parameters are varied over a range of values to determine the effects of each on the interference pressure. It is shown that the exact shape of the afterbody representing the blockage due to the

wake is generally not very important to the total suction force resulting from the interference pressures. The entrainment factor is quite significant. The streamwise and circular jet exits are more useful for lifting-jet applications than the blunt exit because of their favorable coupling of the blockage and entrainment effects and their relatively small wake production.

CHAPTER I

INTRODUCTION

The Jet-in-Crosswind Phenomenon

Jet-in-crosswind phenomena have received considerable attention in recent years because of their rather broad applications in all Mach number regimes. According to its most general definition, a jet in a crosswind may be the injection of one fluid stream into another at any finite angle. Clearly then vector control jets for missile guidance or fuel venting systems or air injection cooling systems for turbine blades are usually in the category of jet-in-crosswind phenomena. For these applications at least one stream--either the jet or the cross-flow or both--is compressible. The subsonic jet in a subsonic cross-wind is particularly pertinent to two areas of current interest: air pollution and lifting jets for V/STOL aircraft. Fumes exhausting from stacks into a breeze are jets in crossflows, as are lifting jets or lifting fan wakes on V/STOL aircraft when the craft is in the transition phase of flight, that is, when it has attained some forward speed but is still dependent on the fan or jet for most of its lift. Much experimental and analytical effort has been directed toward these two applications [1-49]*, and because the flow regimes of these applications are similar, research directed primarily toward one problem may be

* Numbers in brackets refer to items in the Bibliography.

useful to the investigation of the other. The present work is concerned with the interference effects pertinent to the lifting jet application of the jet-in-crosswind.

Experimental investigations have shown that lifting fan or lifting jet powered V/STOL aircraft in the transition phase of flight encounter aerodynamic interference effects which result in severe lift loss and stability problems [1-11]. In particular, low pressure regions develop on the lower surfaces of wings or fuselages and the distribution of the pressure is usually such that a nose-up pitching moment is produced. It is therefore of interest to study this interference problem in order to find means of reducing the adverse effects or even of controlling the flow sufficiently to gain favorable effects.

The experimental investigations of references [1-11] employed various aircraft and jet or fan configurations, so that, although interference effects adverse to V/STOL applications were consistently observed, it was very difficult to analyze the details of the interference phenomenon. Attention was then given to simplified problems which include the principal features of the jet-in-crosswind interference but eliminate the complications due to three-dimensional flow about complex finite bodies. Both experimental and analytical investigations [12-49] have considered simplified problems wherein turbulent subsonic jets exhaust into a subsonic crossflow without impinging on any solid boundary. In most of these investigations the jets issued from flat plates or isolated wings. All of these efforts were directed toward achieving a greater understanding of the precise mechanisms and the

effects of the interference, and ultimately achieving a method of predicting these effects. However for the most part these research programs were quite diverse. Recently attempts have been made to unify this research effort. At the Georgia Institute of Technology a research program has been undertaken involving both experimental and analytical phases. The early stages of this program are concerned with greatly simplified jet-in-crosswind problems with the emphasis on understanding basic phenomena. In the course of the program greater complexity will be introduced. The present work is the initial analytical effort in this program, and is undertaken in conjunction with a parallel experimental effort [46], [47] and [49] from which most of the experimental data necessary for this work is drawn.

The experiments of references [46], [47], and [49] considered a subsonic turbulent jet issuing normally from a large flat plate into a subsonic crossflow. The experiments were sized in such a way that the jet did not impinge on the wind tunnel walls. It was felt that several jet exit shapes should be studied because suitably shaped jet exits could conceivably minimize adverse interference effects. For instance, it was suspected that a jet plume with a small frontal area, that is, a jet issuing from a slot aligned with the free stream or from an in-line cluster of circular jets aligned with the free stream, would disturb the crossflow less than a jet issuing from a wider exit. Three jet exit shapes were considered in this initial work: a circular exit, a relatively wide, round-ended slot with its longer dimension aligned with the free stream, and the same slot with its longer dimension

perpendicular to the free stream. The first of these slots is called the "streamwise" exit, and the second the "blunt" exit. The cross-sectional area of all the exits was the same. These exits were chosen to study the effects of jet exit shapes both because they are practical from the standpoint of fabrication and because they are reasonable approximations to cluster arrangements of round exits. In the course of the experimental investigations plate pressure measurements, flow direction surveys, and jet penetration measurements were made for jets issuing from each of these exits at jet-to-crossflow speed ratios of 4, 8, 10, and 12 with a constant tunnel speed. Plate pressure measurements were also made with the blunt exit and a speed ratio of 20 obtained by reducing the tunnel speed. These speed ratios were chosen because it was felt that they were representative of flight conditions of V/STOL aircraft in transition [3], [4], [7], [8], [16] and [19]. For instance a heavily loaded fan or a lifting jet would probably have exhaust velocities on the order of 500 feet per second, and an aircraft equipped with such devices in the transition phase of flight would have forward speeds ranging from zero to perhaps 200 feet per second. Thus the jet-to-crosswind speed ratio would range from approximately 2.5 to infinity. However, until the aircraft has attained some altitude and some forward speed the jet plume or fan wake would impinge upon the ground. Therefore the speed ratio range of interest in considering simplified problems with no impingement is more reasonably 2.5 to 20 or so.

These experimental investigations, as well as numerous others

[12-16], [20], and [21], indicate that the interference that develops when a jet issues perpendicularly from a large flat plate into a crossflow may be considered in two interrelated parts: (1) the action of the crossflow on the jet and (2) the effect of the jet on the crossflow. The crossflow produces aerodynamic forces on the jet and the jet entrains crossflow fluid, and therefore momentum, so that because of the presence of the crossflow the jet spreads, deforms, and deflects as shown in Figure 1. The action of the jet on the crossflow includes the entrainment of part of the crossflow fluid into the jet, the displacement of the crossflow by the jet, and the formation of a low pressure region downstream of the jet plume, as was observed in references [15], [16], [20], and [46]. These three factors shall be called the entrainment effect, the blockage effect, and the wake effect respectively. As far as V/STOL applications are concerned, the most important results of this interference are the general reduction of plate pressures and the production of a pitching moment due to the distribution of those pressures. Therefore the present study is principally concerned with the action of the jet on the crossflow as evidenced by the plate pressures.

Of the three principal types of disturbance in the crossflow, the wake effect is perhaps the most difficult to analyze. Oil film photographs [49] clearly show the presence of a wake region on the plate. (See Figure 2.) Plate static pressure measurements both with the jet exhausting and with a solid rod replacing the jet were made by Vogler [19] and Bradbury and Wood [20], and it was concluded that the low static pressure region behind the jet is generally larger than that

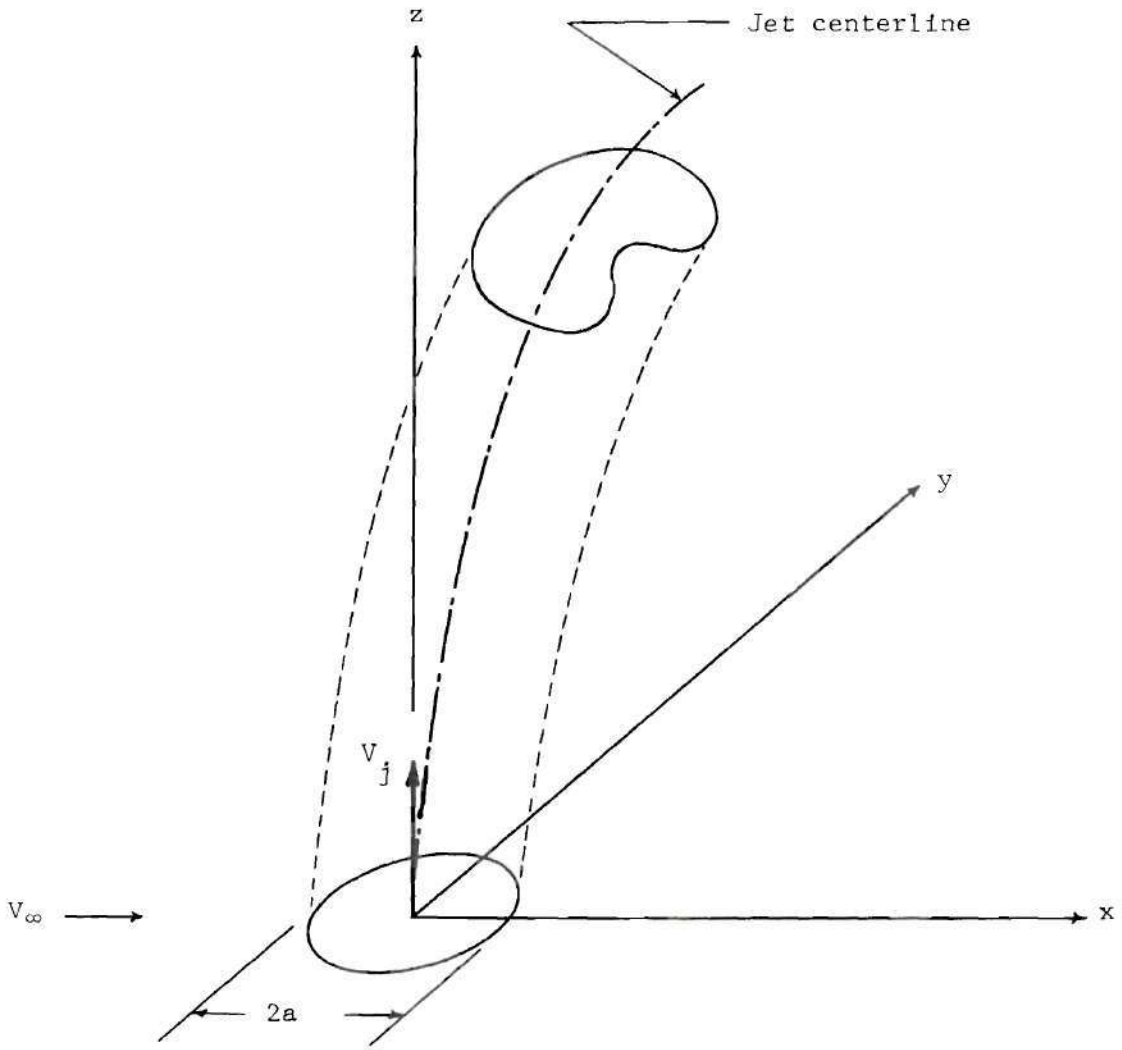

Figure 1. Three Dimensional Coordinate System With Jet Geometry Indicated

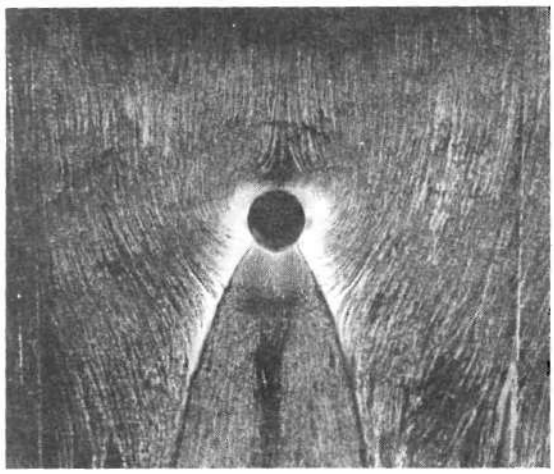

Figure 2. A Typical Oil Film Photograph, $V_j/V_\infty = 12$ (Reference 49)

behind the rod. In the case of the solid rod the low static pressures in the wake region are a result of a loss of total pressure due to the separation of the crossflow as it flows around the rod, but it is difficult to determine if the same separation phenomenon is present when the crossflow flows around the jet plume, for in this case low static pressures may result from acceleration of the flow due to entrainment. Total pressure measurements by Jordinson [15] show that, in the case of a jet issuing from a circular exit, a low total pressure region does exist downstream of the jet and it extends several jet exit diameters away from the plate. The fact that the low total pressure region extends far from the plate indicates that the wake is not local to the vicinity of the plate; that is, the wake cannot be due entirely to the entrainment of plate boundary layer air. However, the presence of the low total pressure region does not conclusively prove that the crosswind separates as it flows around the jet plume. Since so few details are actually known about the wake region and its effects, no attempt will be made in this study to analyze the wake in detail.

The entrainment and blockage effects are easier to identify and analyze. Examination of oil film photographs [49] reveals that both effects are present and more or less distinguishable, as seen in Figure 2. The blockage is observed in two features of the photographs: (1) a dark region upstream indicating a significant deceleration of the flow, and (2) the curvature of the streamlines in the vicinity of the jet exit indicating that the crossflow actually flows around the jet. However, some streamlines terminate at the edges of the jet exit and

wake, indicating entrainment into the wake as well as into the jet itself. The oil film photographs represent only the effects near the plate, and since the jet-in-crossflow problem is basically three-dimensional, care must be taken not to over-emphasize the conclusions drawn from them. However, a flow direction survey taken by Mosher [49] at distances of several jet radii off the plate also clearly indicates the presence of both blockage and entrainment. There seems to be a region near the jet in which both blockage and entrainment are significant and their relative importance depends on both jet exit configuration and speed ratio, while in a larger region further from the jet the crossflow field seems to be dominated by entrainment effects.

In order to develop a means of describing and predicting interference pressures for this problem it is necessary to determine the important parameters involved. For the case of a jet issuing normal to a flat plate from a circular exit Bradbury and Wood [20] have stated that dimensional analysis shows that the interference plate pressure coefficient

$$C_p = \frac{p - p_\infty}{1/2\ \rho_\infty V_\infty^2} \tag{1}$$

is dependent on only three dimensionless parameters, provided that the plate boundary layer may be specified by a single parameter. If that single parameter is the momentum thickness θ, the three dimensionless parameters are: (1) the ratio of the jet speed to the undisturbed crosswind speed, V_j/V_∞, (2) the ratio of the plate boundary layer

momentum thickness to a representative length dimension of the jet exit, in the case of a circular jet exit θ/a, where a is the jet exit radius, and (3) the jet efflux Reynolds number, $V_j a/\nu$. The speed ratio is a simplification of the momentum flux ratio $(\rho_j V_j^2/\rho_\infty V_\infty^2)^{\frac{1}{2}}$ which is permissible if density variations are small. It has already been argued that for lifting jet V/STOL aircraft speed ratios in excess of 2.5 are of particular importance. Experimental results of Bradbury and Wood [20] indicate that for θ/a less than 0.3 the plate pressure is only weakly influenced by variations of the second parameter θ/a. In most of the experiments referenced, the value of θ/a is of the order of 0.1, so variations in the momentum thickness of the plate boundary layer are expected to be of secondary importance to the interference pressure. Considering the third parameter, the jet efflux Reynolds number, it is noted that turbulent jets and free shear layers are generally rather insensitive to Reynolds number changes. Since jets become turbulent at small Reynolds numbers, it appears that the jet-in-crosswind interference flow should be insensitive to variation in Reynolds number. It is noted that the agreement of plate pressure data from different sources [19], [20], and [49] and of jet centerline data [12], [15], [32], and [49] obtained under diverse experimental conditions seem to support this argument. It is also noted that the dimensional analysis of Callaghan and Ruggeri [13] shows jet deflection to be a function of jet efflux Reynolds number, speed ratio, density ratio, viscosity ratio, and the ratio of duct width to jet exit diameter, but their final deflection relation determined from their experimental results is a

function of speed and density ratios alone. The density ratio was necessary because their tests were for a hot jet in a cold crossflow. Since their tests covered a Reynolds number range $30{,}000 \leq V_j a/\nu \leq 250{,}000$ their results support the argument for Reynolds number insensitivity. It then appears that for circular jet exits and speed ratios of practical interest the interference plate pressure is primarily a function of the speed ratio V_j/V_∞ alone. This conclusion is further supported by the fact that experimental formulas [15], [16], [27], [30] accurately describing the jet deflection path for these cases have been established solely as a function of the speed ratio. For non-circular jet exit configurations it would seem that these same arguments concerning the important parameters should apply. However, it is clear that the shape of the jet exit has an effect, which may be seen in the oil film photographs and plate pressure data of reference [46]. In particular these data show that plate pressure losses, pitching moments, and blockage effects as indicated by the photographs become more severe at a given speed ratio as the jet exit becomes more bluff. If it is chosen to describe the jet exit shape by two dimensions, the length ℓ and the width w, and the same techniques of dimensional analysis are applied, an additional parameter w/ℓ, the jet exit thickness ratio, is obtained. (See Appendix A.) It then appears that the primary parameters affecting interference pressures should include the jet exit thickness ratio w/ℓ as well as the speed ratio V_j/V_∞.

It should be noted that the weak dependence of the interference pressure on the variations of the Reynolds number and the parameter θ/a

does not imply that the role of viscosity in the interference problem is negligible. Since there exists a significant wake region and entrainment is definitely present, viscous effects are indeed important in the mixing regions. However, it appears that the crosswind may be represented by potential flow except in the mixing regions immediately surrounding the jet plume and in the wake.

In order to formulate a proper three-dimensional potential model for the jet-in-crosswind it is necessary to have information concerning entrainment rates, jet cross-sectional deformation, and jet deflection, as was pointed out by Rubbert [42]. Entrainment rates were measured by Keffer and Baines [16] and were extracted from the work of Margason [12] by Heltsley and Kroeger [41]. Semi-empirical evaluations of entrainment rates were attempted in references [26], [32], and [38]. At present, however, none of these efforts is considered entirely definitive.

There has been little analytical effort dealing with the spreading and deformation of the jet in the crossflow. Recently, however, some attention has been given to the possibility of extending the early work of Lu [22], which dealt with the time-dependent problem of the deformation of a circular column of fluid in a two-dimensional flow, to the three-dimensional steady flow problem of a jet in a crossflow. In particular Soukup [29], Margason [39], and Hackett and Miller [36] have taken this approach and jet cross-sections are obtained which agree qualitatively with the experimental observations of Jordinson [15]. Vortex elements originally distributed around a cylinder are seen to roll up at the sides of the cross-section to form the characteristic

kidney-shaped cross-sections of the jet plume. Semi-empirical analyses involving cross-sectional growth were undertaken by Wooler, et al [26] and Skifstad [38], but cross-sectional deformation was not of primary concern in these efforts. At present then useful information concerning cross-sectional deformation comes primarily from experimental observation [15] and [33].

There are several semi-empirical analyses concerned with the jet deflection path when the jet issues from a circular exit. Good agreement between semi-empirical results and experimental jet paths was reported by Vizel and Mostinskii [31] and Crowe and Riesebieter [33] considering only the aerodynamic drag on the jet, and by Keffer and Baines [16], Platten and Baines [32], Fearn [45], and McAllister [28] considering only the entrained momentum. In addition to these approaches, Wooler, et al [26], reported good jet path agreement using both drag and entrained momentum. It appears that the effects of aerodynamic drag and entrained momentum cannot be distinguished from one another by examining the jet path alone. It is intuitively reasonable that entrainment has importance in both the spreading and deflection of the jet plume, but presently available experimental data are insufficient to permit a quantitative assessment of this importance. Nevertheless, since the use of semi-empirical analyses ignoring the entrained momentum seems to require the postulation of an excessively large drag coefficient ($C_d = 4$) [13] or a normal value of the drag coefficient and an excessively wide jet plume (in reference [16] the width is on the order of twice the width indicated by Jordinson's

data [15], it appears that the entrained momentum does contribute significantly to the deflection of the jet.

Potential Flow Models in the Literature

Clearly there is not sufficient information about the basic characteristics of the jet-in-crosswind interference to accurately model the potential crossflow. Nevertheless, in an effort to gain some insight into this problem numerous potential models have been investigated. In 1965 Monical [25] reported a vortex lattice model whereby a wing and a jet efflux tube (jet plume) could be represented. The positions of vortex elements were fixed using experimental jet path data and a system of linear equations was solved by matric inversion for the vortex strengths, subject to zero normal flow boundary conditions at control points on the wing and efflux tube surfaces. Then knowing the strengths and positions of the elements, the interference velocities and pressures were calculated. Reasonable prediction of total lift coefficients was reported. However, this model did not in any way account for entrainment of cross-sectional growth of the jet plume. In 1969 Heltsley and Kroger [41] reported a similar model which was more general in that the boundary conditions on the jet efflux tube were adjusted to permit normal flow to match entrainment rates extracted from Margason's experimental work [12]. Streamline directions calculated in the plane of symmetry downstream of the jet matched experimental observations well, but no interference pressure calculations were made.

Wooler [27] proposed a vortex model wherein a horseshoe vortex system was placed along an experimentally determined jet centerline.

The strengths of the vortices were determined so that lifting forces accounted for plume bending and a constant momentum flow was maintained along the jet path. This resulted in remarkably good plate pressure agreement with the data of Bradbury and Wood [20] far from the jet exit, but the agreement was poor in the regions immediately upstream and downstream of the jet exit.

As was previously mentioned, Margason [39] and Hackett and Miller [36] have extended the work of Lu [22] in an attempt to model the jet-in-crosswind. Margason, however, has reported that pressure calculations made with his model do not yield good agreement with experimental data. This could be partly due to a lack of growth of vorticity along the jet plume, as seen by Keffer and Baines [16]. Preliminary experimental data of reference [34] also indicates that the vorticity specified by this model is not sufficiently strong. Furthermore, there is no representation of entrainment.

Skifstad [38] has done some work on a vortex-sink model in which a line sink is placed between two counter-rotating line vortices of known strength. The vortices assume stable positions by lateral motion, and an interative solution yields jet centerline and vortex position coordinates and a sink distribution along the centerline. The basic formulation of this model would seem to be sound, in that it can account for jet deflection, cross-sectional growth, and entrainment. However preliminary results indicate that many refinements in computational techniques are needed.

A rather sophisticated model wherein series expansions for the

velocity potential are written for a region far from the jet and are asymptotically matched to series expansions for the potential near the jet has been proposed by Werner [44]. Results of matching the zeroth, first, and second partial sums are interpreted as having the effect of a distribution of doublets along the jet in a uniform stream and a downwash due to a trailing vortex system.

A very elaborate potential model was proposed by Rubbert [42]. Vortex, source and/or doublet panels represent a wing with an inlet, fan, and fan centerbody, and trailing jets. However, Rubbert notes that the success of such a model is highly dependent on the choice of correct potential elements and panel spacing. Furthermore, lack of adequate information about entrainment renders proper specification of boundary conditions on the jets impossible. He recommends the choice of a much more simple model wherein the jet is represented by a tube of jet exit cross-section placed along an experimentally determined centerline. Normal flow boundary conditions in the form of series derivatives of the velocity potential are placed on this tube so that the zeroth order terms represent a distribution of doublets or vortices (blockage) along the jet. Higher order terms would represent refinements to these entrainment and blockage elements, but Rubbert reasons that these would be influential only quite near the jet. He further suggests that variations of the higher order terms along the jet may not be very important to interference pressures on the surface from which the jet issues. However, it is noted that the lack of entrainment data restricts the use of this model, too. Rubbert suggests a

theoretical solution in which the series terms are adjusted to reproduce experimentally measured plate pressures, thus determining distributions of blockage and entrainment elements.

Another interesting point presented in reference [42] is that the difference between the influence of a doublet and that of a vortex pair of comparable blockage is very small at points far from either element. As has been seen, many of these previous models have represented blockage by vortex systems. In particular the models of references [27] and [38] attempt to represent the vortex roll-up observed in the plume. However, Keffer [35] notes that vortex pairs are the dominant feature of the jet plume only after the potential core has disappeared and significant bending has taken place. Thus it would seem that, for modeling the flow field in order to obtain plate or wing interference pressures, the blockage could be described to sufficient accuracy by doublets rather than vortices.

A model utilizing doublets for blockage was proposed by Wooler, et al [26], prior to the publication of reference [42]. An entrainment function was proposed, a drag coefficient was assumed, and the equations of motion along the jet were solved to yield jet trajectory and cross-sectional growth subject to the proper adjustment of the entrainment coefficients. Thus an entrainment distribution along the jet was also obtained. Then sinks of proper strength to simulate the entrainment were distributed within the jet and doublets of proper strength to represent the cross-sectional growth were placed along the jet path. The jet was assumed to issue from a rectangular wing which was treated

by lifting surface theory. Interference pressures were calculated and compared to corresponding experimental data. The agreement was generally acceptable over most of the wing, but was quite poor near the jet.

One series of two-dimensional models was recently reported by Rosen, et al [43]. Plate pressure coefficients from reference [19] were matched at a chosen radial distance from the center of the jet by a truncated Fourier series. Various two-dimensional potential models were then assumed and the strengths of the potential elements were adjusted to give the Fourier coefficients. In particular, a doublet-source-uniform stream model, a doublet-sink-vortex pair-uniform stream model, and two source-free stream models were used. However, while pressures could be matched at the chosen radius, the agreement was generally poor.

Of the nine three-dimensional potential models it is noted that, while all represent blockage, only the models of references [26], [38], [41] and [42] attempt to specifically simulate entrainment, and none represent wake effects. The limitations of these models appear to be due to a lack of sufficient experimental observations concerning wake formation and entrainment.

The Present Work

In recognition of the great difficulties of properly modeling the jet-in-crosswind interference, the objective of the present work is to provide a simple, approximate model which is capable of representing two of the major effects of the interference, namely blockage and entrainment. Like the previously described models, the model developed

here is of the steady potential type. However, for simplicity, the present model is two-dimensional in the x,y plane. (See Figure 1.) Arguments based on experimental observations recorded in the literature showing that a two-dimensional model should be successful for speed ratios of 8 or more are detailed in Chapter II. It is recognized that a steady, two-dimensional potential model can not simulate flow conditions in regions of energy loss such as the wake region, so the wake region is excluded from consideration in this model. It is shown that, except for the case of jets issuing from very bluff jet exits, the exclusion of the wake does not seriously detract from the effectiveness of the model.

This model is then similar in concept to the approach of reference [43] in that a potential model is assumed and the strengths of the potential elements are adjusted so that experimental plate pressure data are matched. However, the present model is significantly different from the models of reference [43] in that it is always a blockage-sink representation. Blockage is always simulated by potential elements closely approximating a jet exit shape plus an afterbody simulating the blockage of the wake. Entrainment, which is shown to be truly important to the interference in Chapter II, is consistently represented by a sink placed downstream of the center of the jet exit. The method of matching plate pressures, detailed in Chapter II, is also different from that of reference [43].

This blockage-sink representation is also similar to the three-dimensional model of reference [26]. However, since it includes the

wake-blockage afterbody, it is not a simple reduction of the model of Wooler, et al [26]. Furthermore, the present model more successfully represents the physical situation by placing the entrainment-simulating sink aft of the center of the jet exit in accordance with the observed entrainment into the wake [16], [32], [35], [46], and [49].

Although the model is two-dimensional, it is considered to be more general than the previously proposed models in that non-circular as well as circular jet exit cases are represented. To the author's knowledge non-circular jet exits were not considered in the other theoretical investigations of references [25-27], [38], and [41-44]. However, it is noted that it should be possible to extend the models of references [25], [41], and [42] to these cases without encountering undue complexity. In particular the model is applied to the three jet exits examined experimentally in references [46], [47], and [49] for speed ratios of 8, 10, 12, and the blunt exit of those references for speed ratio 20. Through the method of plate pressure matching, a semi-empirical evaluation of entrainment rate as a function of speed ratio and exit geometry is obtained. By interpolation of the curves for the model parameters presented in Chapter II it is possible to formulate theoretical models for jet exits and speed ratios other than those that have been experimentally investigated.

In order to gain insight into means of controlling the adverse effects of the interference, the model is used in a parametric study to show the effects of varying entrainment and afterbodies for each of the three jet exits considered. This parametric study and the results are

described in detail in Chapter III.

Since relatively simple blockage and sink elements are used, the interpretation of the effects of each is straightforward. However, even for speed ratios equal to or in excess of 8 there is some three-dimensionality in the flow, so this model two-dimensionally represents the net effects of the three-dimensional flow. Thus the wake-blockage afterbodies actually represent some plume spreading as well as blockage due to the wake. Also the position of the sink probably reflects the effect of some plume bending as well as the combined effect of entrainment into the wake and into the plume itself. Because of this, the entrainment rates obtained from this model are only approximate. However, the qualitative trends indicated by the parametric study are considered to be accurate for speed ratios equal to or in excess of 8.

CHAPTER II

THE TWO-DIMENSIONAL MODEL

General Requirements on the Two-Dimensional Blockage-Sink Model

The simplicity of a potential flow blockage-sink model makes that approach to the analysis of this problem very attractive. In the first place, potential models of this type are rather uncomplicated from a mathematical point of view. Secondly, the potential elements representing blockage and those representing entrainment are quite distinct, and hence the effects of each of these two factors may be seen separately, or when both are present the effect of their coupling may be observed. Therefore the interpretation of the results of the model is comparatively simple. Furthermore, because of additional simplifications, a two-dimensional model is highly desirable, even though this may result in a somewhat restricted range of application. Consider, then, the general requirements on a simple, two-dimensional blockage-sink model.

Exclusion of the Wake Region

The presence of the viscous wake region causes considerable difficulty in the formulation of a potential model for the jet-in-crosswind interference. All of the previous potential models [25-27], [36], [38], [39], [41-44] treat the entire crossflow as inviscid. However, experiments show the existence of an extensive region of low total pressure behind the jet [15], [46]. Therefore a constant total pressure

steady potential model could hardly be expected to give good results in this wake region, although three-dimensional models involving trailing vorticity [27], [41], [44] may give fair approximations. Since a steady two-dimensional potential model cannot, in any way, accurately represent the details of a low total pressure region, the wake region will be excluded from consideration in the present work. The situation is somewhat analogous to the steady potential flow solution for flow about a right circular cylinder. The theory agrees well with experimental data over the upstream portion of the cylinder but fails to predict the low pressure wake region behind the cylinder.

It is then necessary to estimate the region of the flow that is strongly influenced by the wake, and which therefore must be excluded from the potential flow model. Oil film photographs [46] show that, for speed ratios of interest, i.e., greater than 2.5, the width of the wake is in general of the order of four times the jet exit width w at a distance of approximately 4w downstream of the jet exit. However, the photographs also show a dependence of wake width on speed ratio and jet exit thickness ratio w/ℓ. That is, for a given jet exit configuration the wake width increases perceptibly with increasing speed ratio, and at a given speed ratio the wake appears to be wider for more bluff exits. Therefore it appears that the wake itself may be considered to cover a total angle of 50 degrees to 60 degrees in the region immediately downstream of the jet, at least on the plate. For the circular jet exit case total pressures surveyed above the plate [15] indicate that the region of total pressure loss covers a similarly large region even

several jet exit diameters off the plate. However, while the oil film photographs show the wake as clearly defined, the total pressure surveys lack this sharp definition. The data of reference [15] are presented as curves of constant total pressure coefficient defined as the difference between local and free stream total pressure divided by the difference between the total pressure of the jet at the exit and the free stream total pressure. Therefore, although an orderly presentation of the data is made, it is difficult to draw definite conclusions when directly comparing data for different speed ratios. It is implied, but not stated directly, that all tests were made with the same crossflow velocity and total pressure. Assuming this to be true, the indication from the total pressure surveys is that as speed ratio is increased the wake does become wider, but at the same time it becomes weaker; i.e., there is a wider region of reduced total pressure, but the actual total pressure loss is less. Therefore it is very difficult to state definitely the size of the wake. However, since only low speed flows are considered, the influence of the wake undoubtedly extends over a much larger region of the flow than that occupied by the portion of the fluid that has experienced a severe total pressure loss. For all of these reasons, in this study a region downstream of the jet covering a total angle of 90 degrees ($\beta > 135^\circ$) is excluded and is referred to as the "wake region". With the exclusion of this arbitrary wake region very promising agreement with experimental data results, as is demonstrated in the following example.

Consider a very simple two-dimensional model with a line doublet

and a line sink placed along the z-axis, simulating respectively the blockage of a circular jet and entrainment by the jet. Using the coordinate system shown in Figure 3, the plate pressure coefficient for this flow is

$$C_p = (1/r)^4 + 2K \cos\beta\,(1/r)^3 + (2\cos 2\beta - K^2)(1/r)^2 \qquad (2)$$

$$- 2K \cos\beta\,(1/r) \ ,$$

where r is the radial coordinate non-dimensionalized by a_e, the effective jet radius, K is the dimensionless entrainment coefficient defined by

$$K = \frac{m}{2\pi a_e V_\infty} \ , \qquad (3)$$

and m is the sink strength, representing the volume of air entrained into the jet per unit length of jet per unit time. The effective radius a_e is the radius of a circle having the same area as the jet exit under consideration. Hence in this case $a_e = a$. The integrated interference force coefficient for the area $1 \leq r \leq R$ and $0 \leq \beta \leq \beta_o$ is defined by

$$C_s = \int_0^{\beta_o} \int_1^R C_p \, r \, dr \, d\beta \ , \qquad (4)$$

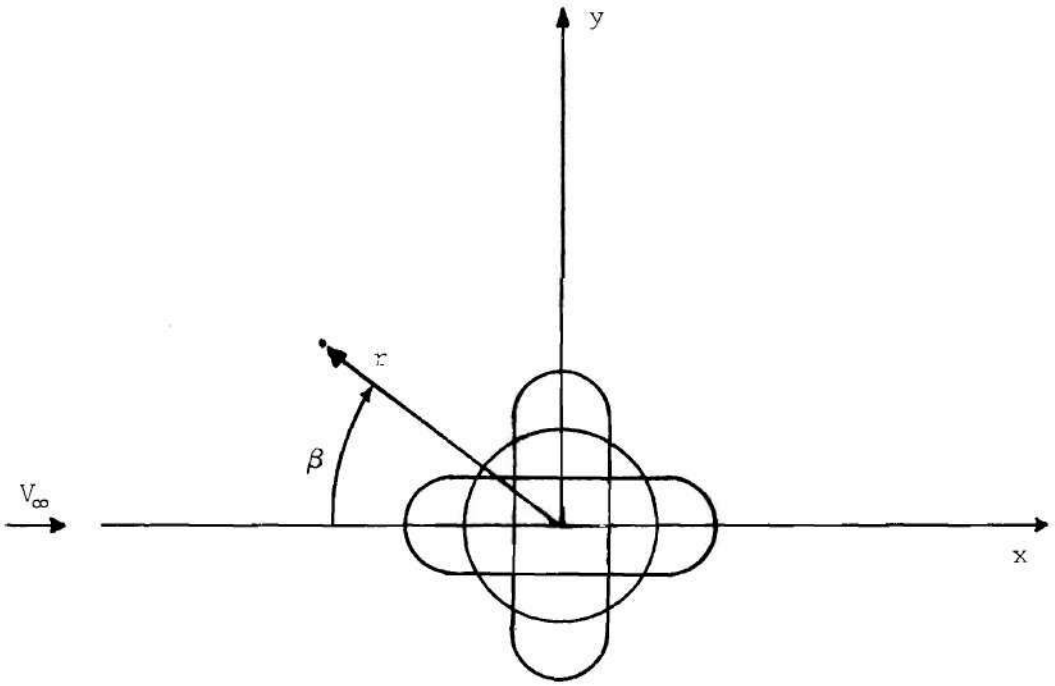

Figure 3. Coordinate System in the Plane of the Plate

which for this case becomes

$$C_s = \left(\frac{1}{2R^2} - \frac{1}{2} - K^2 \ell nR \right)\beta_o + 2K\left(2 - R - \frac{1}{R}\right)\sin \beta_o \qquad (5)$$

$$+ \ell nR \sin 2\beta_o \ .$$

For the case of a free jet exhausting into still air ($V_\infty = 0$) the appropriate dimensionless entrainment parameter is $m/(2\pi a_e V_j)$. Experimental data [50] for the circular free jet case gives $m/(2\pi a_e V_j) = 0.08$. For the case of a jet in a crossflow, $m/(2\pi a_e V_j) = KV_\infty/V_j$. With $V_j/V_\infty = 8$ the convenient value of $K = 1.0$ corresponds to $m/(2\pi a_e V_j) = 0.125$, which is comparable in magnitude to the free jet value. Using $K = 1.0$, C_s values are calculated and compared with experimental values [49] for the speed ratio $V_j/V_\infty = 8$ in Table 1, which shows that the calculated C_s values including the wake region are much smaller than the experimental values, while the values excluding the wake region are of the proper order of magnitude.

Since the concern of this work is the effects of interference on plate pressures, it is necessary to observe the contribution to the suction force due to low plate pressures in this arbitrarily excluded wake region. The experimental work of reference [49] provides plate pressures for jets exhausting from three different exits and for a range of speed ratios. Therefore it is possible to calculate from these data the integrated interference force coefficient with the upper limit $R = 5$, 10, and 15, including and excluding the wake region, for

Table 1. Comparison of Calculated and Experimental Interference Force Coefficients, Wake Included and Wake Excluded

	Interference Force Coefficient			
	Wake Included ($\beta_o = \pi$)		Wake Excluded ($\beta_o = 3/4\pi$)	
R	Calculated (K = 1)	Experiment ($V_j/V_\infty = 8$)	Calculated (K = 1)	Experiment ($V_j/V_\infty = 8$)
5	-6.6	-22.0	-11.0	-17.7
10	-8.8	-46.4	-20.4	-38.2
15	-10.2	-67.5	-28.8	-56.3

jet exits with thickness ratio $w/\ell = 0.3$, 1.0, and 3.4 and for speed ratios $V_j/V_\infty = 8$, 10, 12, and 20. The results are shown in Figures 4, 5, and 6 in terms of $\Delta C_{s_{wake}} / C_{s_e}$, where $\Delta C_{s_{wake}}$ is the difference between the integrals calculated by including and excluding the wake rehion. The calculations were carried out numerically using the trapezoidal rule. It is interesting to note that the contribution of the wake region to the suction force diminishes with increasing speed ratio for all three jet exit configurations. This seems to be in agreement with the previous conclusion that the wake becomes weaker with increasing speed ratio. For the streamwise and circular jet exit ($w/\ell = 0.3$ and 1.0) it is seen that the contribution of the wake region is greatest near the jet exit and diminishes as the upper limit of integration is increased, while for the bluff exit ($w/\ell = 3.4$) the opposite is generally true. For the speed ratio range $8 \leq V_j/V_\infty \leq 20$ the contribution of the wake region is never greater than 20 percent of the total suction force for the circular jet exit and 15 percent for the slender exit, which is significant in light of the fact that the wake region is 25 percent of the plate area. For these cases the low pressure effects in the wake region are less important than the effects of blockage and entrainment over the rest of the plate in terms of suction force. Therefore a properly specified blockage-sink model excluding this wake region should be useful for studying interference effects in terms of plate pressures. For bluff exits the contribution to suction force due to the wake region is generally quite large. Except in the case of relatively high speed ratios a potential model excluding the wake

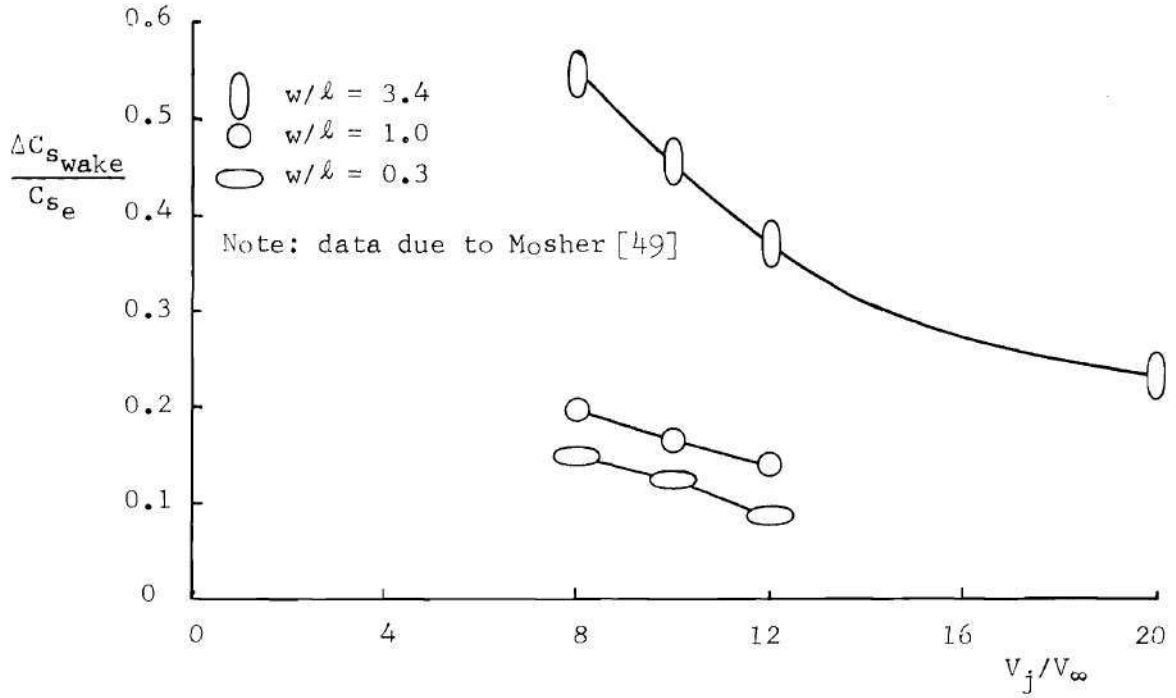

Figure 4. Portion of Suction Force Occurring in the Wake Region, R = 5

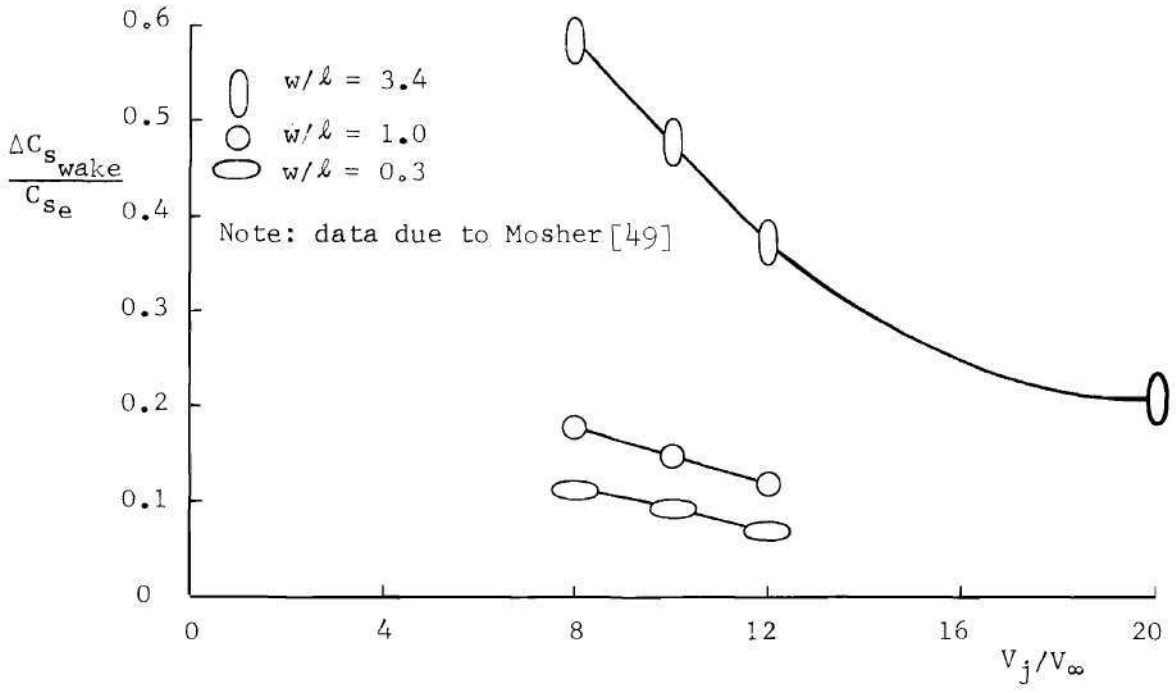

Figure 5. Portion of Suction Force Occurring in the Wake Region, R = 10

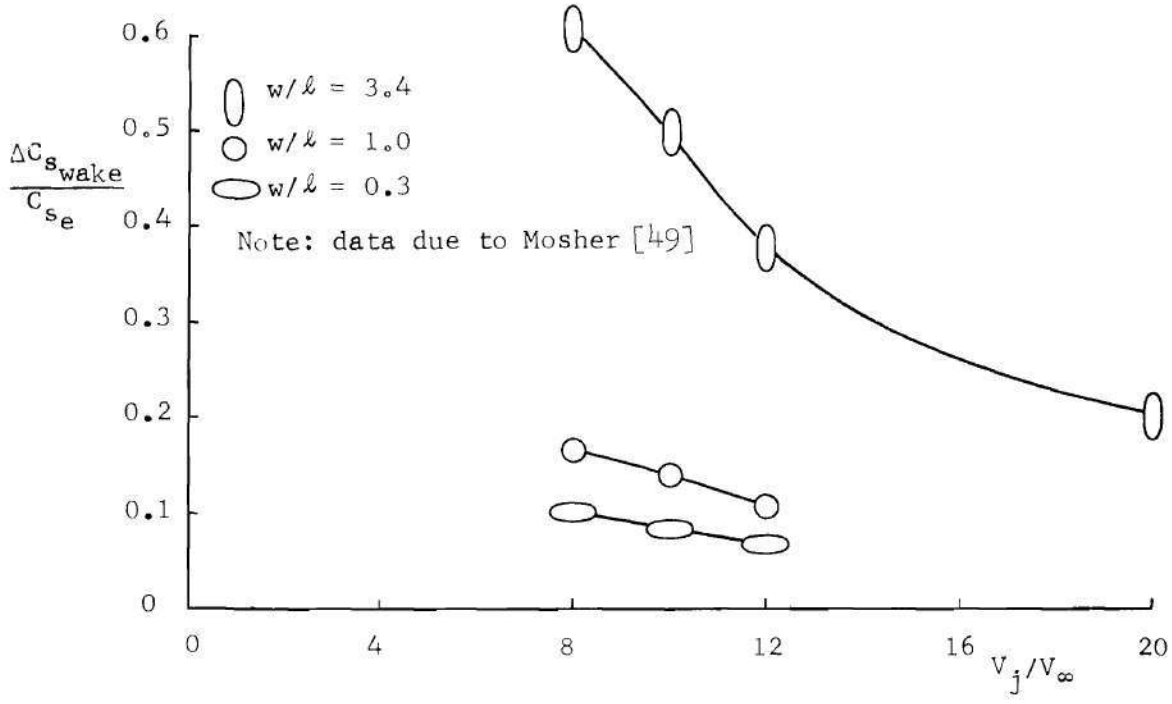

Figure 6. Portion of Suction Force Occurring in the Wake Region, R = 15

region may be very useful in representing the effects of blockage and entrainment upstream and to the side of such a jet, but it would grossly underestimate the suction force or lift loss for V/STOL application. While the effects of blockage and entrainment for jets exhausting from very bluff exits are of interest, the tendency of such jets to produce extensive low pressure wakes would appear to make them impractical for lifting jet applications.

The Importance of Entrainment

The question has also arisen as to whether entrainment is truly significant in the determination of interference pressures. The analyses of references [25], [27], [36], [39], and [44] incorporated no procedures to account for entrainment effects. Bradbury and Wood [20] undertook an analysis of the effect of entrainment on the suction force and concluded that the contribution of C_s from the entrainment is small in a blockage-sink representation including the wake as a part of the potential flow region. However, they neglected the effect of the free stream velocity on the local dynamic pressure, so that their result was in error. This may be seen in Table 2 in which C_s values are calculated both by including ($K = 1.0$) and omitting ($K = 0$) the entrainment effect and including ($\beta_o = \pi$) and excluding ($\beta_o = 3/4\ \pi$) the wake region and are compared to experimental values for $V_j/V_\infty = 8$. Clearly the calculated values omitting entrainment, even excluding the wake region, are too small, but whether or not the wake region is excluded, the contribution of entrainment to the calculated values of C_s is very significant. It can be seen, for example, that for the case in which the wake is

Table 2. The Effect of Entrainment on the Interference Force Coefficient, Wake Included and Wake Excluded

	Interference Force Coefficient					
	Wake Included ($\beta_o = \pi$)			Wake Excluded ($\beta_o = 3/4\pi$)		
R	Calculated (K = 1.0)	Calculated (K = 0)	Experiment ($V_j/V_\infty = 8$)	Calculated (K = 1.0)	Calculated (K = 0)	Experiment ($V_j/V_\infty = 8$)
5	-6.6	-1.5	-22.0	-11.0	-2.7	-17.7
10	-8.8	-1.6	-46.4	-20.4	-3.5	-38.2
15	-10.2	-1.6	-67.5	-28.8	-3.9	-56/3

excluded the contribution of entrainment to the calculated C_s values is itself of the order of magnitude of the experimental values of C_s. Clearly then the effect of entrainment on the plate pressures is quite significant, especially if the wake is excluded.

In order to represent entrainment by a sink or sinks it is necessary to make some reasonable estimate of the entrainment rate and the region in which entrainment takes place. Unfortunately reliable data from which information about the entrainment rate may be extracted directly are scarce. Keffer and Baines [16] present an entrainment parameter for initially circular jets based on experimental observations in which they compared volume flow rates across consecutive plume cross-sections. However, because it is extremely difficult to define the flow direction in the jet plume, this method of measuring entrainment is probably inaccurate. Reference [16] gives an indication of a trend toward increasing entrainment rate with increasing speed ratio but it is difficult to evaluate the validity of this trend. Although it is easy to criticise the work of reference [16], it is extremely difficult to find means of improving the experimental technique of that work. In the absence of more definitive entrainment data it is necessary to evaluate entrainment rates semi-empirically.

Experimental observations are considerably more helpful in determining the region in which entrainment takes place. Examination of oil film photographs [46] and flow direction surveys [15], [49] shows that entrainment occurs in the wake as well as in the jet itself; this same conclusion was reached by McAllister [28] and Platten and Baines [32].

In particular it appears that as the jet plume is deformed, a pair of counter-rotating vortices is formed and these vortices effectively pump crossflow fluid into the plume. Thus entrainment in the jet-in-crossflow situation is more complicated than in the simple free jet case, involving not only the mixing entrainment due to the velocity difference of two streams but also a vortex-induced pumping phenomenon. In their analysis of the jet deflection path Platten and Baines [32] present an interesting approach to a semi-empirical evaluation of entrainment rates. They use two entrainment parameters, considering one to represent the free jet type of entrainment and the other to represent the vortex-induced entrainment. These were both varied until a simultaneous solution of plume continuity and vertical momentum equations yielded a good approximation to the jet path. The values of the resulting "free jet" entrainment parameter corresponded generally to the order of the entrainment rate for free jets reported by Ricou and Spalding [50]. However, the analysis of reference [32] is applicable only to the region of the jet plume that has experienced much deflection and makes a relatively small angle with the crossflow.

The fact that entrainment does occur in the wake suggests that in a blockage-sink model the entrainment effect may be better represented by a distribution of sinks entending into the wake region. Unfortunately no experimental information is presently available concerning the nature of this distribution. One simple approximation for the distribution might be the use of two sinks, one at the center of the jet exit and one in the wake. The difficulty then comes in assigning the strengths

of the two sinks. The results of Platten and Baines cannot be used in a two-dimensional model since their approach assumed large deflection of the plume and the two-dimensional model applies to the portion of the jet plume that is deflected very little. Since the addition of a second sink of unknown strength compounds the difficulty of determining the model parameters by matching experimentally obtained plate pressures, a two-sink model contradicts the present goal of providing a simple model. However, some preliminary calculations were made assuming, in conjunction with a line doublet along the z-axis, a continuous distribution of infinitesimal sinks (sink sheet) lying in the x-z plane between x = 0 and x = 4 with a constant strength per unit length in the x-direction. It was found that the resultant interference plate pressures were very little different from those obtained from a model consisting of the doublet and a single line sink of equivalent strength placed at x = 2. Furthermore for any sink distribution there would be a mean location at which a single sink of equivalent strength would produce virtually the same effects on the flow outside the wake region. Therefore in this study a single sink located at a distance x_s downstream of the origin is used to represent the combined effect of jet and wake entrainment.

Range of Validity of the Two-Dimensional Model

While it is recognized that the jet interference problem is basically three-dimensional and the results of a two-dimensional analysis can at best be approximate, the simplicity and versatility

resulting from the use of a two-dimensional model makes the approach attractive. To determine the range of speed ratio for which the two-dimensional representation may be reasonable, the effects of jet deflection, jet deformation, and variation of entrainment rate along the jet path, none of which can be adequately accounted for in the two-dimensional model, were examined.

To detect the three-dimensional effects of jet deflection, calculations were made with the empirical jet centerline formula for an initially circular jet [27]

$$x = G(\cosh z/G - 1) \tag{6}$$

where

$$G = 0.38(V_j/V_\infty)^2 \quad . \tag{7}$$

This formula, which is conservative in that it describes greater deflections than are observed experimentally, results in jet deflections of less than one jet exit radius at a plane six radii away from the plate surface when $V_j/V_\infty \geq 8$. It then would not be expected that the effect of jet deflection would be very significant for speed ratios greater than or equal to 8. To verify this conclusion for the circular jet exit case, the plate pressure distribution was computed using a large number of three-dimensional doublets and sinks distributed along the jet centerline path given by the above formula for the case $V_j/V_\infty = 8$. The resulting plate pressures were compared with the plate

pressure distribution obtained for the corresponding two-dimensional doublet-sink model as shown in Figure 7. It is seen that the effect of jet deflection is indeed very small for this speed ratio. For $V_j/V_\infty > 8$ the jet deflects even less and the effects of jet deflection are expected to be even less important. However, similar calculations for $V_j/V_\infty = 4$ showed that at lower speed ratios bending does have a significant influence. (See Figure 8). Thus it appears that the effect of jet deflection is not very important for $V_j/V_\infty \geq 8$ for the case of a circular jet exit configuration. It is reasonable to assume that for the case of non-circular jet exit configurations the same conclusion holds, provided that the jet plume penetration is not much less than that for the circular jet exit case at $V_j/V_\infty = 8$.

The effects of jet deformation may be examined by considering characteristics of potential elements in conjunction with experimental observation. The velocity induced at a given point in the flow field by a three-dimensional blockage element is inversely proportional to the cube of the distance between the point and the element, and the velocity induced by a sink element is inversely proportional to the square of the distance [51]. In three-dimensional models the total induced velocity at a point is the cumulative effect of a closely spaced distribution of small three-dimensional elements. Therefore, even if the strength of the individual elements changes considerably as distance along the plume is increased, the influence of the elements near the plate dominates the total effect in the region of the plate near the jet exit; but it does not necessarily dominate the total

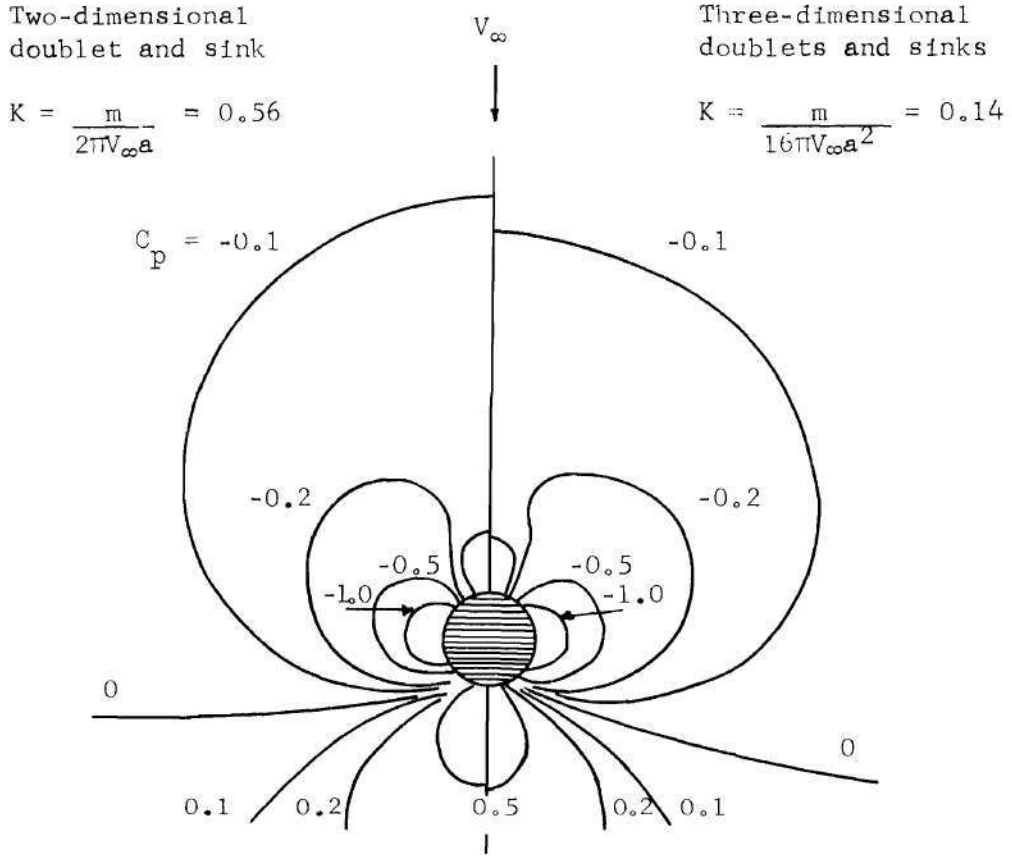

Figure 7. Effect of Jet Path on Pressure Distribution, $V_j/V_\infty = 8$

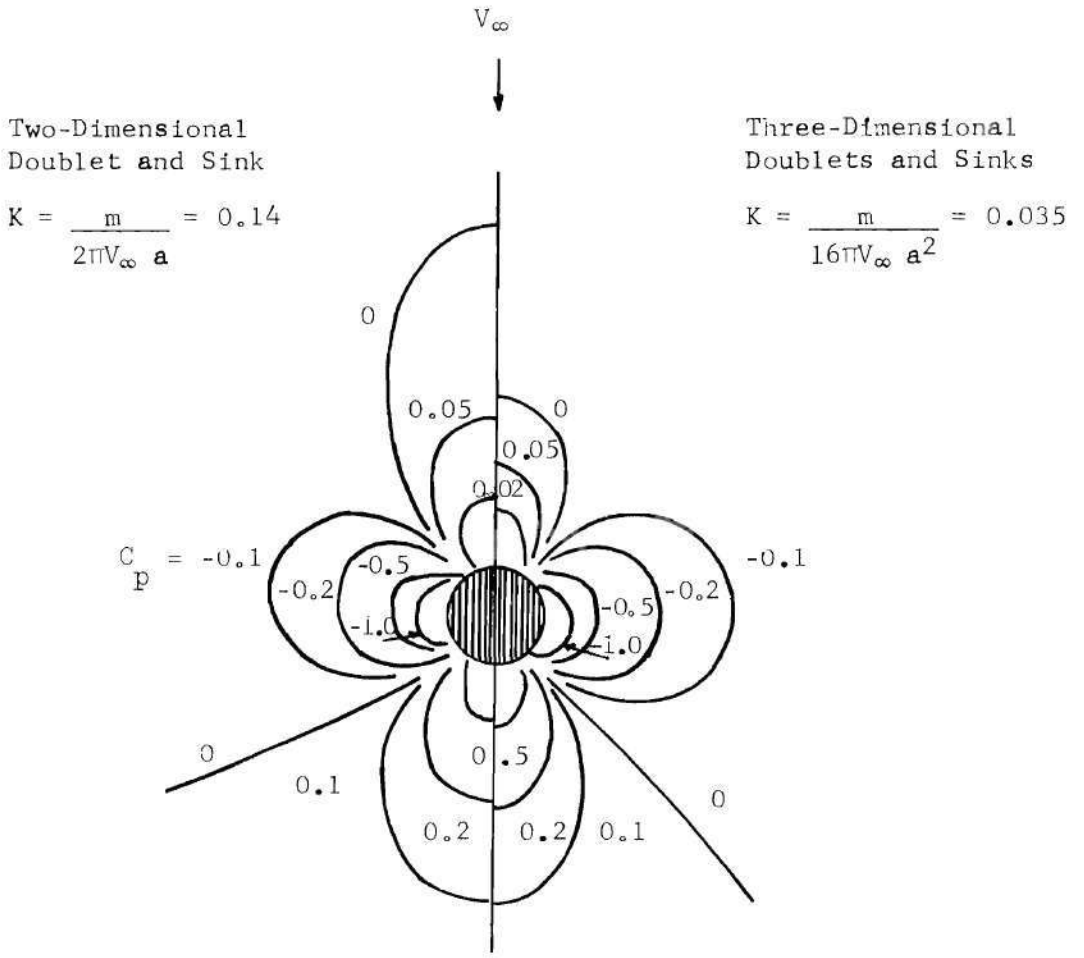

Figure 8. Effect of Jet Path on Pressure Distribution, $V_j/V_\infty = 4$

induced velocity in regions far from the jet. For the case of a circular jet exit existing experimental information indicates [26] that the change of jet exit shape from a circle to a characteristic kidney form takes place in the region $0 \leq z \leq 0.6\ V_j/V_\infty$. It then appears that in regions close to the jet exit the influence of the jet shape change is not very important for speed ratios $V_j/V_\infty \geq 8$. The same conclusion may be drawn concerning the influence of entrainment rate change, provided the entrainment rate does not change by as much as an order of magnitude in the first ten jet exit diameters or so along the jet plume.

It should be noted that, while the effects of deflection and deformation and variation of the entrainment rate along the plume are not expected to be large near the jet exit, they will be present. These effects on the plate may be approximately simulated by small alterations to the basic two-dimensional model. For example, instead of using a blockage element which, in the presence of a uniform stream, closely simulates the exact shape of the jet exit, the model may employ a blockage element which forms a somewhat wider shape, thus approximating the effect of plume spreading. Similarly, an aftward shifting of the sink position may be used to simulate the effect of entrainment into the plume which has been physically deflected downstream.

It then appears that a two-dimensional model should give good results in terms of plate pressures near the jet exit (less than 10 jet exit radii in the case of a circular exit or an equivalent distance for non-circular exits) for speed ratios of about 8 or greater, provided that the wake region is excluded.

Details of the Two-Dimensional Model

The General Method of Computation

All calculations for all variations of the model are treated in the same manner; i.e., the velocities at a point due to the blockage elements in the crossflow and those due to the sink elements are superposed to form the total velocity, from which the plate pressure coefficient is calculated. Let u and v be the velocity components (non-dimensionalized by V_∞) in the x- and y-directions, respectively. Then

$$u = u_b + u_s \,, \tag{8}$$

$$v = v_b + v_s \,, \tag{9}$$

where the subscript b denotes crossflow velocity components as affected by blockage only and the subscript s denotes those due to the sink. The components u_s and v_s are obtained by the relations

$$u_s = \frac{K(x_s - x)}{(x_s - x)^2 + y^2} \tag{10}$$

$$v_s = \frac{-Ky}{(x_s - x)^2 + y^2} \tag{11}$$

where x_s is the dimensionless sink location and K is the dimensionless entrainment parameter. Since this is a two-dimensional model, u and

v are the velocity components on the plate. The plate pressure coefficient is then simply

$$C_p = 1 - u^2 - v^2 \quad . \tag{12}$$

Additional information is found by integrating the plate pressure coefficient along radial lines to form the force distribution coefficient C_F, defined by

$$C_F = \int_{R_o}^{R} C_p \, r \, dr \quad , \tag{13}$$

where R_o is the periphery of the jet exit non-dimensionalized by a_e. Note that C_F is a function of the angle β. The integrated interference force coefficient is then defined by

$$C_s = \int_{0}^{\beta_o} C_F \, d\beta \quad . \tag{14}$$

Since the algebraic expressions for the velocity components are generally rather cumbersome and involve complex numbers, the computation of C_p is accomplished by use of a digital computer, as are the integrals C_F and C_s. Appendix B gives the details of these routine computations.

Blockage Elements Without Afterbodies

The most simple blockage element is a doublet in a uniform stream which can be used to represent the blockage due to a jet issuing from a circular exit. The effect of the doublet, like those of all the blockage elements that follow, is most simply described mathematically by the complex potential function. Let the complex number Z describe the non-dimensional coordinates of the plane of the plate; i.e., let

$$Z = x + \mathcal{L}y \quad . \tag{15}$$

Then the complex potential function for the doublet in a uniform stream V_∞ in the x-direction, non-dimensionalized by V_∞ and a_e, is

$$w = - \left(Z + \frac{1}{Z} \right) \quad , \tag{16}$$

and the complex velocity is simply

$$\frac{dw}{dZ} = - u_b + \mathcal{L}v_b = - \left(1 - \frac{1}{Z^2} \right) . \tag{17}$$

In addition to a circular jet exit, reference [46] considered jets issuing from a round-ended slot exit which consists of a straight-sided slot of width 1.0 inch and semi-circular ends of radius 0.5 inch so that the total length of the exit is 3.56 inches. The configuration is shown in Figure 9. The area of this exit is the same as the area of the circular exit of radius 1.0 inch also investigated in reference [46],

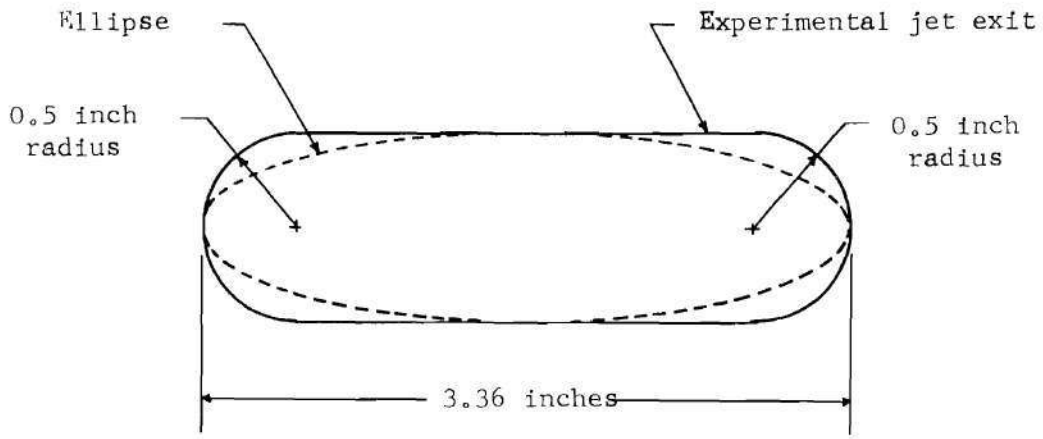

Figure 9. Shapes of Jet Exits

so that the effective radius a_e = 1 inch. This exit was designed so that it could be installed in the plate with its longer dimension aligned with or perpendicular to the crossflow so that relative to the crossflow it represents two exit configurations. When the longer dimension of the slot is aligned with the crossflow, the configuration is termed "streamwise"; in the other orientation it is referred to as the "blunt" configuration. These configurations are approximated by an ellipse having major axis of 3.56 and minor axis of 1.0. This ellipse is also shown in Figure 9. It should be noted that this ellipse has about 16 percent less area than the jet exit used in the experiment. Nevertheless, for the equivalent radius in the calculation, the value a_e = 1.0, corresponding to the test exit, is used. By rotating this ellipse relative to the free stream two elliptic blockages are obtained corresponding to the streamwise and blunt test configurations.

These elliptic blockages and the flow about them are obtained by standard conformal transformations. Consider flow about a circle of radius a_ζ in the ζ-plane ($\zeta = \xi + \imath\eta$). The dimensionless complex velocity for this flow is

$$\frac{d\omega}{d\zeta} = -\left(1 - 1/(\zeta/a_\zeta)^2\right) . \tag{18}$$

The circle $|\zeta| = a_\zeta$ is transformed to an ellipse with semi-major axis A and semi-minor axis B by the relation

$$Z = \zeta \mp \tfrac{1}{4}\left(A^2 - B^2\right)\frac{1}{\zeta} , \tag{19}$$

provided that $a_\zeta = \frac{1}{2}(A + B)$, where $Z = x + iy$ describes the plate plane. The upper sign is used for the blunt configuration and the lower for the streamwise. This convention is used in the remainder of this work. The complex velocity in the Z-plane is then simply

$$\frac{d\omega}{dZ} = \frac{d\omega}{d\zeta} \Big/ \frac{dZ}{d\zeta} \quad , \tag{20}$$

where

$$\frac{dZ}{d\zeta} = 1 \pm \tfrac{1}{4}\left(A^2 - B^2\right)\frac{1}{\zeta} \quad . \tag{21}$$

In order to obtain the ellipse shown in Figure 9 these relations are used with the specific A = 1.678 and B = 0.500.

Calculations were made using these simple blockage models in conjunction with a single sink located at x_s. Several cases were considered for each jet exit shape so that the sink was located successively at several values of x_s and the appropriate corresponding values of K were computed. (See the section "Method of Choosing the Sink Parameters and the Best Fit Models"). It was found that good agreement with the experimental data [49] could be obtained over a large region upstream of the circular jet exit, but the agreement grew progressively worse with increasing β. Similar results were obtained with the streamwise ellipse model which resulted in the best agreement with experimental data for $V_j/V_\infty = 12$, as shown in Figure 10 and 11. For the blunt ellipse model the results were very good for $\beta \leqq 90$ degrees,

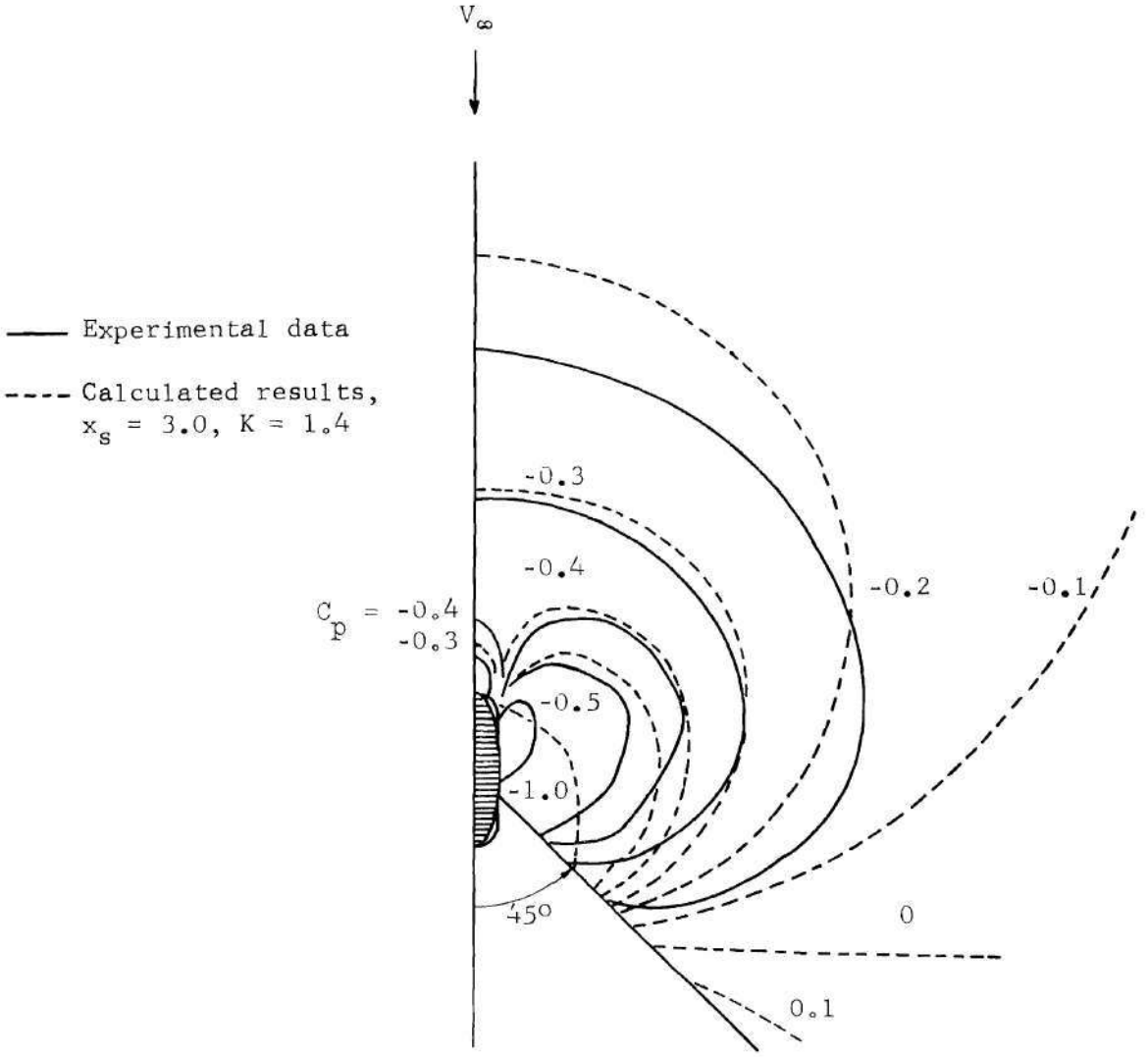

Figure 10. Plate Pressures for the Streamwise Exit, V_j/V_∞ = 12, Simple Model

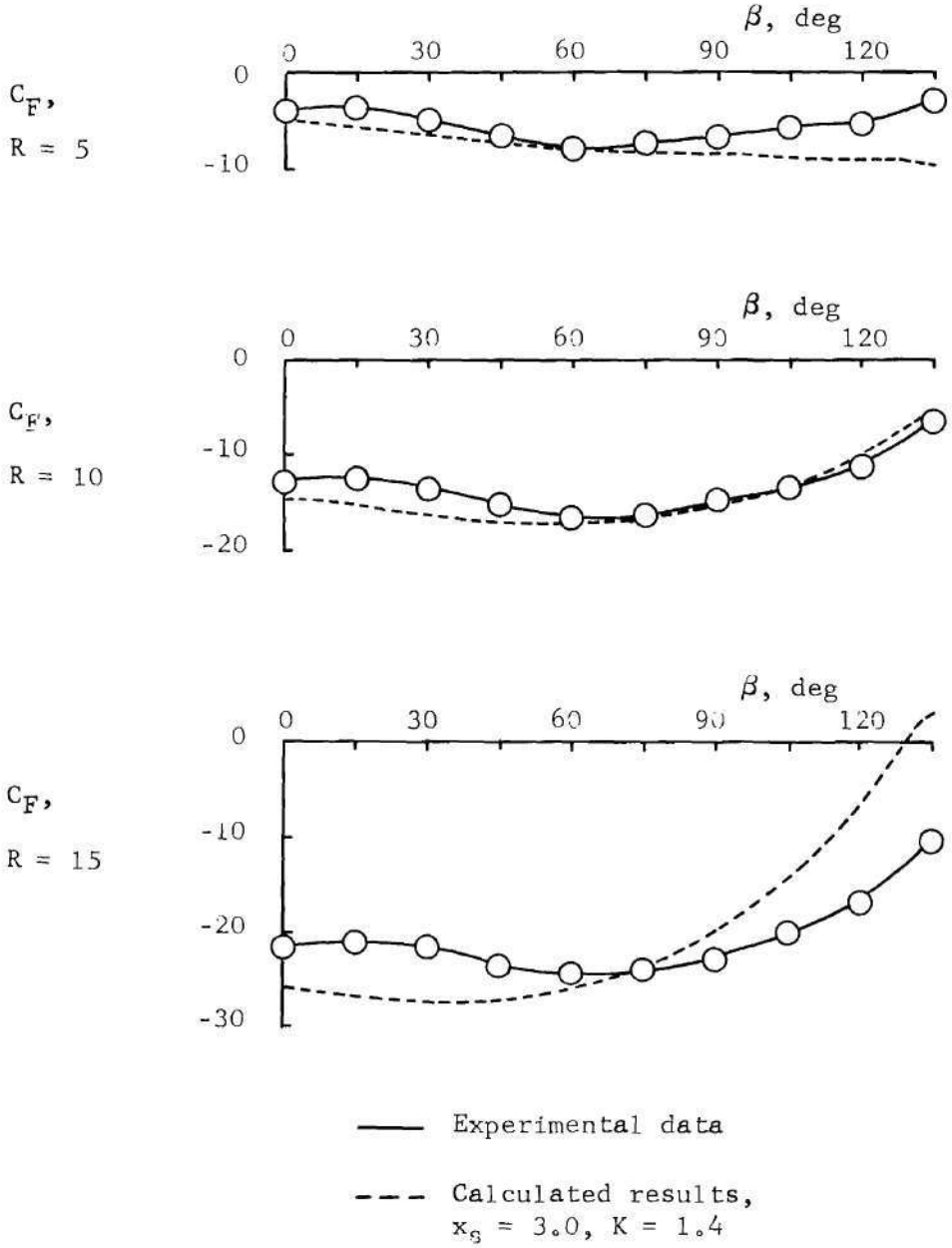

Figure 11. Force Distribution for the Streamwise Exit, $V_j/V_\infty = 12$, Simple Model

but for $\beta > 90$ degrees the results of the model did not agree at all with the experimental data, as may be seen in Figures 12 and 13. The progressive deviation of the theoretical results (dashed curves) from the experimental data (solid curves) is easily seen in all these figures. The results from the simple blockage-sink models were encouraging, but the inadequacies near the wake region were disturbing.

The Afterbody Forms

The results cited above suggest that the wake region has an important blockage effect. At present the wake is not amenable to detailed description. However, this blockage effect can be incorporated in the blockage-sink model by the addition of an afterbody to the basic blockage element. The afterbodies must represent the wake blockage in terms of width and point of intersection with the basic blockage element. Although the oil film photographs tend to indicate that the width of the wake increases with increasing speed ratio for a given jet exit shape, careful study of the total pressure data of Jordinson [15] tends to indicate that the region of severe total pressure loss actually decreases in width with increasing speed ratio. Therefore, it would appear that the width of the afterbody representing blockage by wake fluid which has experienced severe total pressure loss should decrease with increasing speed ratio for a given jet exit configuration. With all other parameters of the theory held constant, the point of intersection of the afterbody with the basic blockage element controls the total width of the blockage so that as the intersection point moves aft on the basic blockage element the total width is reduced. Now in the physical situation the plume actually deforms, becoming wider with

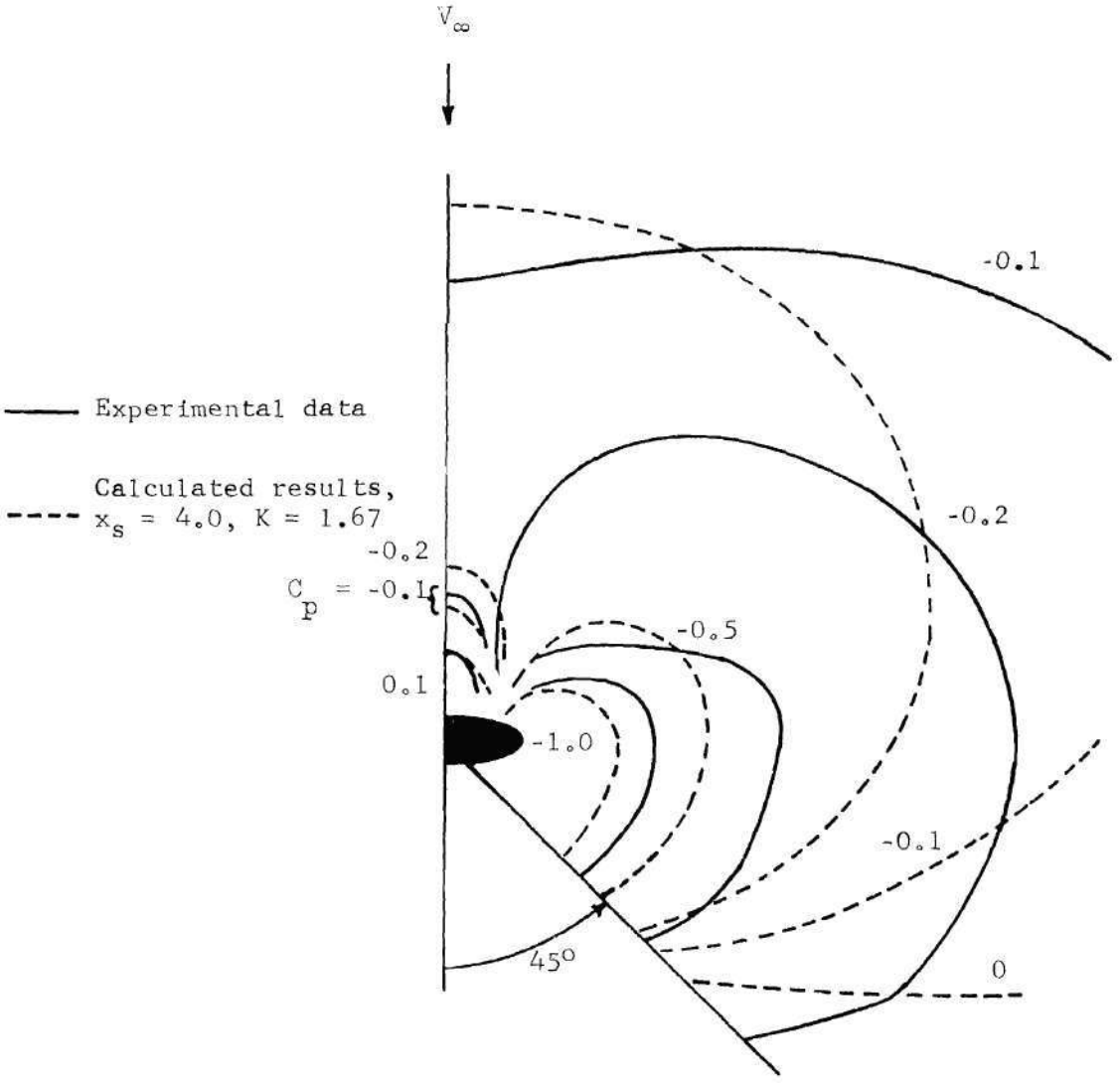

Figure 12. Plate Pressures for the Blunt Exit, V_j/V_∞ = 12, Simple Model

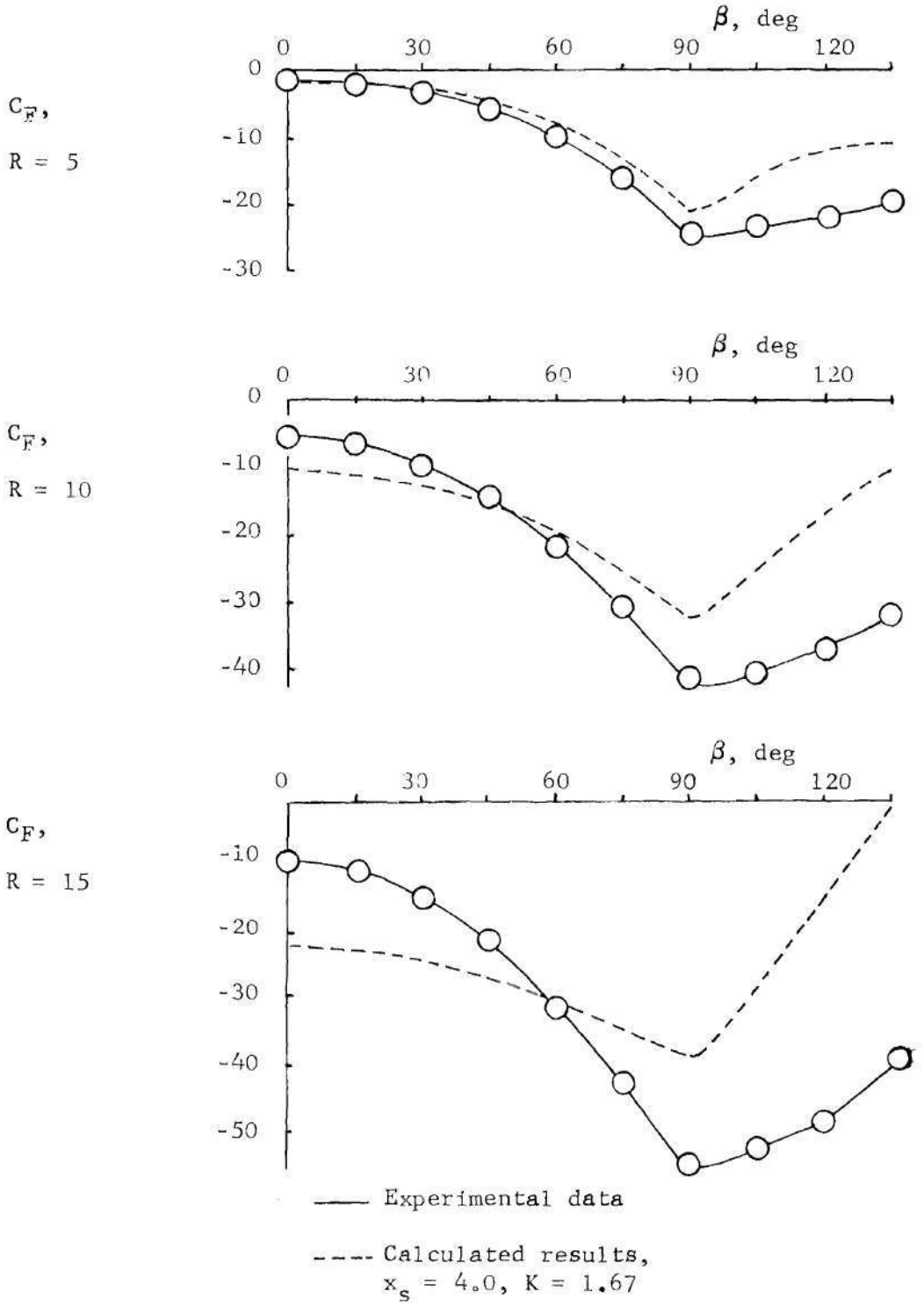

Figure 13. Force Distribution for the Blunt Exit, V_j/V_∞ = 12, Simple Model

increasing distance from the plate. Since the present model is two-dimensional, it can not directly represent this deformation. However, by specifying the point of intersection so that the total width of the blockage is somewhat wider than the jet exit, some of the effects of the deformation may be simulated in terms of plate pressure. Therefore the point of intersection should move aft on the basic blockage element with increasing speed ratio since with increasing speed ratio the plume deforms less at a given distance off the plate.

The use of an afterbody to represent the blockage due to the wake is well illustrated by the case of a solid right circular cylinder. It has been shown in reference [20] that the pressure distribution around a solid circular cylinder calculated from potential theory accounting for only the cylinder blockage differs significantly from the experimentally observed pressure distribution on a plate to which a solid circular cylinder is attached perpendicularly. It is noted that the tested solid cylinder case, aside from the plate boundary layer effect, is truly two-dimensional. Figure 14 presents a comparison of the calculated and experimentally obtained constant pressure contours shown in terms of the pressure coefficient C_p. The dashed curves are calculated contours and the solid curves are experimental. It is seen that the simple potential theory fails to show the lateral spread of the low pressure region for $\beta > 90$ degrees. Since the effect of plate boundary layer on the plate pressure is of secondary importance [20], it is suspected that the effect of blockage of the crosswind by the wake is of considerable importance. Accordingly, constant pressure contours on the plate were calculated using a solid cylinder-afterbody repre-

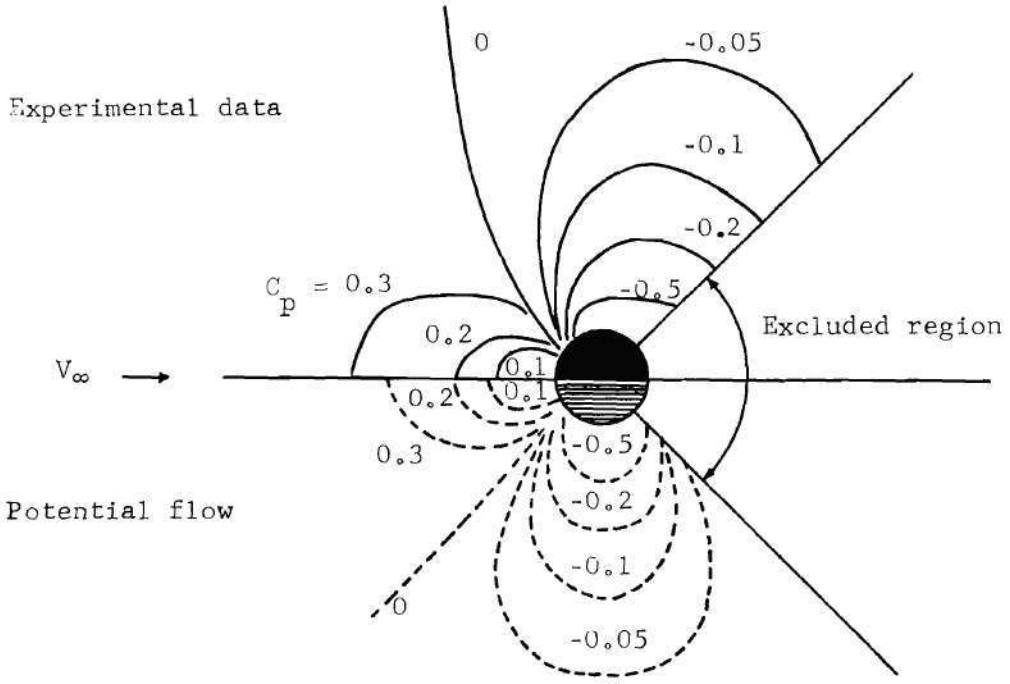

Figure 14. Constant C_p Contours Around a Circular Cylinder, Potential Flow -- Circular Cylinder Only

sentation and compared with the experimentally measured pressure distribution around a circular cylinder in Figure 15. Again, the dashed curves are calculated contours and the solid curves are experimental. The shape of the afterbody used in the calculation is also shown in Figure 15. The agreement between the two sets of contours is quite good outside the excluded wake flow region; in particular, the solid cylinder-afterbody model results in a lateral spread of the low pressure region for $\beta > 90$ degrees. A comparison of Figure 14 and Figure 15 shows clearly that the addition of the afterbody significantly improved the blockage representation.

The afterbodies used in this work are obtained in the following manner: consider a Rankine oval placed in the ζ'-plane ($\zeta' = \xi' + i\eta'$), as shown in Figure 16. The Rankine oval has half-length ℓ_a and half-width w_a and in general the upstream stagnation point ξ_3' is displaced from the origin of the ζ' coordinate system. All lengths are non-dimensionalized by a_e. The Rankine oval is formed by a source-sink pair of strength S separated by a distance D immersed in a uniform stream V_∞. These parameters are related by the equations

$$w_a^2 - \tfrac{1}{4} D^2 = D w_a \cot\left[\frac{D w_a}{\ell_a^2 - \tfrac{1}{4} D^2}\right], \tag{22}$$

and

$$\frac{S}{V_\infty} = \frac{\ell_a^2 - \tfrac{1}{4} D^2}{D}. \tag{23}$$

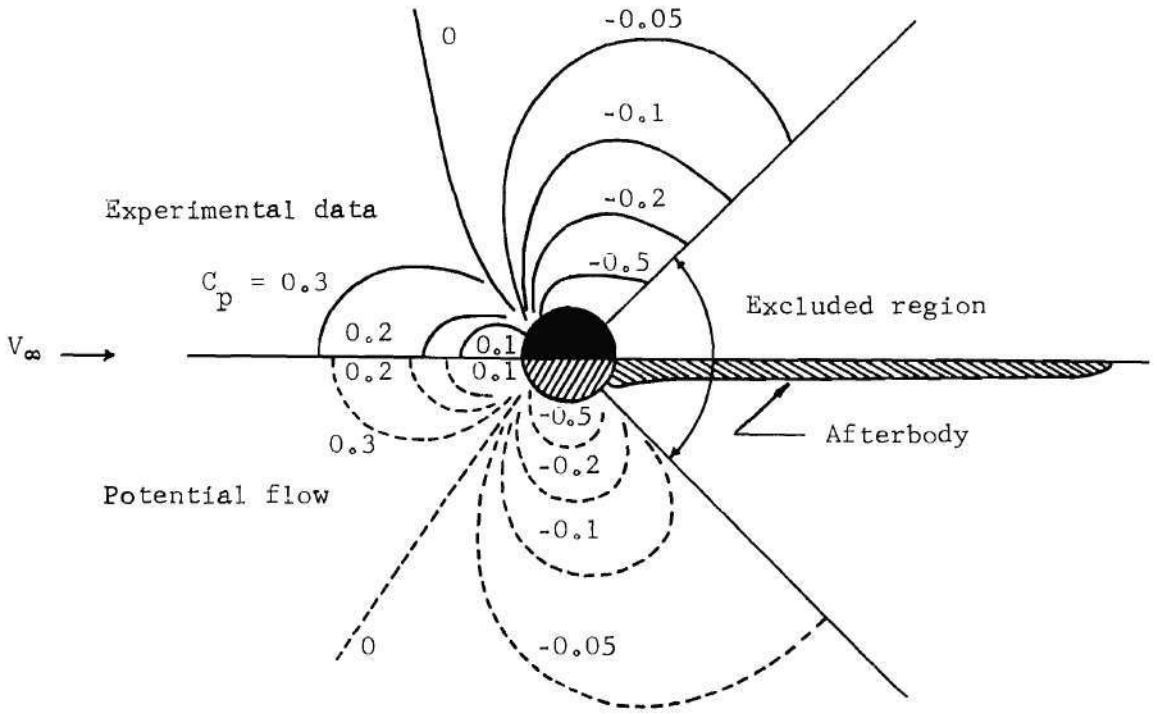

Figure 15. Constant C_p Contours around a Circular Cylinder, Potential Flow -- Circular Cylinder with Afterbody

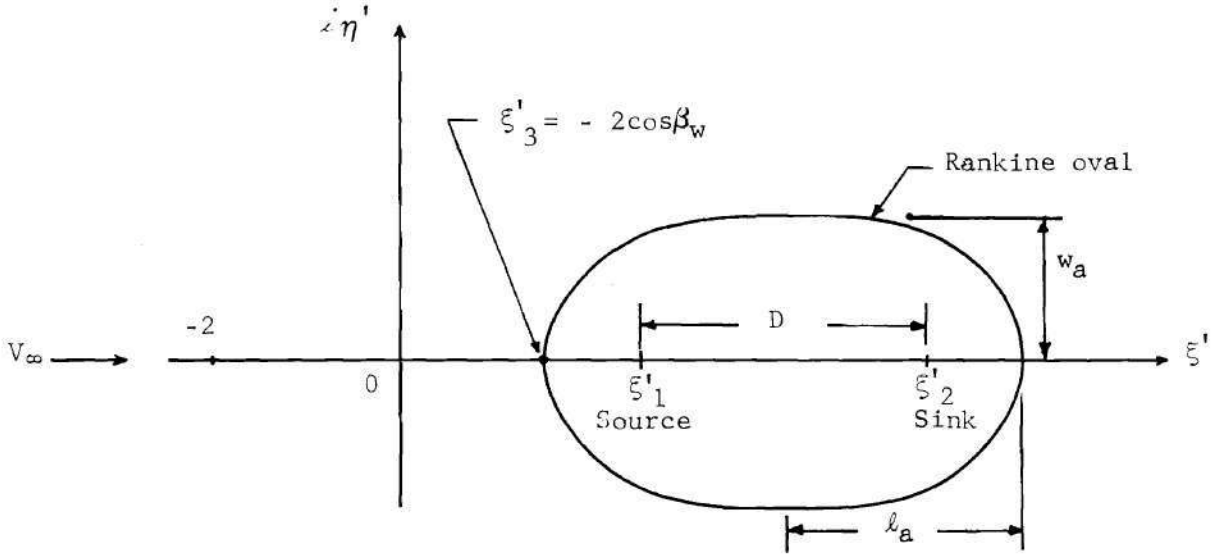

Figure 16. The ζ' - Plane

Therefore if two of these parameters are specified the others may be calculated. In this work values are chosen for ℓ_a and w_a, and equations (22) and (23) are solved for D and S/V_∞, respectively. The dimensionless complex potential function for flow about the Rankine oval is the ζ'-plane is

$$\omega = -\zeta' - \left(\frac{S}{V_\infty}\right)\ell n(\zeta' - \xi_1') + \left(\frac{S}{V_\infty}\right)\ell n(\zeta' - \xi_2') \quad , \tag{24}$$

where the source is located at

$$\xi_1' = \ell_a - 2\cos\beta_w - D/2 \quad , \tag{25}$$

the sink is located at

$$\xi_2' = \ell_a - 2\cos\beta_w + D/2 \quad , \tag{26}$$

and the upstream stagnation point is at

$$\xi_3' = -2\cos\beta_w \quad . \tag{27}$$

In order to obtain a unit circle with an afterbody, the transformation relation

$$\zeta' = Z + 1/Z \tag{28}$$

is employed. This relation transforms the portion of the ξ'-axis - $2 \leq \xi' \leq \xi_3'$ into a portion of a circle of unit radius, and the Rankine oval becomes an afterbody intersecting the circle at $Z = e^{\lambda(\pi-\beta_w)}$, as shown schematically in Figure 17. The choice of β_w is arbitrary, except that β_w should increase with increasing speed ratio as previously argued. The complex potential in the Z-plane is then

$$w = -(Z + 1/Z) + \left(\frac{\ell_a^2 - \frac{1}{4}D^2}{D}\right) \tag{29}$$

$$\times \left[\ell n(Z + 1/Z - \xi_2') - \ell n(Z + 1/Z - \xi_1')\right]$$

and the complex velocity is

$$-u_b + i v_b = \frac{dw}{dZ} = -(1 - 1/Z^2) \tag{30}$$

$$\times \left[1 + \left(\frac{\ell_a^2 - \frac{1}{4}D^2}{D}\right)\left(1/(Z + 1/Z - \xi_1') - 1/(Z + 1/Z - \xi_2')\right)\right] .$$

To obtain the elliptic blockage elements equations (29) and (30) are simply scaled up so that they represent flow about a circle of radius a_ζ and are placed in the ζ-plane. Then the transformation equation (19) is applied and the complex velocity is given by equation (20).

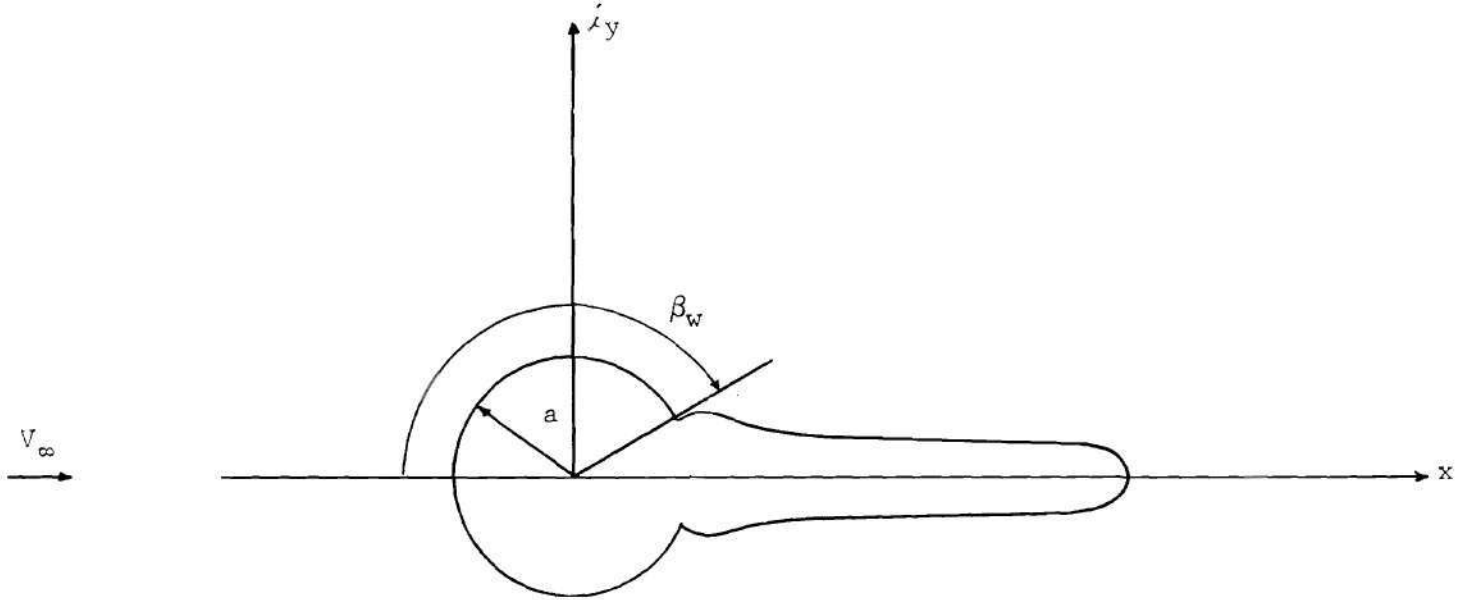

Figure 17. Cylinder with Afterbody (Schematic)

Note that for the elliptic blockage elements with afterbodies the intersection of the afterbody with the ellipse is not described by $Z = e^{\lambda(\pi - \beta_w)}$ because an additional transformation has been employed. For these cases the intersection points occur at

$$x_i = -\frac{1}{2}\left[(A + B) \mp (A - B)\right] \cos \beta_w \tag{31}$$

$$\pm y_i = \frac{1}{2}\left[(A + B) \pm (A - B)\right] \sin \beta_w \tag{32}$$

when the upstream stagnation point of the Rankine oval is specified as $\xi_3' = -2 \cos \beta_w$, as it always is in this work. The multiple signs in the right hand sides of equations (31) and (32) follow the sign convention for blunt and streamwise ellipses; the multiple sign on the left hand side of equation (32) represents the symmetry about the x-axis. Figure 18 shows the coordinates x_i, y_i as functions of β_w for all three jet exit approximations considered.

The choice of the Rankine oval parameters and the afterbody-jet exit intersection point is arbitrary. The variation of β_w (which controls the intersection point) and the general variation of the afterbody width with speed ratio have already been discussed. However, some guidelines for the choice of w_a were obtained. It is reasonable to assume that the afterbody, if it is to represent blockage due to the presence of a wake, should be relatively long. Since the 90 degree total angle wake region is to be excluded from the calculations, it can be anticipated that the most influential portion of the afterbody in

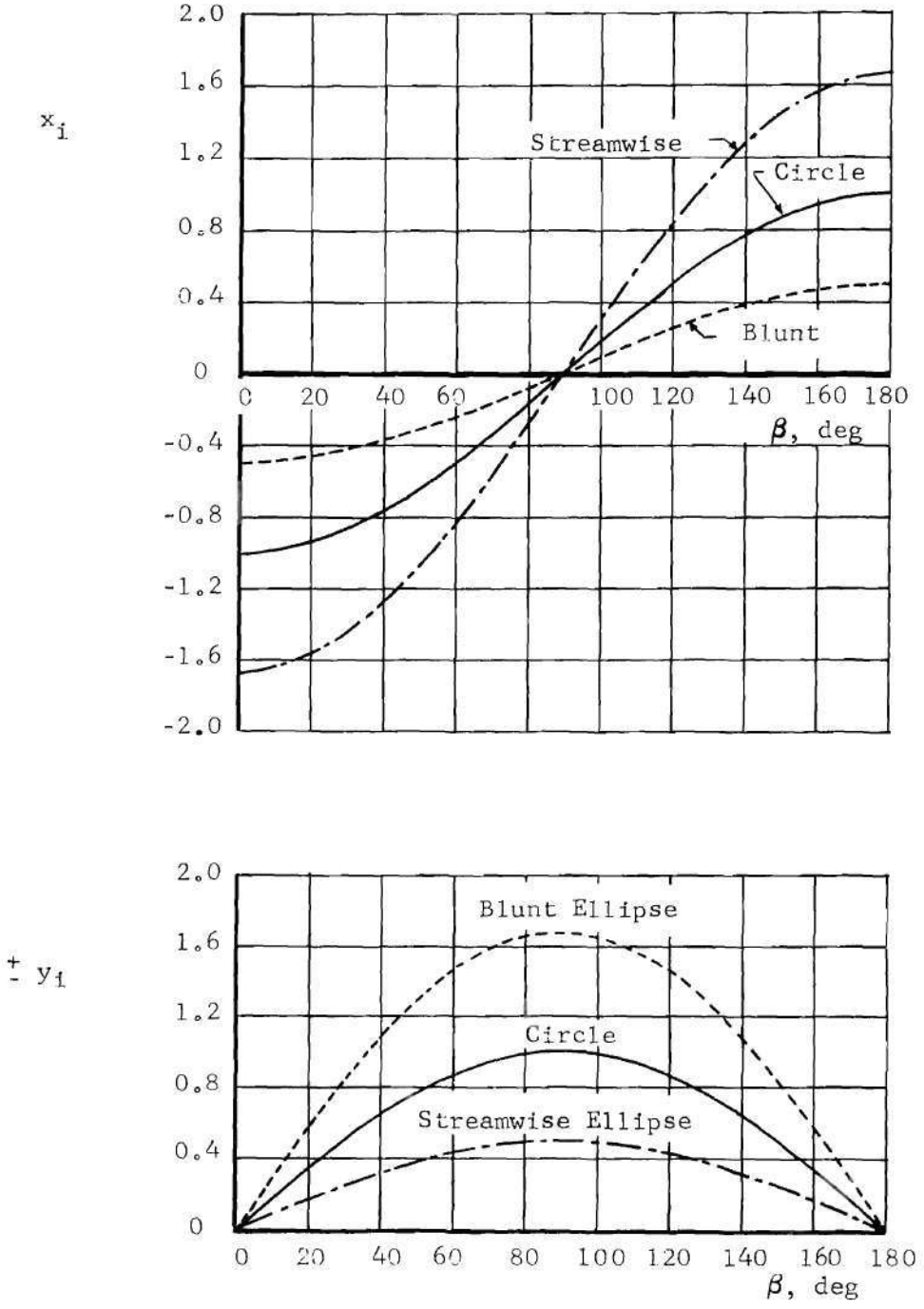

Figure 18. Cartesian Coordinates of Afterbody-Jet Exit Intersection Points

this study is that in the immediate vicinity of the jet exit. Therefore it appears that the half-width of the Rankine oval, w_a, should be of greater importance than the half-length, ℓ_a, since these are rather closely related to the final afterbody width and length, respectively. To check this conclusion some preliminary calculations were made assuming a constant Rankine oval width ($w_a = 1.0$) and varying the half length $2 \leq \ell_a \leq 4.80$. It was found that for this constant width very little change occurred in the pressure field for a circular jet exit with varying half-length, ℓ_a. (See Figure 19.) For the remainder of this work then the value of ℓ_a is arbitrarily chosen to be $\ell_a = 4.80$. With this choice of Rankine oval length a wide range of Rankine oval widths were used in obtaining the best fit models, as described in the following section, and it was found that varying width was indeed important to the detailed pressure field.

It should be noted that the afterbody half-width following the transformations is not the same as the Rankine oval half-width. Generally the downstream portion of the Rankine oval transforms without significant distortion. However, for small real coordinates the distortion of the imaginary coordinates becomes greater so that the effective width of the blockage is slightly increased.

Method of Choosing the Sink Parameters and the Best Fit Models

The method of determining the combination of blockage elements and sink parameters that best represent the experimentally observed plate pressures is as follows:

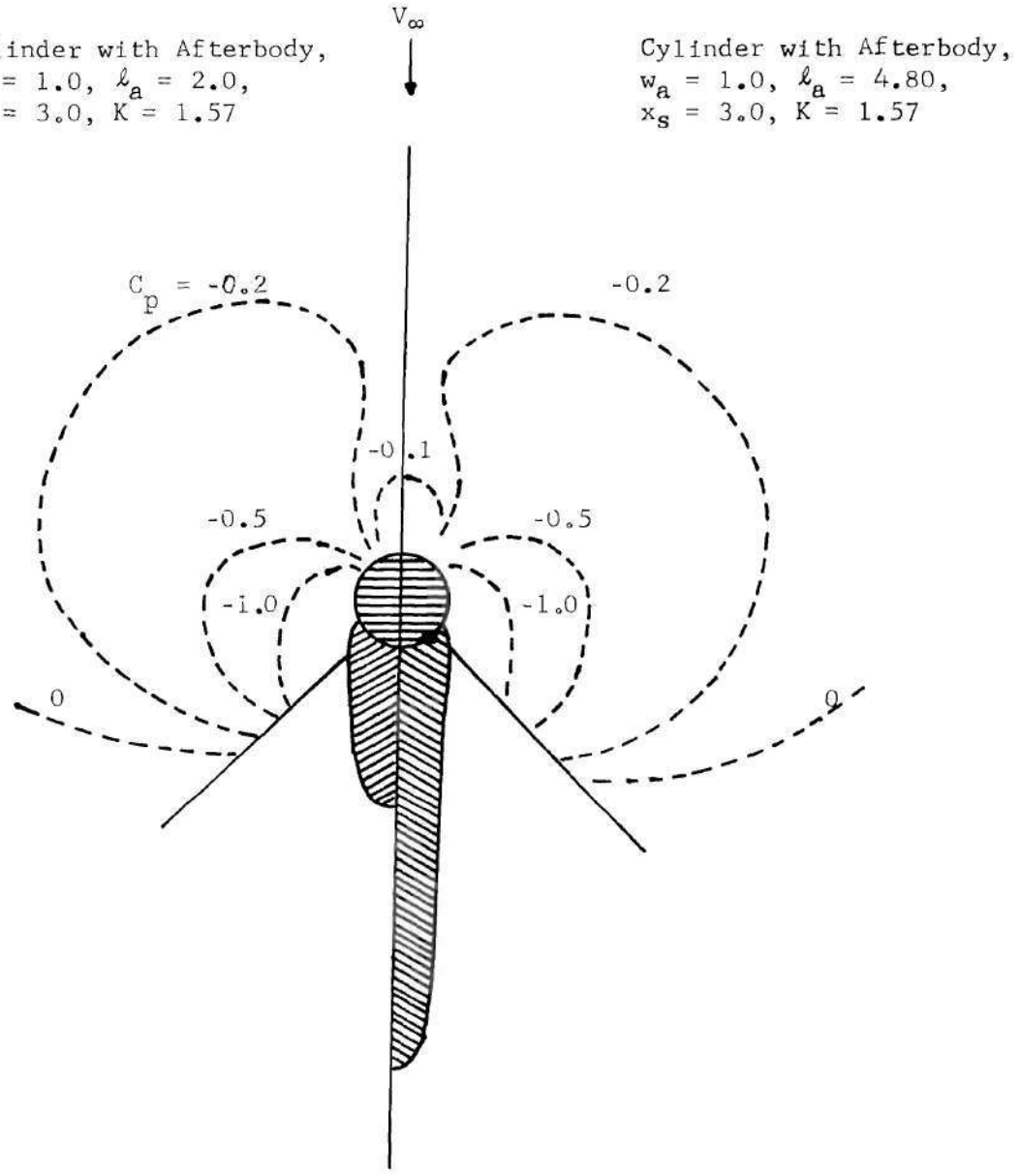

Figure 19. Effect of Rankine Oval Length on Plate Pressures for a Given Rankine Oval Width, Circular Jet Exit

(1) A jet exit shape and a speed ratio are chosen.

(2) A candidate blockage element is chosen. This may be any blockage element representing the jet exit shape and an afterbody, as described in the preceding section.

(3) A sink position x_s is chosen. The first choice is usually $x_s = 0$, that is, the sink is placed at the origin.

The non-dimensional sink strength K corresponding to the choice of blockage element and sink position is calculated by matching the experimentally observed plate pressures [49] on the upstream dividing streamline. The method of this calculation will be given in detail later. At this point a candidate blockage-sink model is completely specified. Then plate pressure coefficients C_p and integrated force distribution coefficients C_F are calculated. Constant C_p contours are plotted and compared to those obtained experimentally [49], and the calculated C_F curves are compared to the corresponding experimental data. Generally the calculated pressure distribution does not agree well with experiment over a large portion of the plate. If this is the case, retaining the same candidate blockage element, a new sink position x_s aft of the previous position is chosen, a new K is calculated, and the resulting plate pressure data are compared to experimental data. This procedure is repeated until the combination of this candidate blockage element and sink parameters resulting in best comparison with the experimental data is found. The criterion for "best comparison" is good general agreement of the C_p contours and the C_F curves when R = 5, as will be discussed later with examples. In general this candidate

"best fit" model results in regions of poor agreement with the experimental data, in which case a new blockage element is chosen; and step 3 is repeated. The choice of new blockage elements is repeated until a wide range of afterbody widths and afterbody-jet exit intersection points has been considered. Comparing the best fitting results from all of the blockage elements a final "best fit" blockage-sink model is chosen. That is, after a wide range of afterbody widths, after-body-jet exit intersection points, sink positions, and sink strengths have been considered, the combination resulting in best comparison to the experimental data for the given jet exit shape and speed ratio is chosen as the best fit model according to the standards to be discussed later. The sink strength is then a semi-empirical measurement of the entrainment rate.

The method of calculating a K compatible with the given blockage element involves matching the experimentally observed plate pressures [49] along the upstream dividing streamline ($\beta = 0$). This method was chosen because in both the experiment and the analytical model the flow direction along this line of the plate is in the x-direction for all jet exit shapes and all speed ratios, so only one component of velocity need be considered. At all other points on or very near the plate the flow direction has never been measured accurately; only experimental plate pressure data are available. It is impossible to accurately convert these pressure data to velocities that may be assigned to either the blockage- or the sink-element in the model. Along the $\beta = 0$ line, then, the total non-dimensionalized velocity is simply u, where in the model

$$u = u_b + u_s \quad . \tag{33}$$

It is clear that if the plate pressures produced by the model are to agree with the experimental data the velocity u must equal the local test velocity u_t; i.e., along the line $\beta = 0$

$$u = u_t = u_b + u_s \quad . \tag{34}$$

Since it is known that the test velocity is in the x-direction, the plate pressure data are readily reduced to the dimensionless velocity according to the relation

$$u_t = \sqrt{1 - C_p} \quad . \tag{35}$$

Therefore the *dimensionless* velocity due to the sink required to match the empirical data is

$$u_s = \sqrt{1 - C_p} - u_b \quad , \tag{36}$$

which is actually a function of x. The sink-induced velocity u_s is then calculated at several points x_j, and at these points the dimensionless entrainment coefficient K_j, used as a positive number, is

$$K_j = (x_s - x_j)\, u_s \tag{37}$$

where

$$K_j = \frac{m}{2\pi a_e V_\infty} \tag{38}$$

and a_e is the radius of a circle having the same area as the jet exit under consideration. Although the actual value of a_e for the elliptic blockage models is about 8.5 percent smaller than the radius of the circular jet exit, the value of a_e for all of the experimental jet exits was the same, and the experimental value was used in these calculations.

Ideally for a given speed ratio, blockage element, and sink position, the K_j's thus calculated should be the same for all x_j. However, in most instances there is some variation in K_j with x_j. The K to be used in calculating the sink-induced velocities on the plate is taken to be the arithmetic average of the values indicated by the experimental data. It should be noted, however, that better results are obtained when the calculating points x_j are chosen to be fairly closely spaced for $x_j > -5$ and sparsely spaced for $-10 < x_j < -5$. This is reasonable when it is recalled that three-dimensional effects are more influential at large distances from the jet exit. In Table 3 a typical choice of calculating points and the resulting values of K are given. A comparison of calculated and experimentally observed pressure coefficients along the line $\beta = 0$ for this case is given in Figure 20.

In order to choose a "best fit" model it is necessary to

Table 3. Variation in Calculated Values of K

x_j	K_j
-1.25	1.69
-2.00	1.45
-3.00	1.34
-5.00	1.13
-10.00	0.72

Average K = 1.27

Model Parameters: Circular jet exit

$\ell_a = 4.80$

$w_a = 0.83$

$\beta_w = 51$ degrees

$x_s = 2.0$

Test Conditions: Circular jet exit

$V_j/V_\infty = 8$

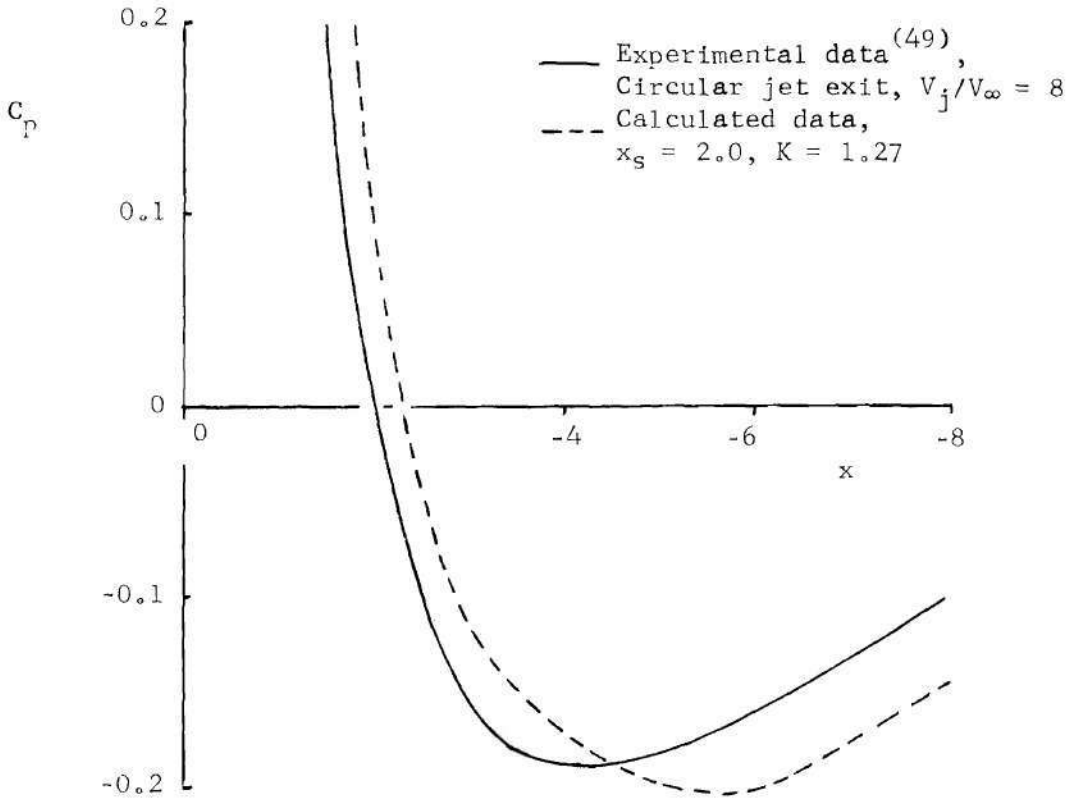

Figure 20. Comparison of Calculated and Experimental Pressure Coefficients Along the Line $\beta = 0$

minimize the errors in some manner. Unfortunately it is extremely difficult to choose an objective means of quantizing the errors incurred by using this method. One cannot choose to compare on the basis of detailed plate pressures, which is the most direct means, for the error in this quantity varies dramatically over the entire plate; since there clearly are regions where the two do not agree, comparisons at points on a closely spaced grid could result in indicated errors ranging from zero to a hundred percent or more. Choosing to compare the pressures at discrete points is not very satisfactory, for by an unfortunate choice of points the indicated error could be very misleading. It seems that the only practical means of basing the test for agreement on the plate pressures is by visual inspection of the C_p contours. However, this is subjective and may be deceptive. For instance, in regions of small pressure gradient the C_p contours may not appear to agree well; but in these regions a point-by-point comparison of the pressure coefficients would show that the agreement is actually reasonably good. The region $\beta < 60$ degrees, $r < 10$ in Figure 21 provides a good example of this difficulty. Since a point-by-point comparison in such regions is extremely cumbersome and time consuming, another criterion was sought. It was reasoned that if the pressure coefficients actually agree well over a region, the integrated force distribution coefficient should agree very well indeed. Again, due to significant variations with β of the error in C_F, the error in these curves cannot be conveniently established quantitatively. However, visual inspection reveals the distribution of the errors and even rather small changes resulting

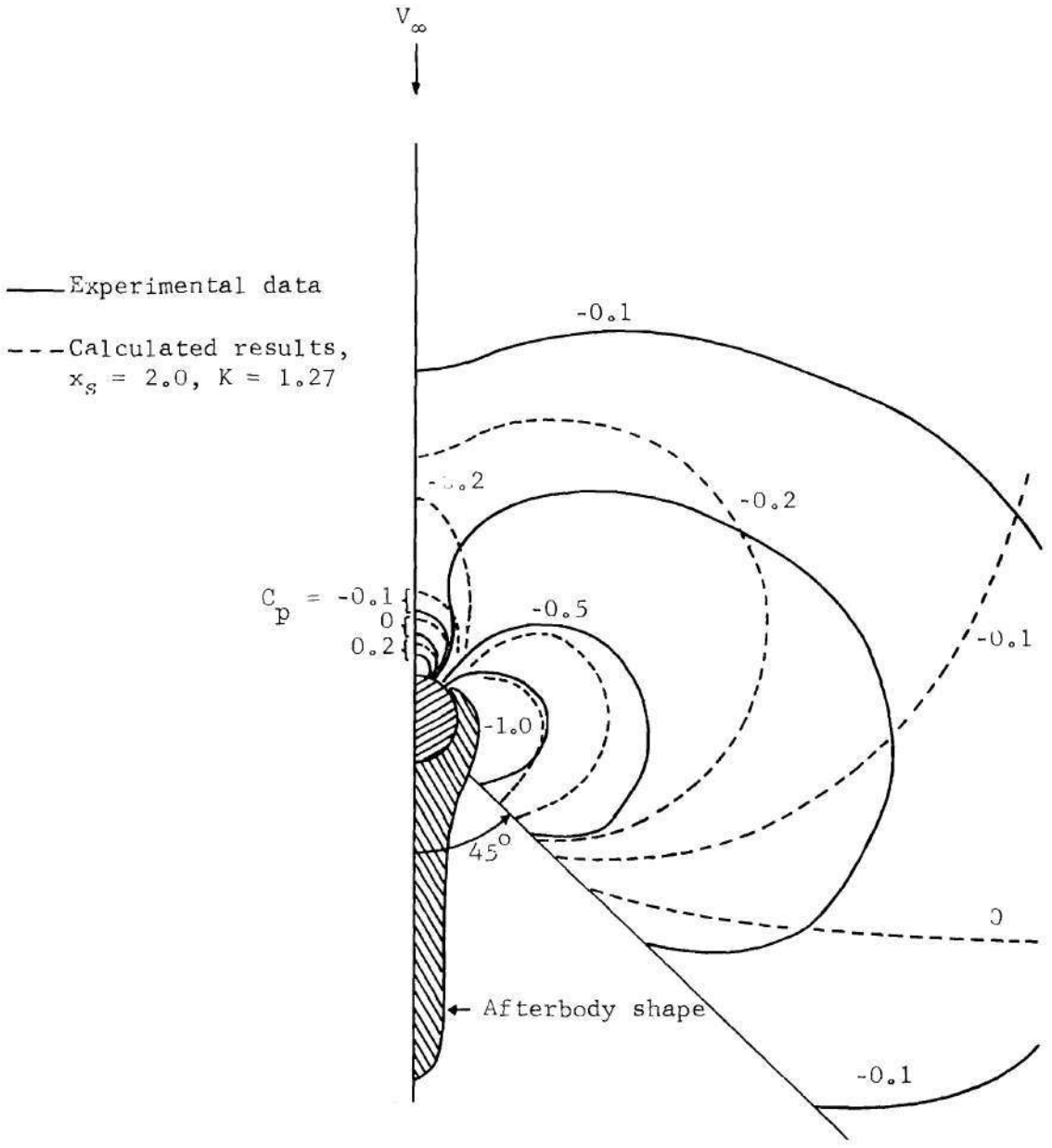

Figure 21. Plate Pressures for the Circular Exit, V_j/V_∞ = 8

from variations in the model parameters. Since the accuracy of the two-dimensional model is expected to diminish with increasing distance from the jet exit, the comparison of C_F curves should be based primarily on values of R = 5.

As an example of the application of the visual comparison of C_p contours of C_F curves in obtaining the "best fit" models, consider the case of a circular jet exit and $V_j/V_\infty = 8$. Figures 21 and 22 show the results of one candidate model in which $x_s = 2.0$ and K = 1.27, as calculated in Table 3. The solid curves are experimental results and the dashed curves are the calculated data. Clearly the C_p contours do not agree very well in the region $\beta > 80$ degrees, $r > 5$ (Figure 21). Furthermore for $\beta > 40$ degrees the integrated force distribution coefficient C_F does not agree extremely well with the corresponding experimental data, although the error does not appear to be serious when R = 5. Following step 2 of the outlined procedure for finding the best fit model, the blockage element was retained and the sink position was moved to $x_s = 3.0$. K was calculated for this new model to be K = 1.54. The resulting plate pressure coefficient contours are given in Figure 23 and the C_F curves are shown in Figure 24. Again the solid lines are the experimental data. Comparing Figure 23 with Figure 21, it is seen that the change in sink parameters has effected some improvement in C_p contour agreement in that the new model provides better agreement in the region $\beta > 80$ degrees. The agreement in the region $0 \leq \beta \leq 80$ degrees and $r < 10$ is somewhat improved. In the region $\beta < 80$ degrees, $r > 10$ the comparison shows generally poorer

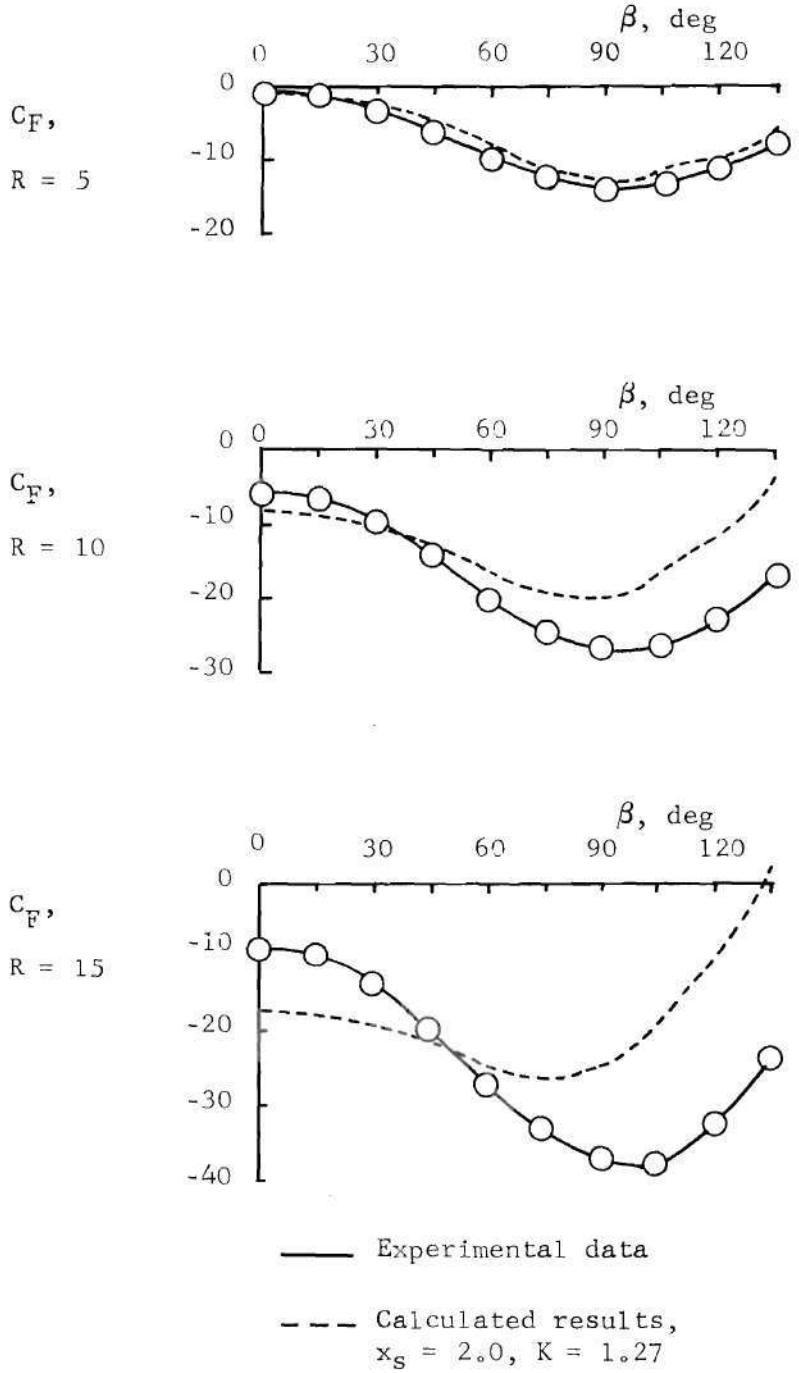

Figure 22. Force Distribution for the Circular Exit, V_j/V_∞ = 8

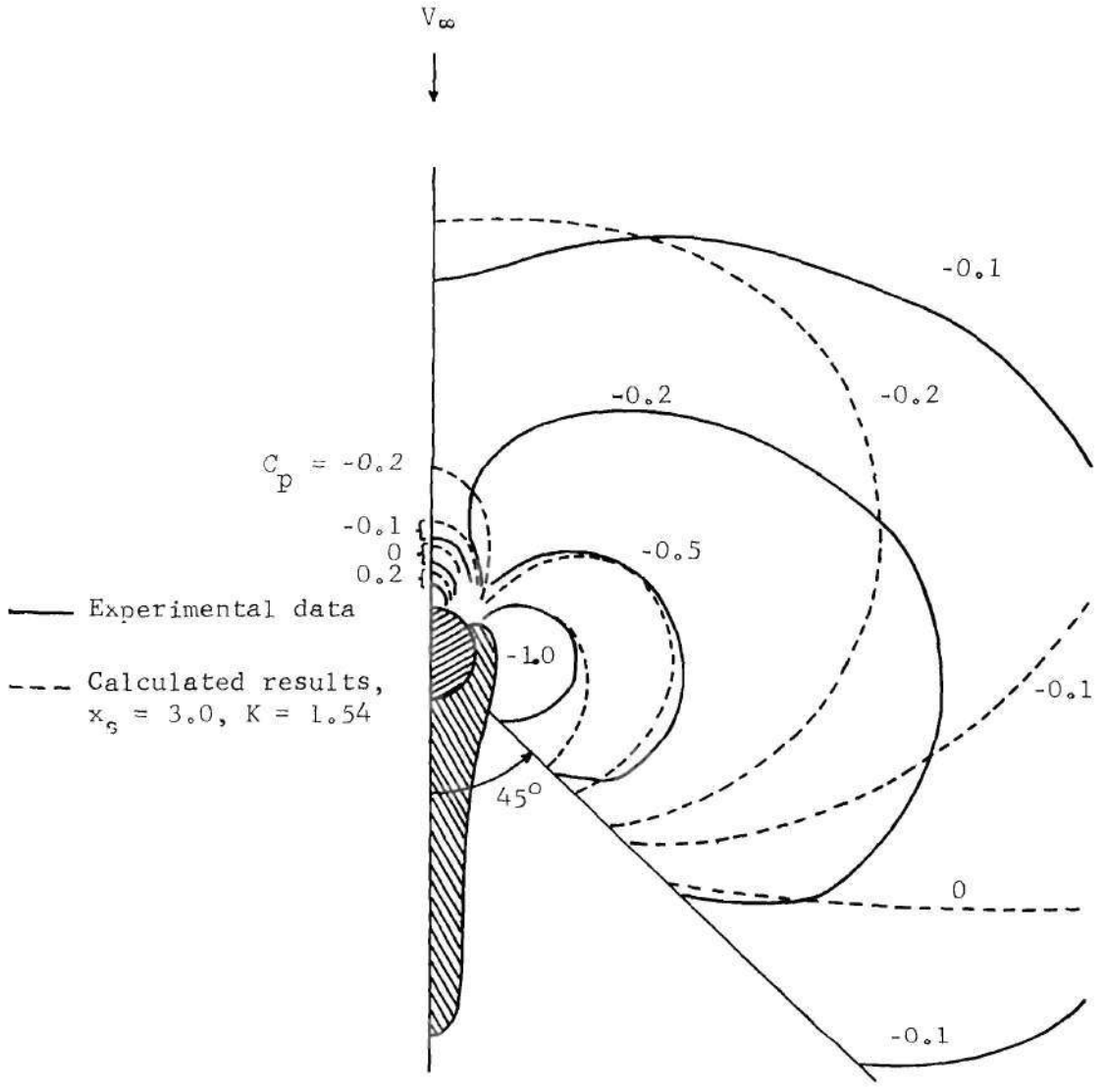

Figure 23. Plate Pressures for the Circular Exit, $V_j/V\infty = 8$

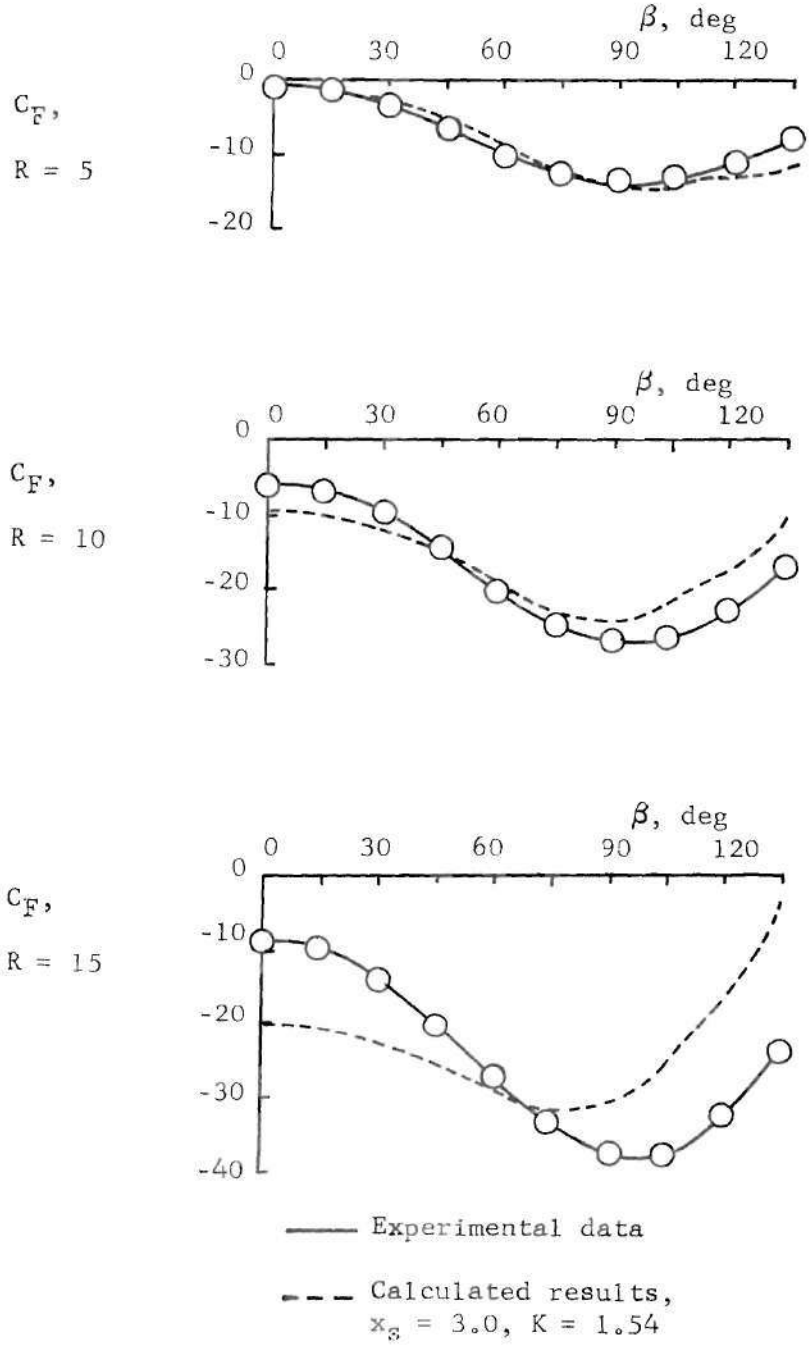

Figure 24. Force Distribution for the Circular Exit, $V_j/V_\infty = 8$

agreement resulting from the new model, but this is not considered serious since any two-dimensional model is expected to be somewhat in error in this region. Furthermore it is noted that the pressure coefficients are rather small in this region so that errors here will not greatly affect the integrated suction force. Comparing Figures 22 and 24 it is seen that a definite improvement in the C_F values, especially when $R = 5$, for $40 \leq \beta \leq 110$ degrees has resulted from the use of the new sink parameters. Therefore the new model is considered to be a better fit. This procedure is repeated using other sink parameters, and then other blockage elements, until a final "best fit" combination of parameters is selected. On the average fifteen candidate models were tried for each jet exit shape and speed ratio before the final best fit was chosen.

It is noted that the integrated suction force coefficient could be used as a means of quantitatively expressing the error. However, this integral over such a large area can conceal the presence of large regions of poor agreement if the pressures in these regions are such that some are excessively small and some are too large. Hence this criterion is not reliable unless it has already been determined that the pressure distribution is in reasonably good agreement.

It also should be noted that even the "best fit" models finally chosen will still produce plate pressures in some regions that do not agree very well with the experimental results. Primarily these regions are immediately upstream of the wake region and the area $r > 10$, $0 \leq \beta \leq 90$ degrees. However, the discrepancies in these regions are

not serious. They appear to be due primarily to the inability of the two-dimensional model to represent the three-dimensional effects of bending and deformation of the plume.

Final Forms of the Model

The constant plate pressure coefficient contours and the C_F curves resulting from the best fit models are shown in Figures 25-44 where the solid curves represent experimental data [49] and the dashed curves show calculated results of the model. The model parameters, afterbody shapes, and test speed ratios are noted on the figures. Comparing Figures 25, 27, and 29, the general effect of sink strength variation may be seen quite clearly, since the other parameters w_a, β_w, and x_s are the same for these cases. As sink strength (K) increases, the low pressure region reaches further to the side and forward. In the region far from the jet exit this effect is dominant and may be seen in all of the pressure contour figures. It is also quite apparent in the C_F curves for R = 15. The effect of the presence of the afterbody was previously shown to be a lateral and aftward spread of the low pressure region (Figures 14 and 15); this effect may also be seen in all of the C_p contour figures, although it is not quite so distinct because of the influence of other parameters. The effect of aftward movement of the sink position is also to decrease the pressure in the region $\beta > 90$ degrees, as seen by comparing Figures 41 and 43. In general the effect of the afterbody is seen more in the region aft of the afterbody-jet exit intersection and relatively near the jet exit, where the pressure decrease is greater with increasing afterbody width;

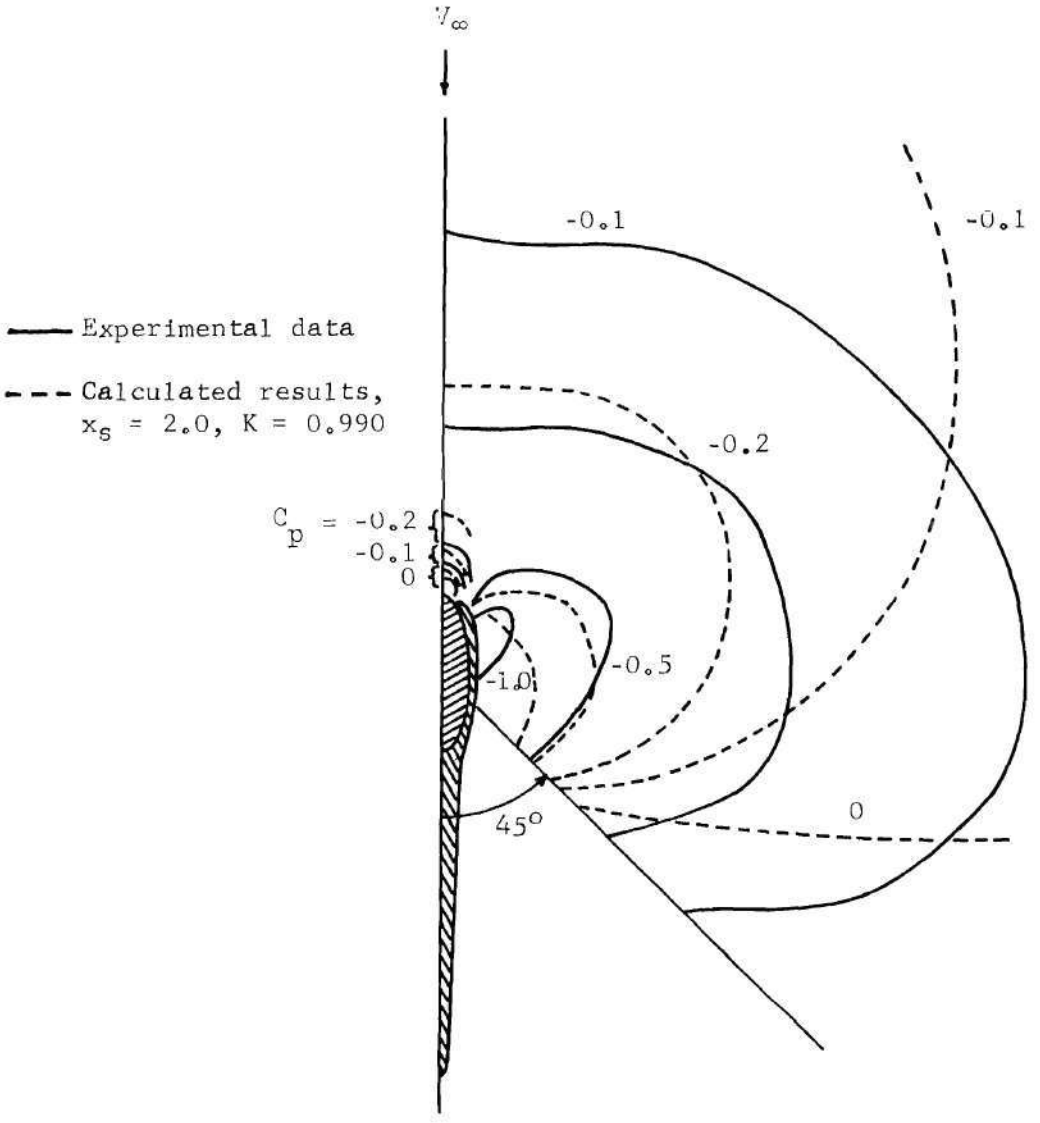

Figure 25. Plate Pressures for the Streamwise Exit, V_j/V_∞ = 8

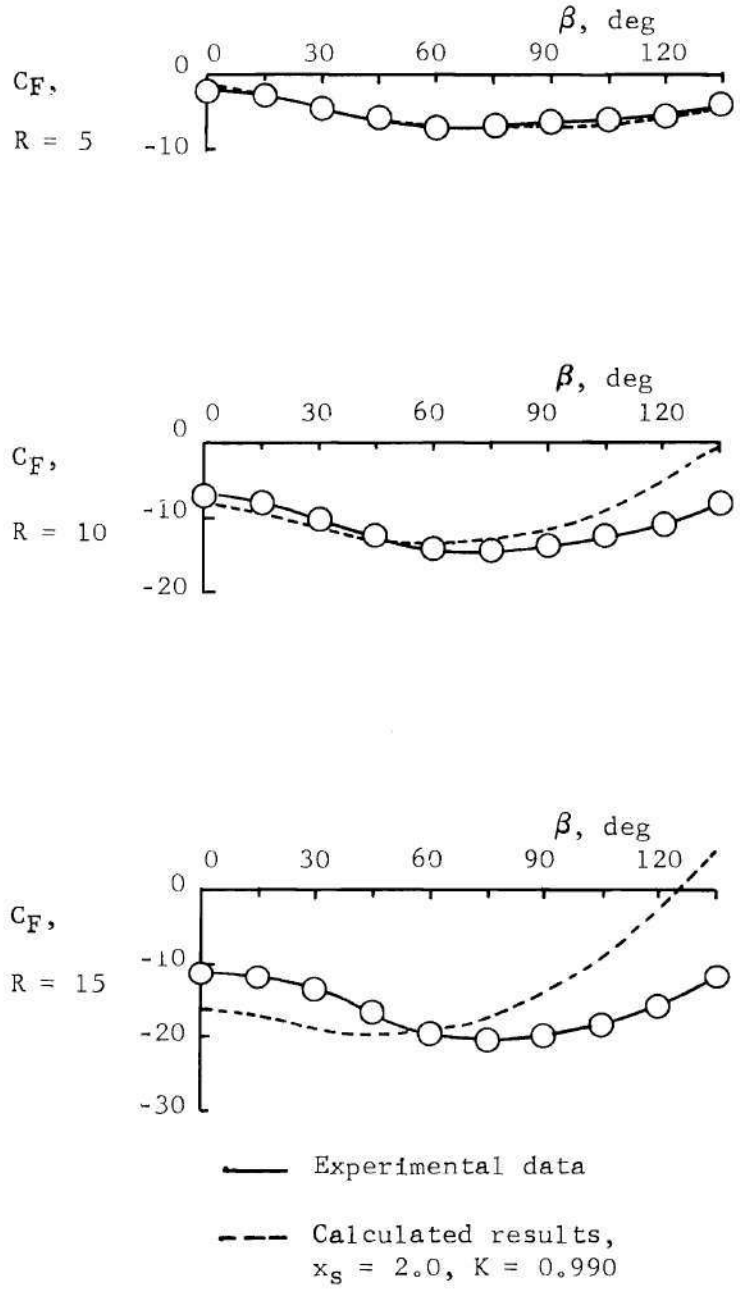

Figure 26. Force Distribution for the Streamwise Exit, $V_j/V_\infty = 8$

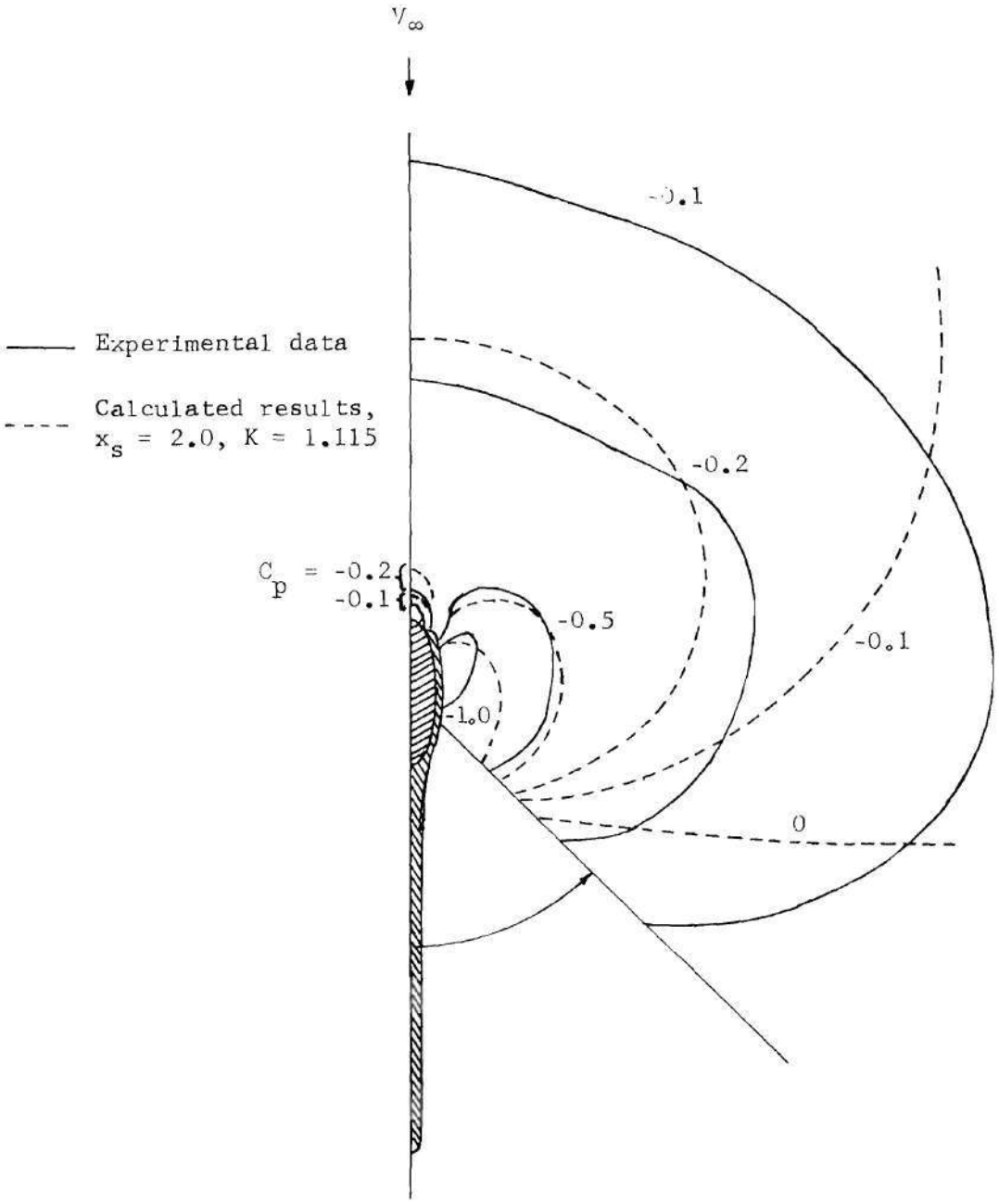

Figure 27. Plate Pressures for the Streamwise Exit, V_j/V_∞ = 10

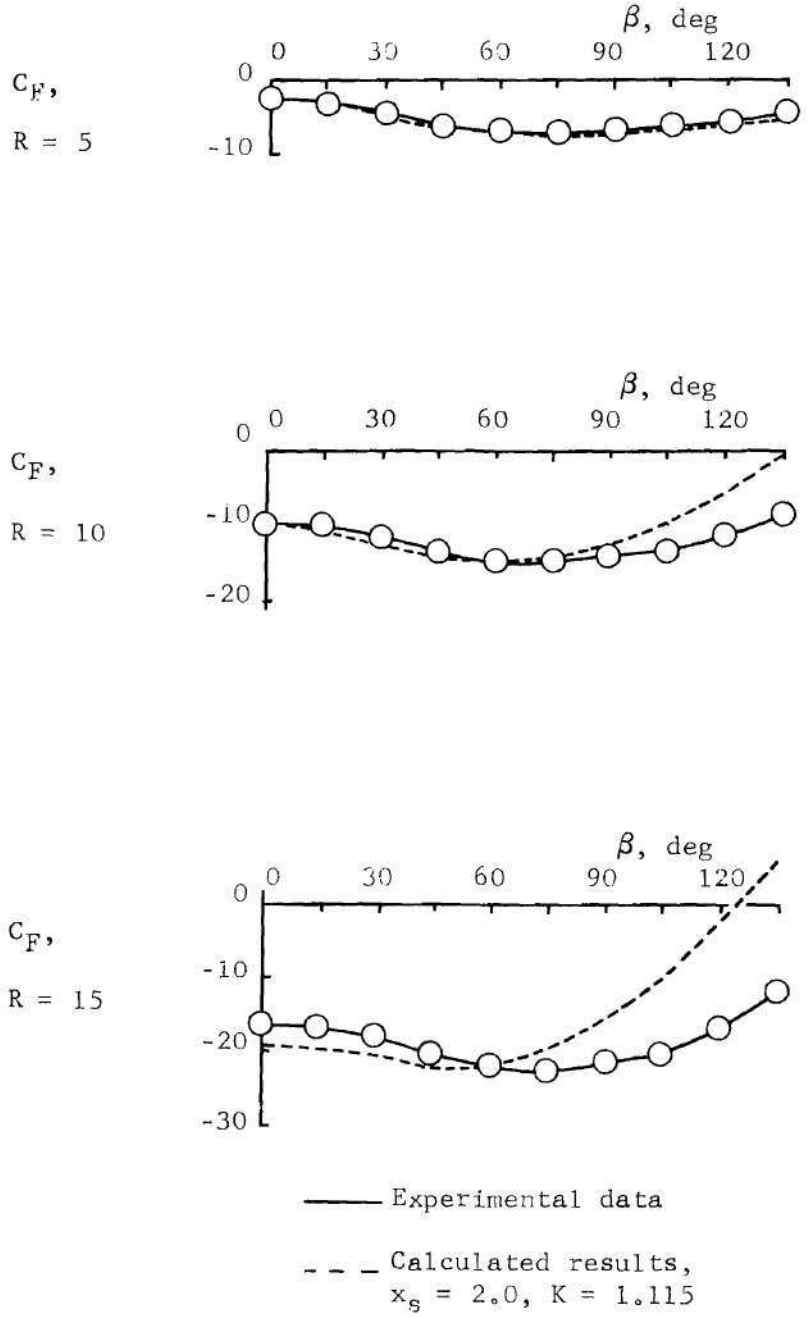

Figure 28. Force Distribution for the Streamwise Exit, V_j/V_∞ = 10

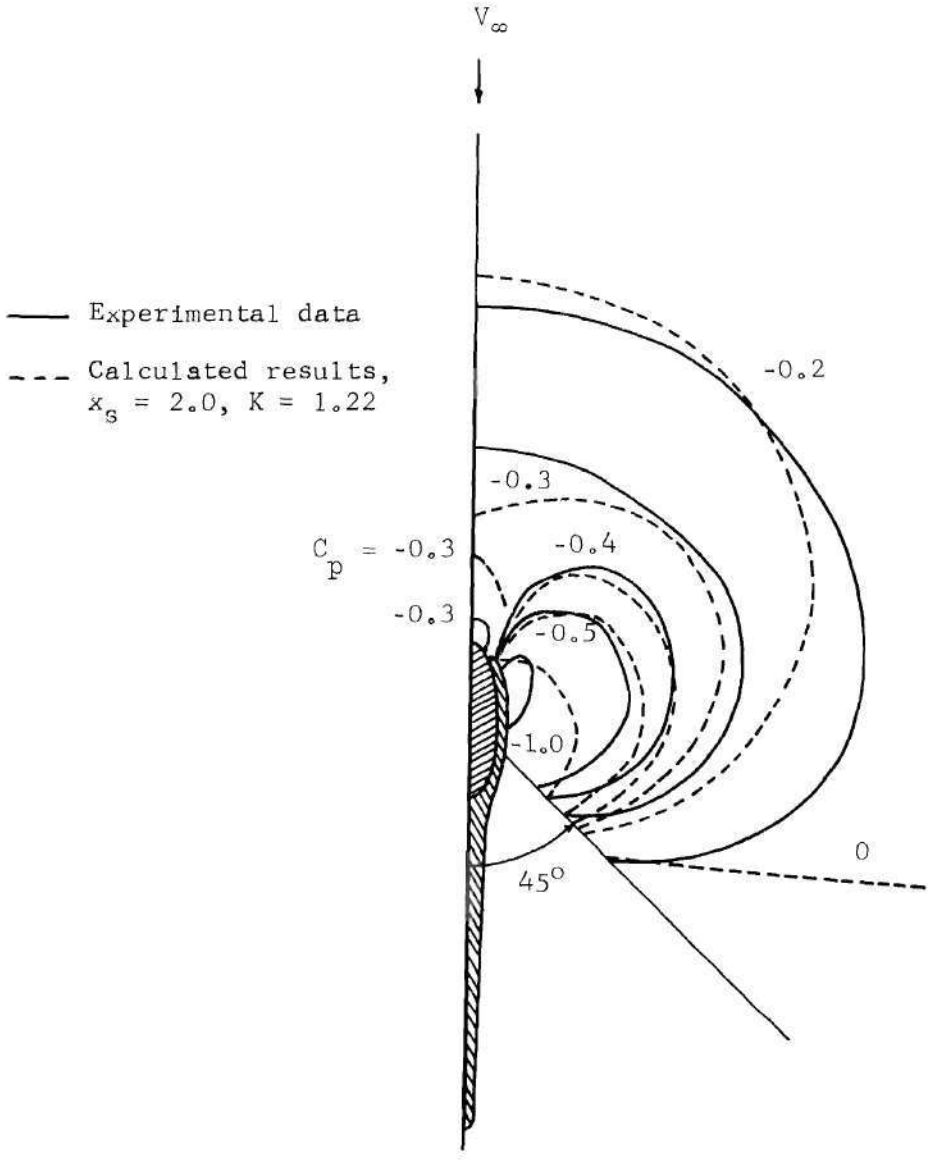

Figure 29. Plate Pressures for the Streamwise Exit, V_j/V_∞ = 12

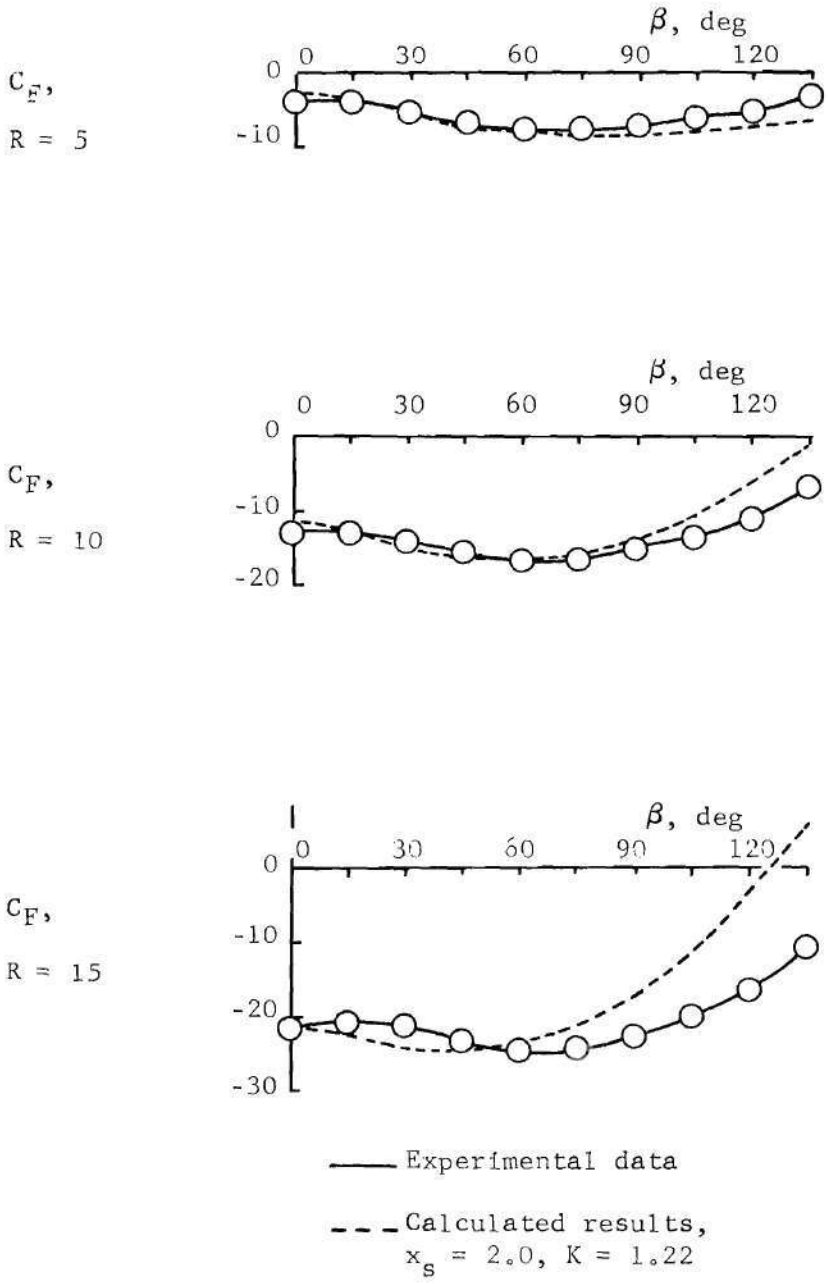

Figure 30. Force Distribution for the Streamwise Exit, V_j/V_∞ = 12

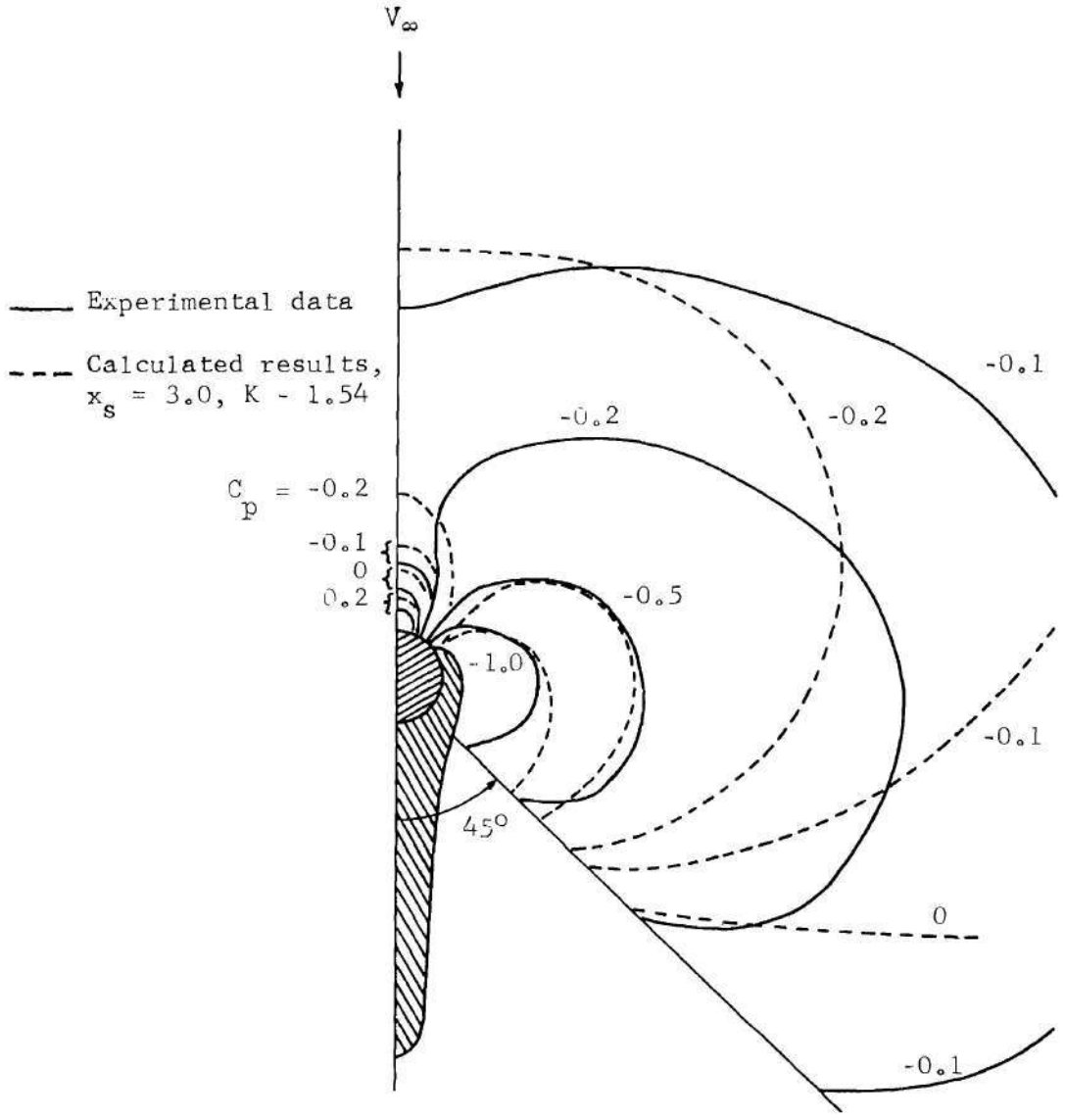

Figure 31. Plate Pressures for the Circular Exit, V_j/V_∞ = 8

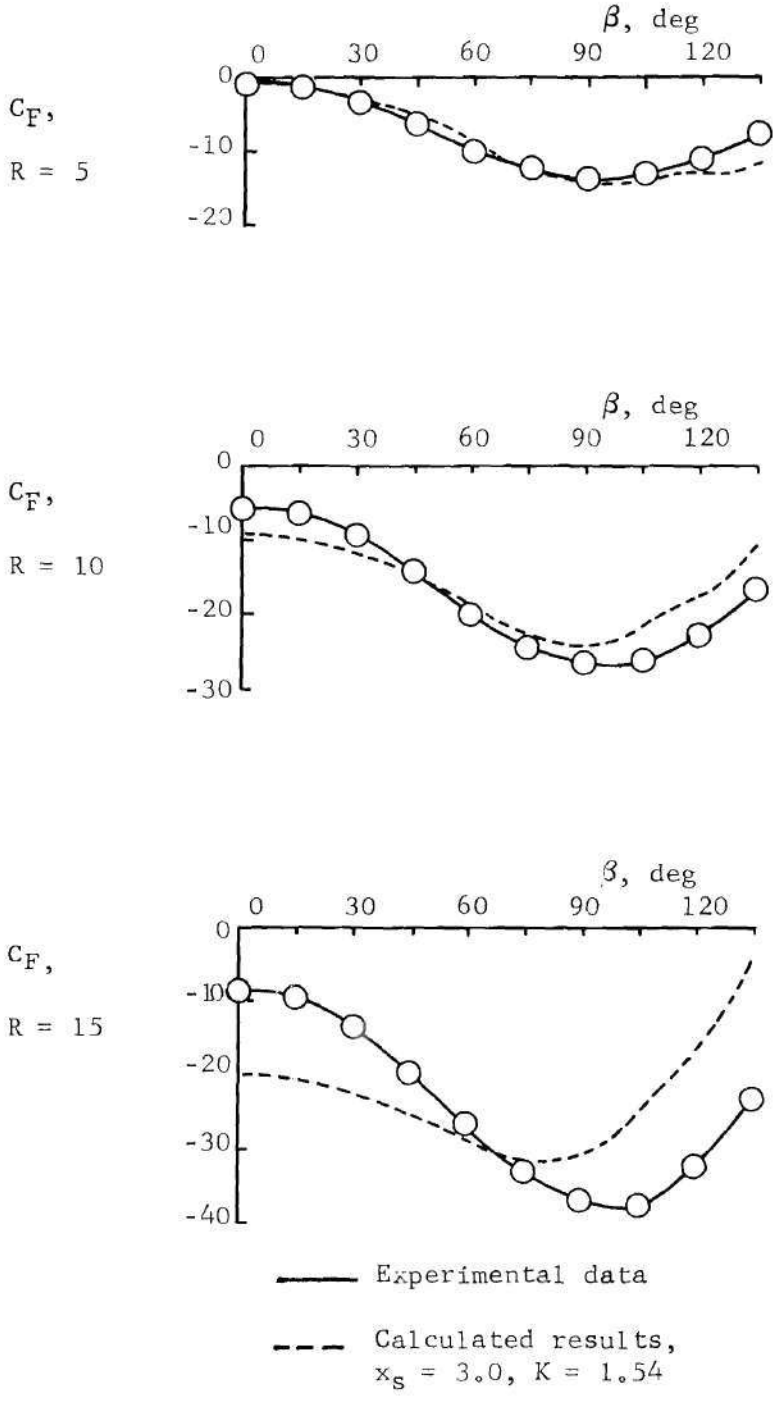

Figure 32. Force Distribution for the Circular Exit, $V_j/V_\infty = 8$

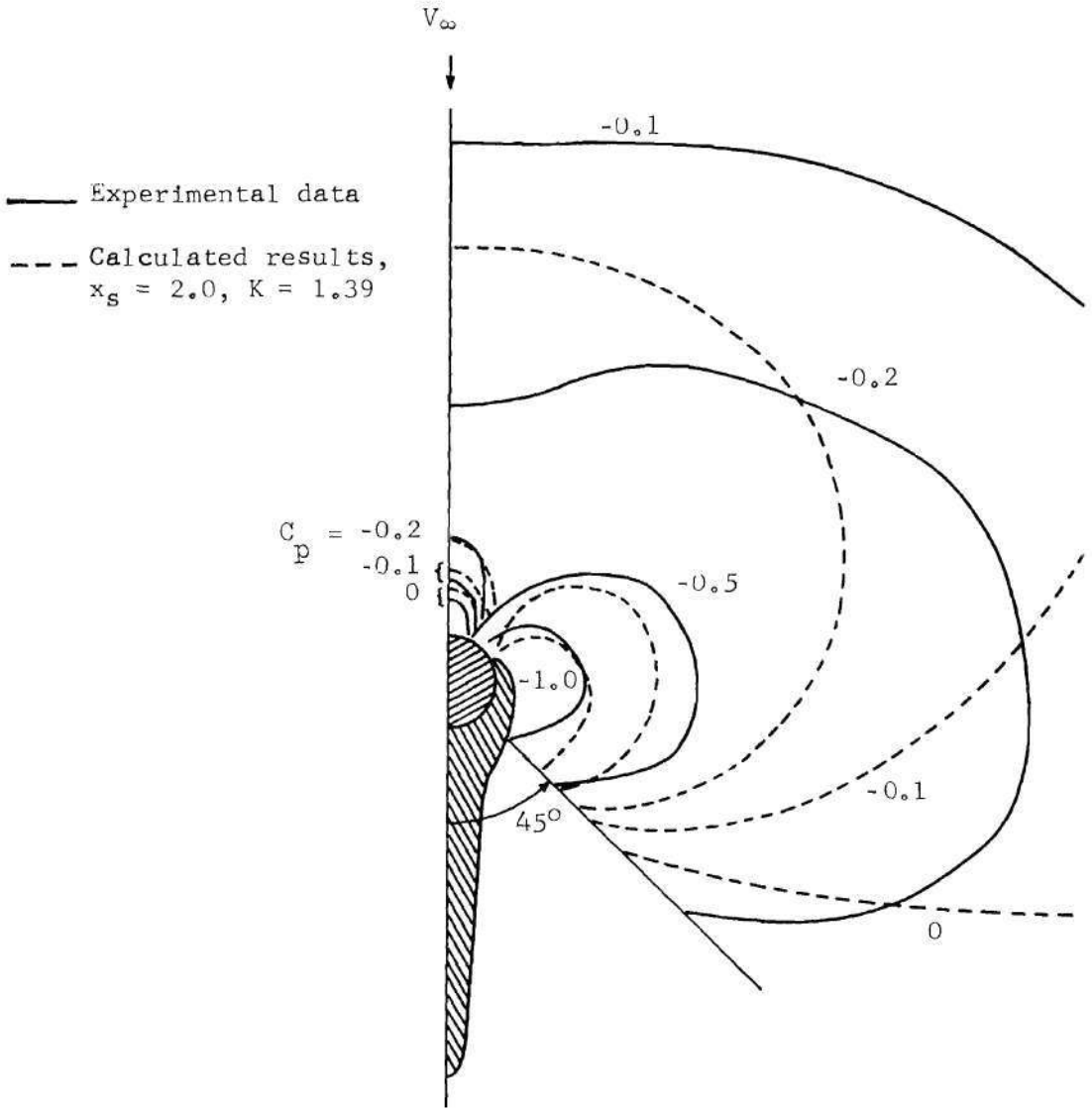

Figure 33. Plate Pressures for the Circular Exit, V_j/V_∞ = 10

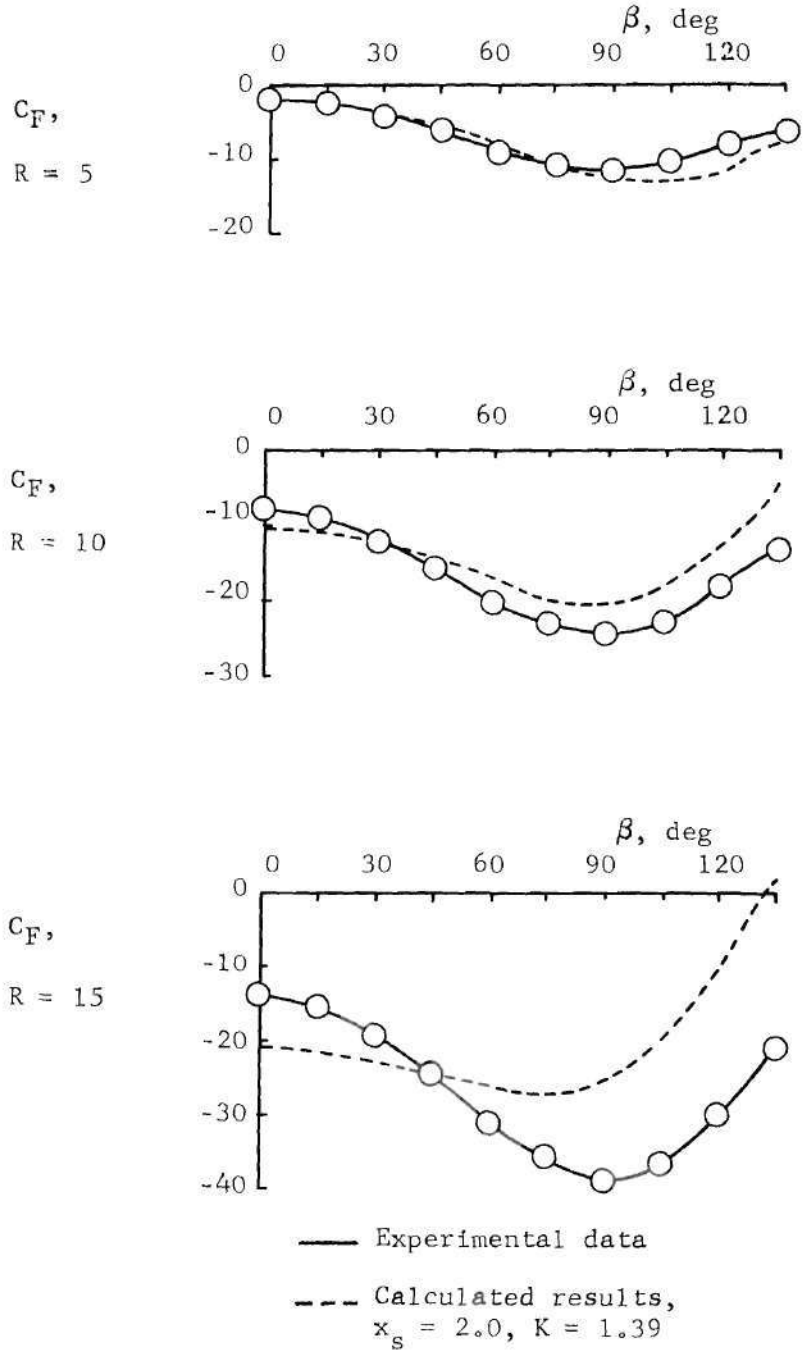

Figure 34. Force Distribution for the Circular Exit, $V_j/V_\infty = 10$

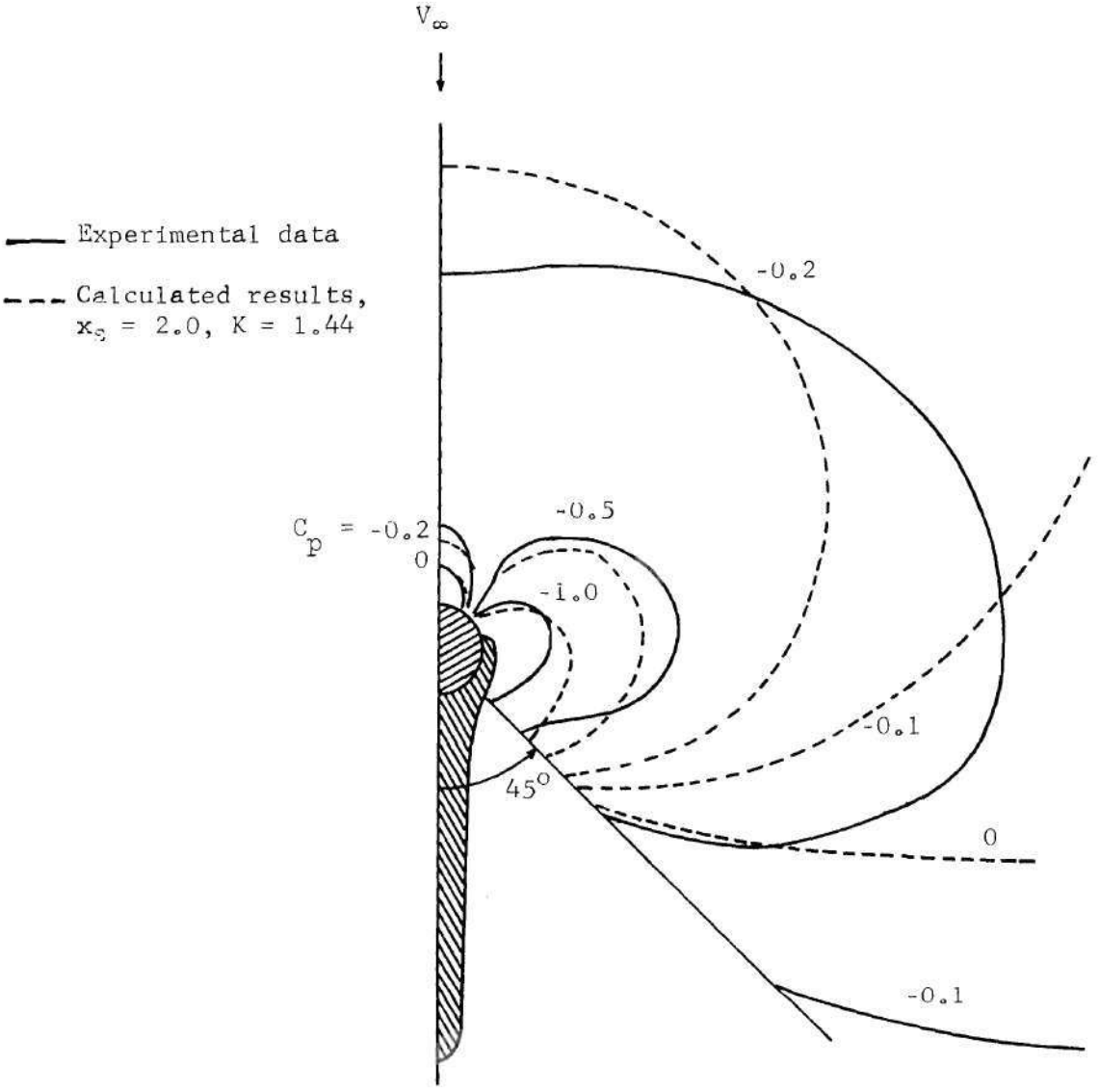

Figure 35. Plate Pressures for the Circular Exit, V_j/V_∞ = 12

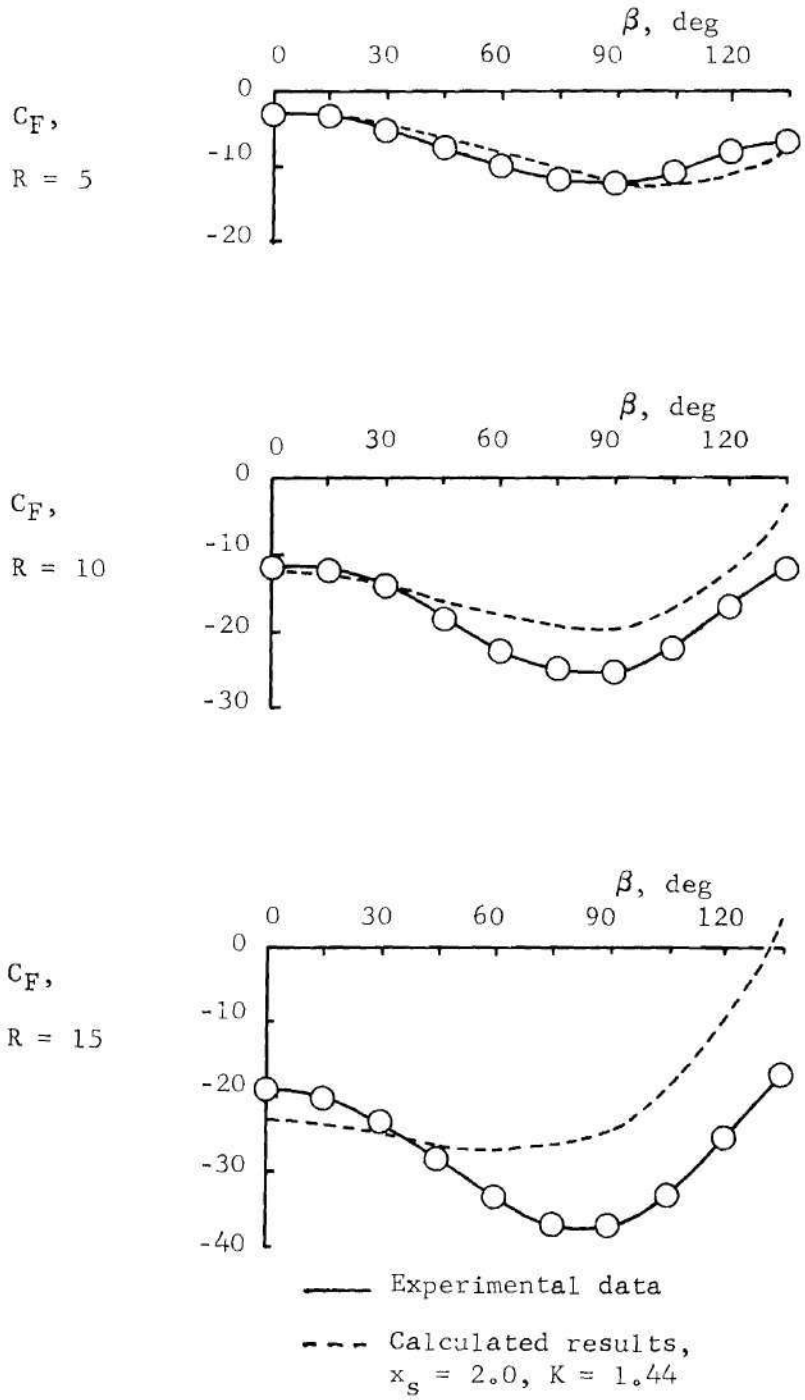

Figure 36. Force Distribution for the Circular Exit, V_j/V_∞ = 12

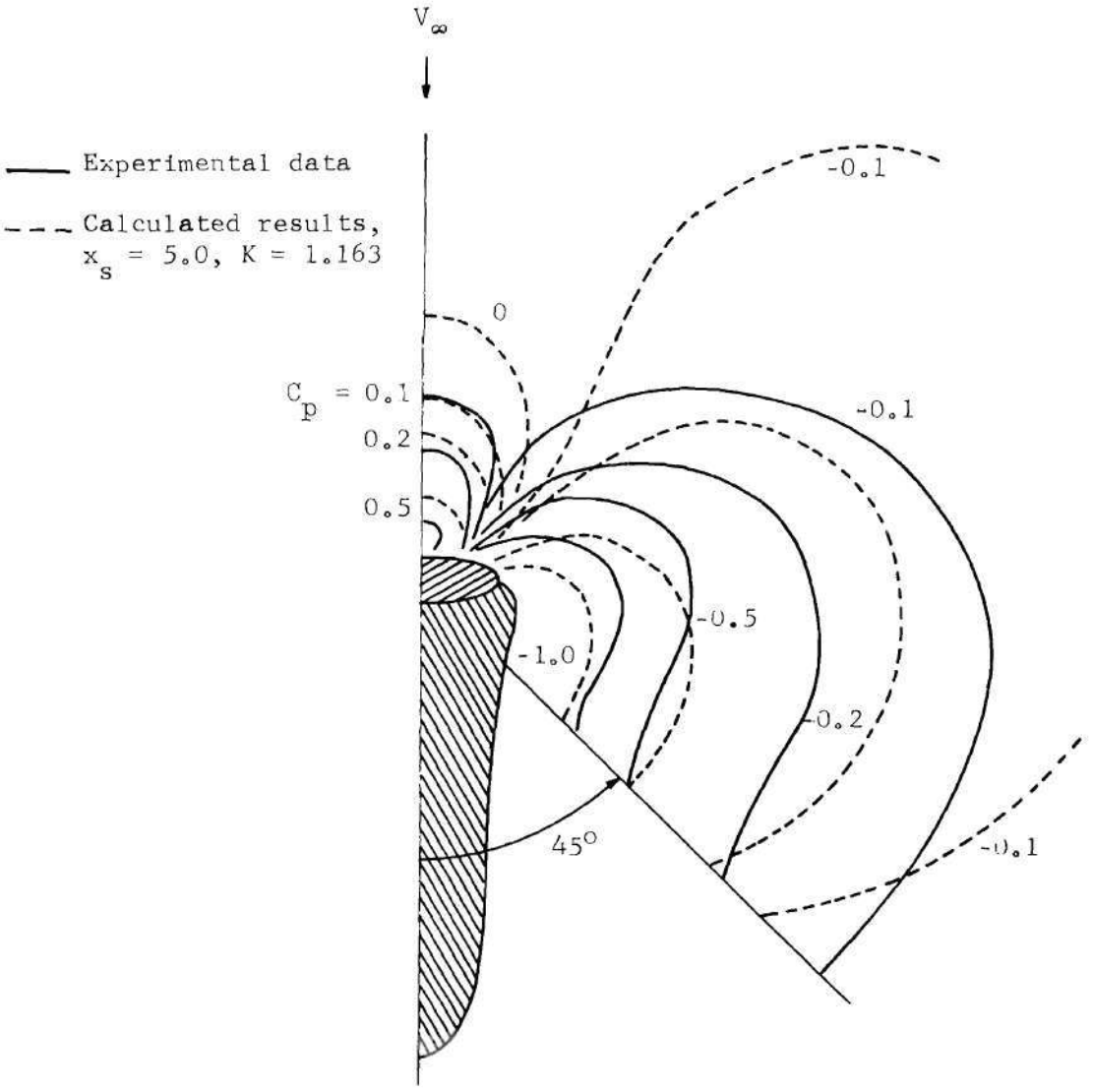

Figure 37. Plate Pressures for the Blunt Exit, V_j/V_∞ = 8

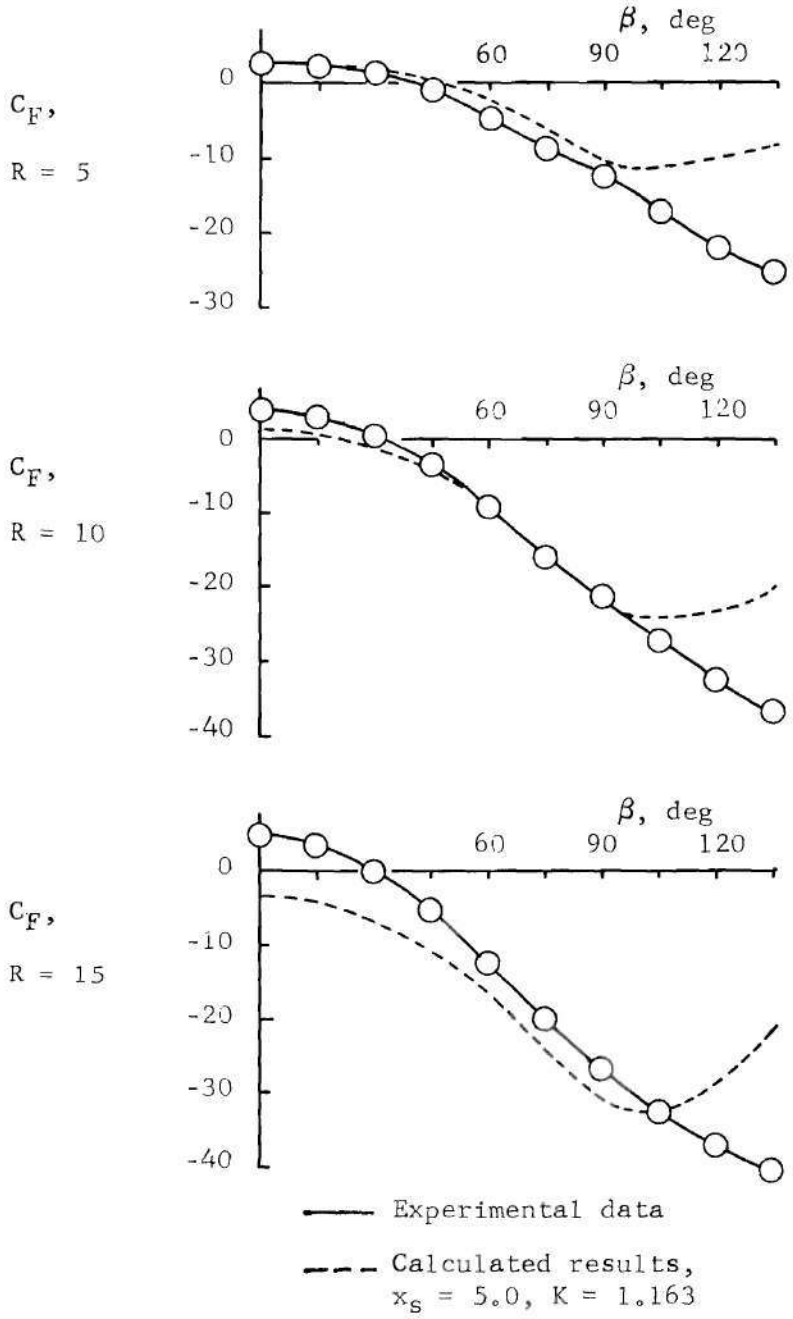

Figure 38. Force Distribution for the Blunt Exit, $V_j/V_\infty = 8$

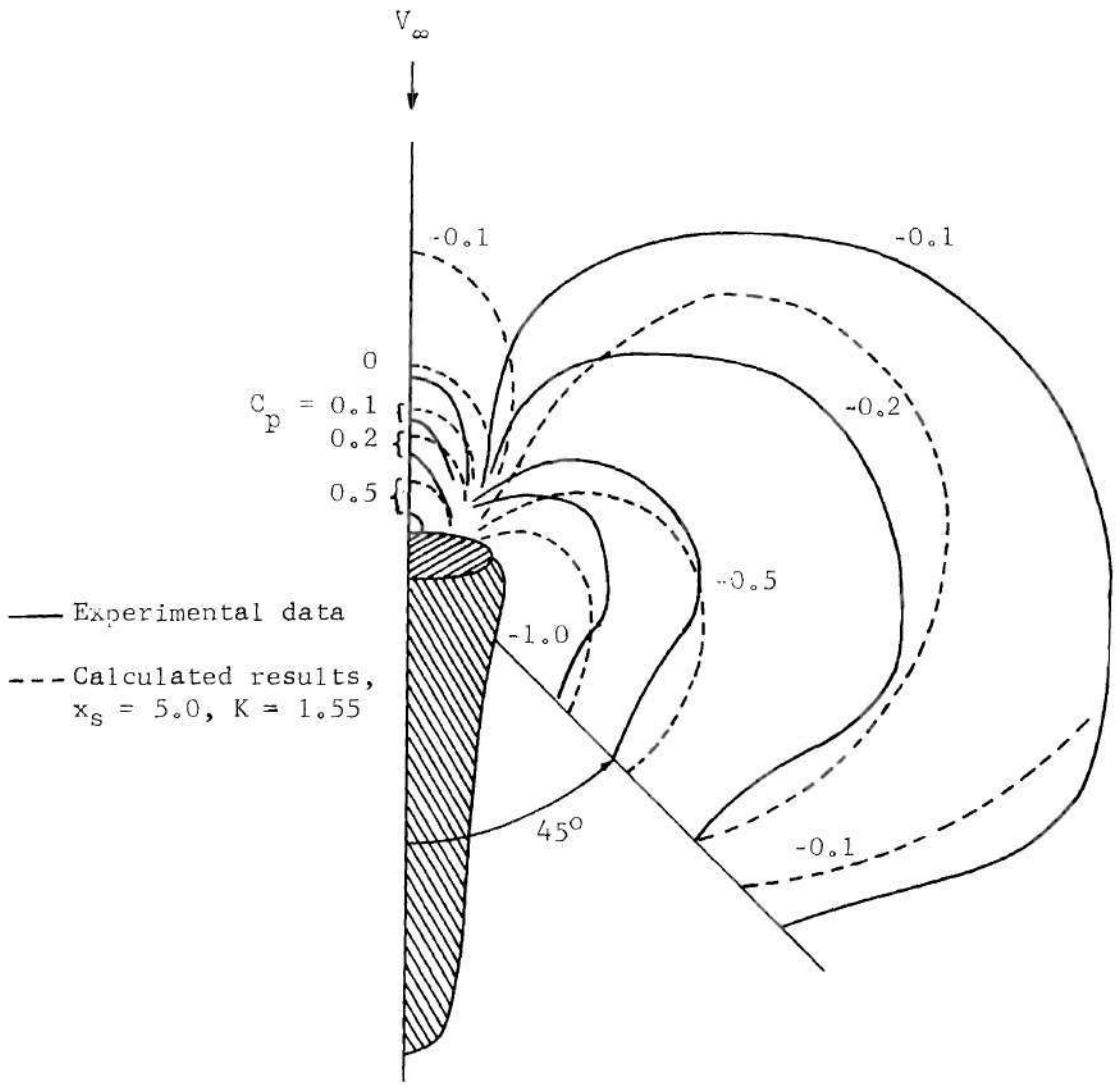

Figure 39. Plate Pressures for the Blunt Exit, V_j/V_∞ = 10

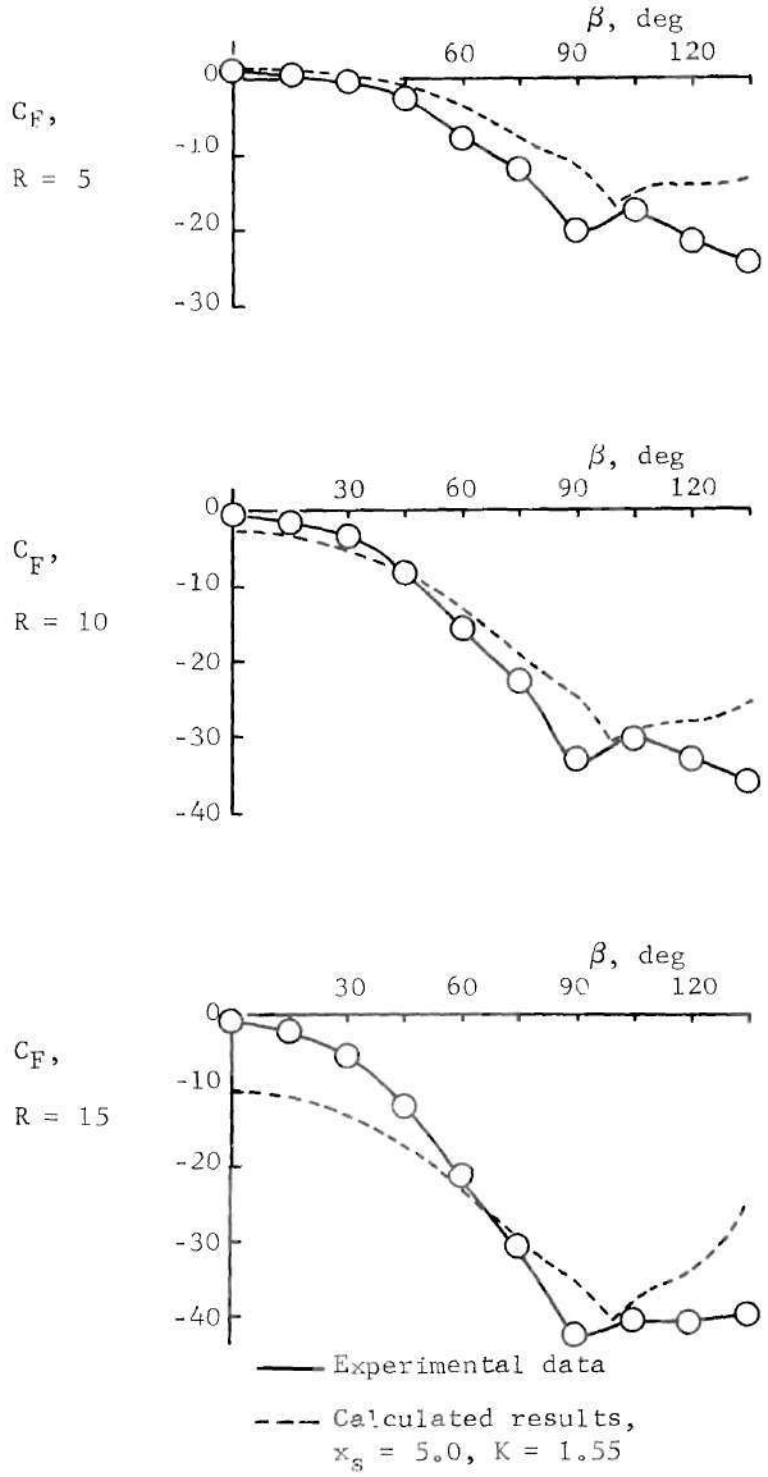

Figure 40. Force Distribution for the Blunt Exit, $V_j/V_\infty = 10$

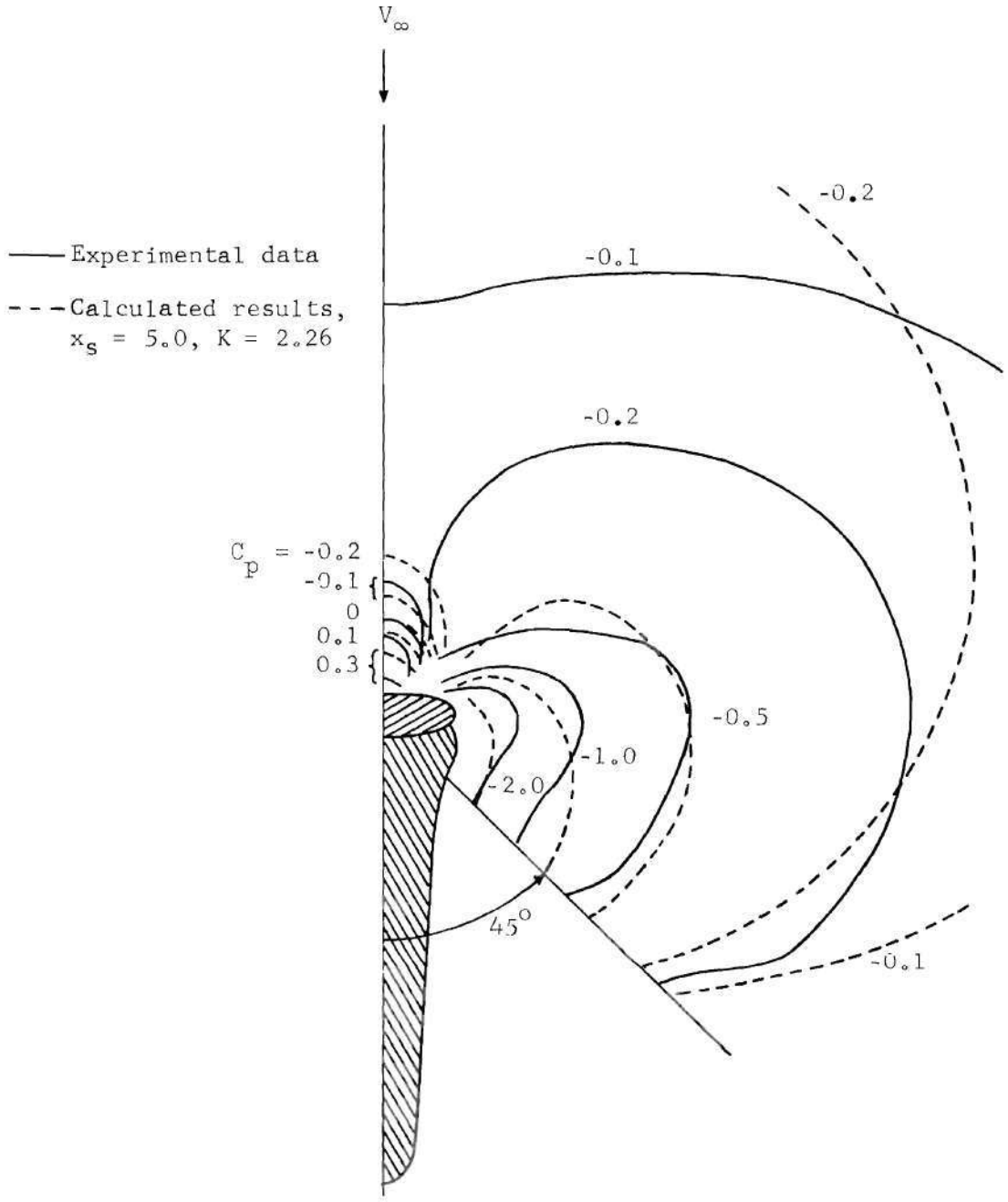

Figure 41. Plate Pressures for the Blunt Exit, V_j/V_∞ = 12

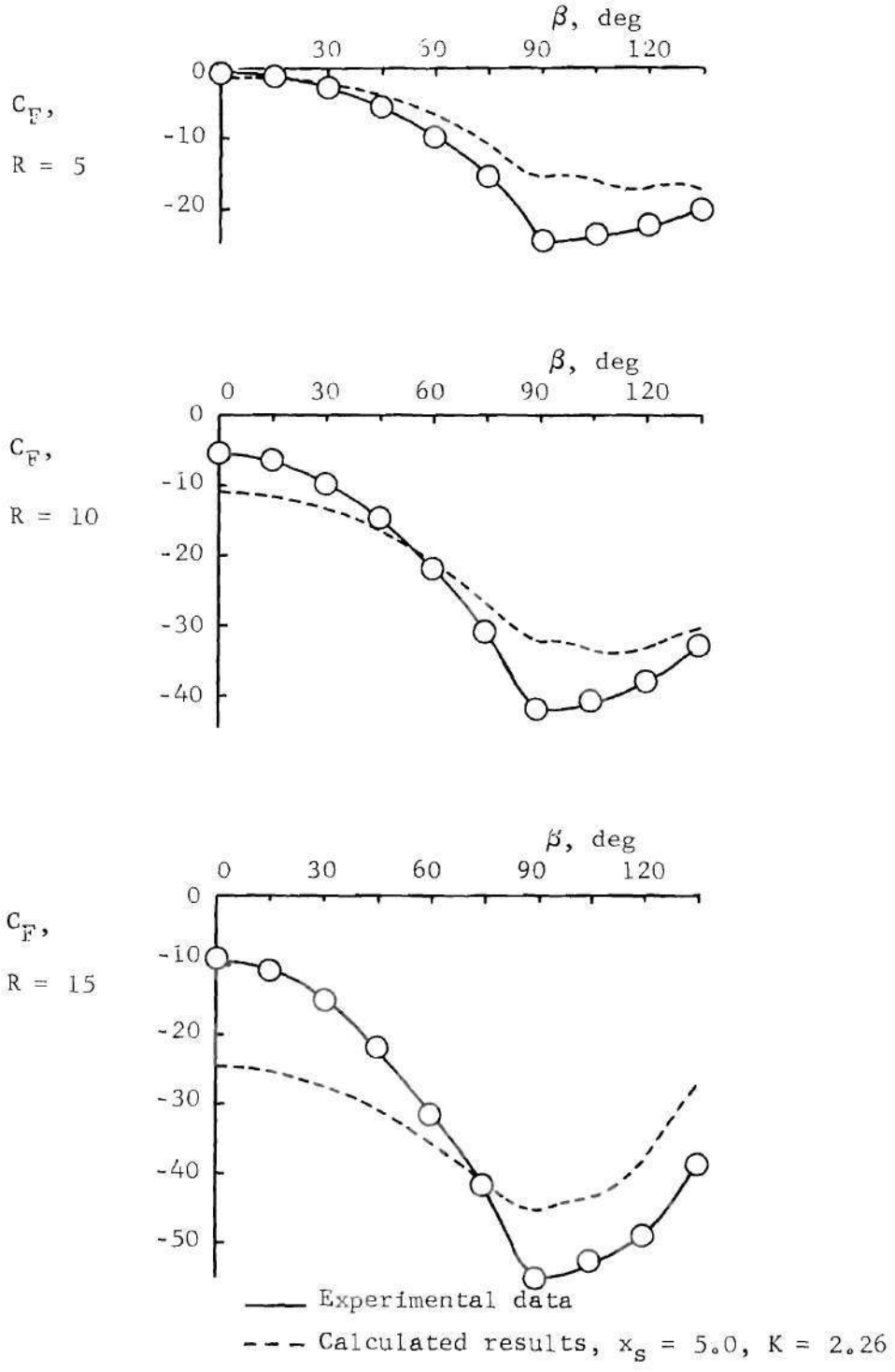

Figure 42. Force Distribution for the Blunt Exit, V_j/V_∞ = 12

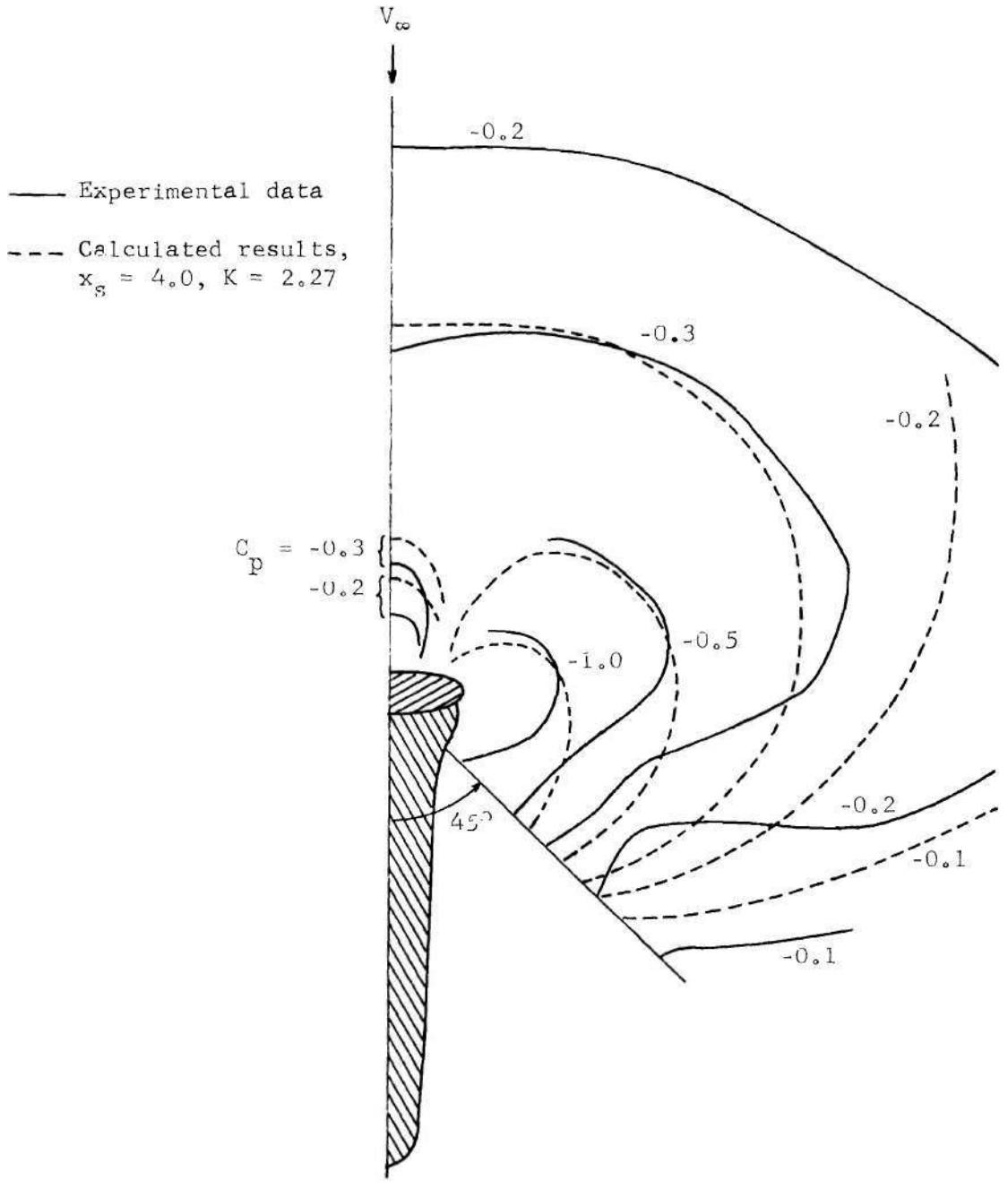

Figure 43. Plate Pressures for the Blunt Exit, V_j/V_∞ = 20

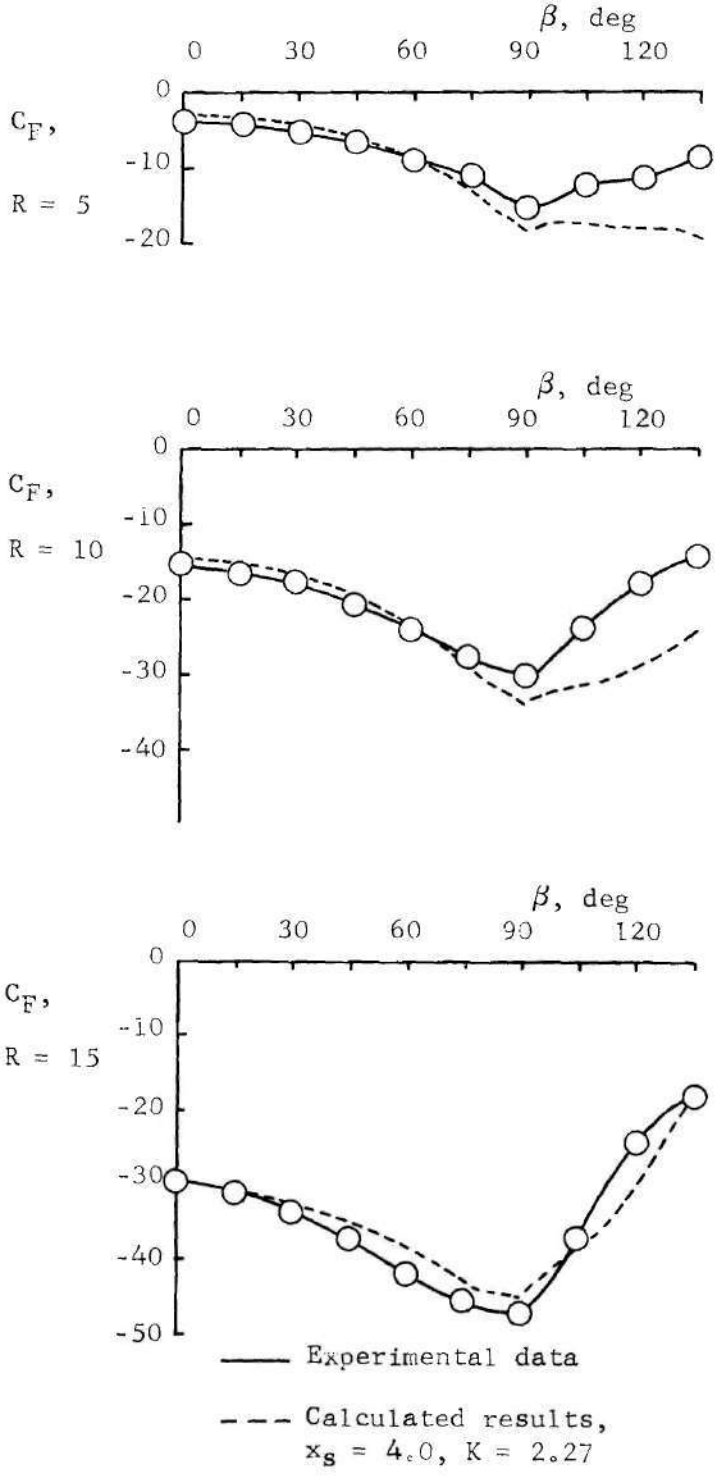

Figure 44. Force Distribution for the Blunt Exit, V_j/V_∞ = 20

and the pressure reduction due to moving the sink aftward is more apparent at larger distances from the jet exit. Again, these effects may also be seen by examining the C_F curves for the various values of R. The effect of the location of the afterbody-jet exit intersection is a slight rise in pressure near the jet exit and immediately upstream of the intersection point, and a decrease in pressure immediately downstream of that point. This may be seen by careful examination of each of the constant pressure contour figures. This effect is of course coupled with the afterbody width effect; i.e., if the afterbody-jet exit intersection is near or upstream of the point of maximum width of the jet exit a perturbation to the effective width of the jet exit results. For the streamwise and circular jet exit cases the afterbody width is fairly small so that the effect of the intersection point appears to be small and quite local and is therefore not readily apparent in the force distribution curves. However, for the blunt jet exit cases where the afterbody width is relatively large the effect on the force distribution curve is observed as a slight "hump" in the theoretical curve in the vicinity of $\beta = \beta_w$ and the minimum of the curve may shift aftward from $\beta = 90$ degrees. (See Figures 38, 40, and 42.) It is seen that in all cases the calculated force distribution for R = 5 deviates from the experimental results somewhere in the region $\beta > 90$ degrees; this deviation becomes progressively more severe going from streamwise to circular to blunt jet exits. There are two reasons for this result: (1) One reason is that the wake becomes larger in the sense that the region of large total pressure loss becomes larger with increasing thickness ratio; even with a good choice

of afterbodies it becomes more difficult to represent the effects of the wake with the steady potential model. (2) The deviation is accentuated by the restricted limits of integration in the afterbody models. The lower limit of integration must be the boundary of the afterbody. With increasing thickness ratio a wider afterbody is used, and hence the area of integration is reduced. The experimental data were obtained by considering the lower limit of integration to be th jet exit. Therefore, the wider the afterbody is, the worse the comparison appears.

The values of the parameters K, x_s, w_a, and β_w used in the best fit models are shown in Figures 45-48 as functions of jet exit thickness ratio w/ℓ and speed ratio V_j/V_∞. Figure 45 shows the variation of K with these variables. It is seen that the entrainment rate is greater for a jet-in-crosswind than for a free jet. The entrainment rate for the streamwise jet increases with speed ratio, but at a slightly slower rate than the equivalent free jet K. Figure 46a shows that as speed ratio increases the effective sink location moves upstream slightly. Figure 46b shows that, relative to the aftmost point of the jet exit, the sink position moves aft with increasing bluffness of the jet exit. Figures 47 and 48 show the decreasing width of the Rankine oval and the aftward movement of the afterbody-jet exit intersection, respectively, with increasing speed ratio.

Using these curves and interpolating, appropriate model parameters may be chosen to predict plate pressures for cases of other jet exit configurations and speed ratios. However, interpolation for the parameter K is very difficult. As an aid to interpolation a different

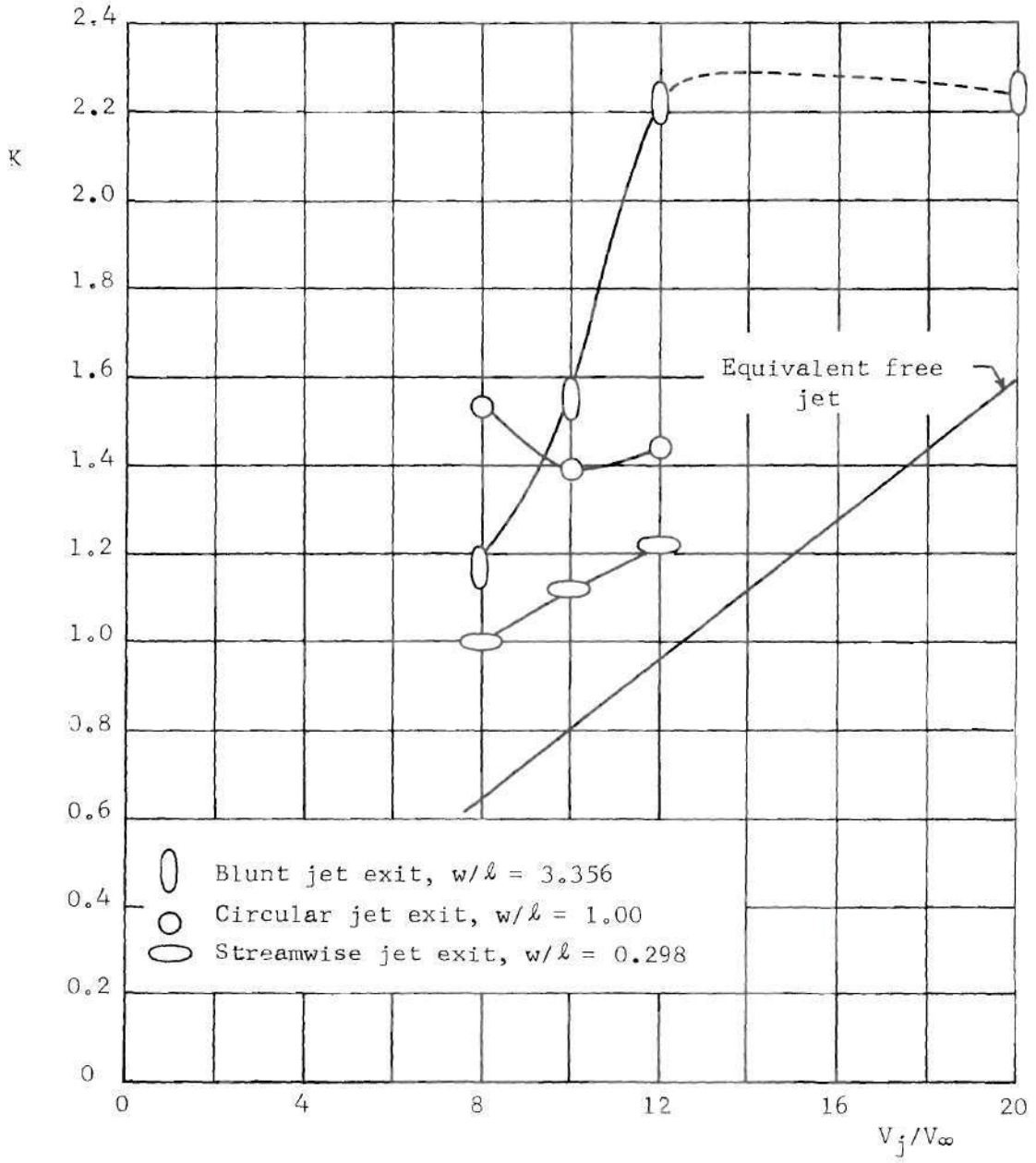

Figure 45. Dimensionless Entrainment Parameter as a Function of Speed Ratio and Thickness Ratio

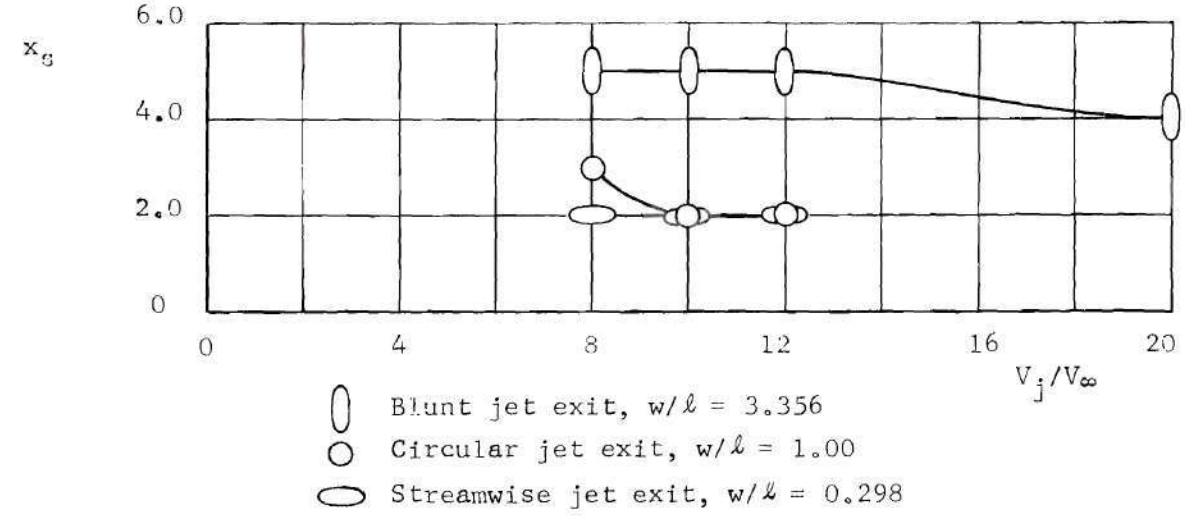

(a) Actual Sink Location

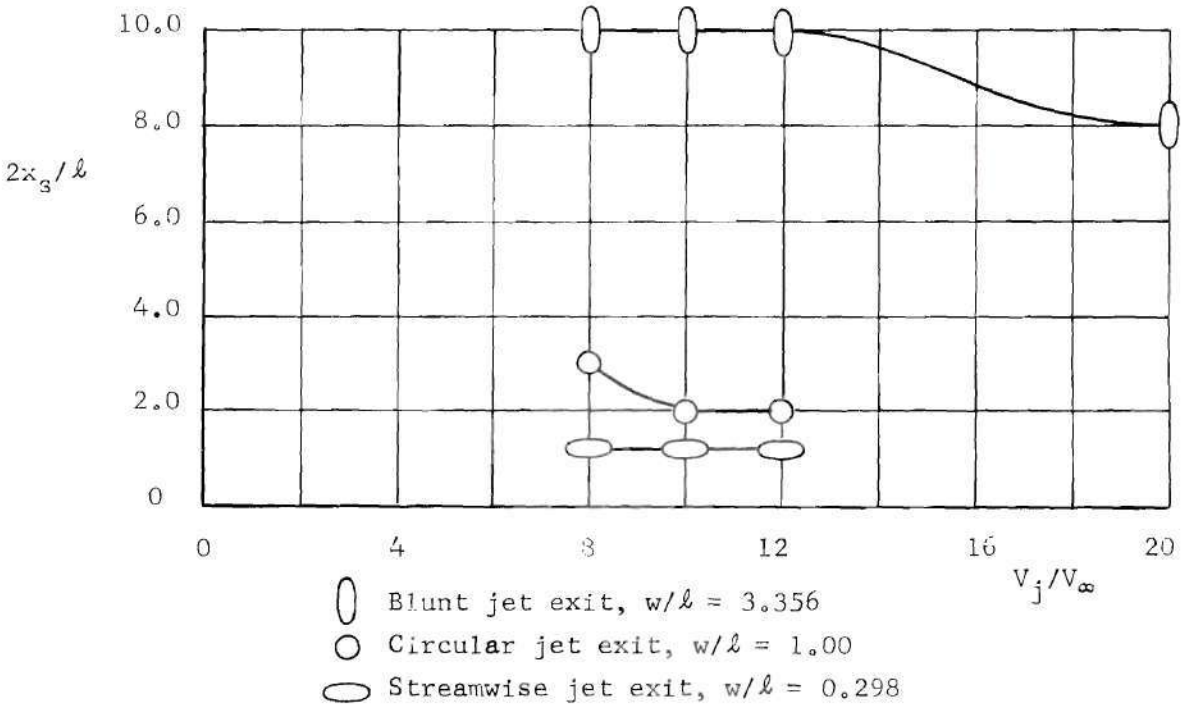

(b) Sink Location Non-Dimensionalized by Exit Half-Length

Figure 46. Sink Location as a Function of Speed Ratio and Thickness Ratio

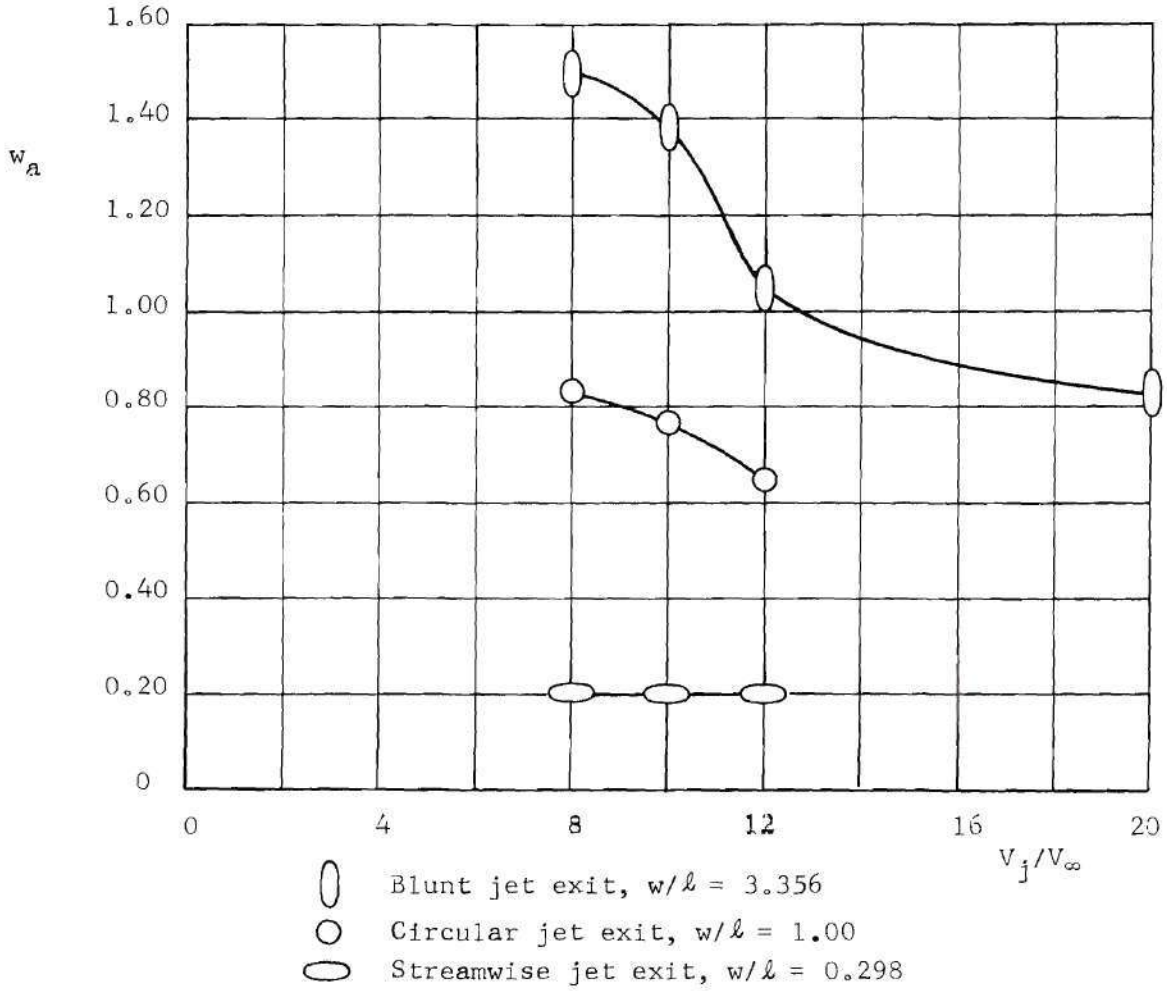

Figure 47. Rankine Oval Half-Width as a Runction of Speed Ratio and Thickness Ratio

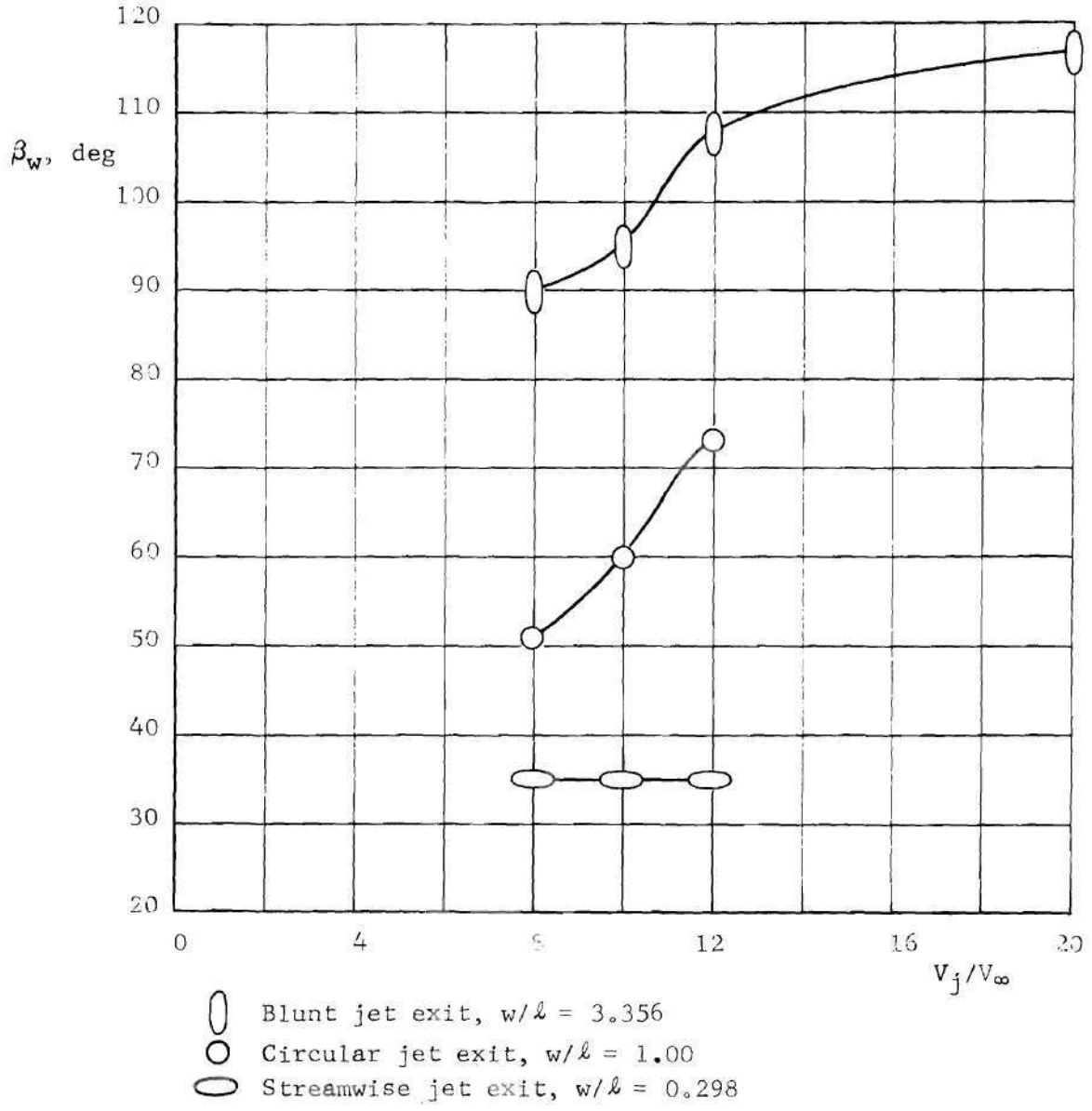

Figure 48. Afterbody Parameter β_w as a Function of Speed Ratio and Thickness Ratio

entrainment parameter E, defined by

$$E = \frac{\mathcal{E}}{\rho V_j \ell} = K \frac{V_\infty}{V_j} \frac{2\pi a_e}{\ell} \quad , \tag{39}$$

where $\mathcal{E}$ is the mass entrained per unit length of jet per unit time, may be plotted against

$$F = (V_j/V_\infty)^{2(\ell/w)^{1/3}} \tag{40}$$

to form a single smooth curve, as shown in Figure 49. This curve does represent a general behavior of entrainment rate; it should be used only for speed ratios within the range of $8 \leqq V_j/V_\infty \leqq 20$. For a given thickness ratio w/ℓ the applicable range of F must be calculated according to this constraint. For instance, suppose plate pressures were desired for the case of a blunt elliptical jet exit with A = 1.414 and B = 0.707, so that the thickness ratio is $w/\ell = 2$. The appropriate range of F is $27 \leqq F \leqq 116$. If the speed ratio under consideration is $V_j/V_\infty = 11$, F = 44.8 and E = 0.82. Hence K = 2.03. From Figures 46-48 it is seen that $x_s \cong 4.0$, $w_a \cong 0.985$, and $\beta_w \cong 90$ degrees would be good choices for the other parameters of the model. Using these values the model should yield a good prediction of the plate pressures.

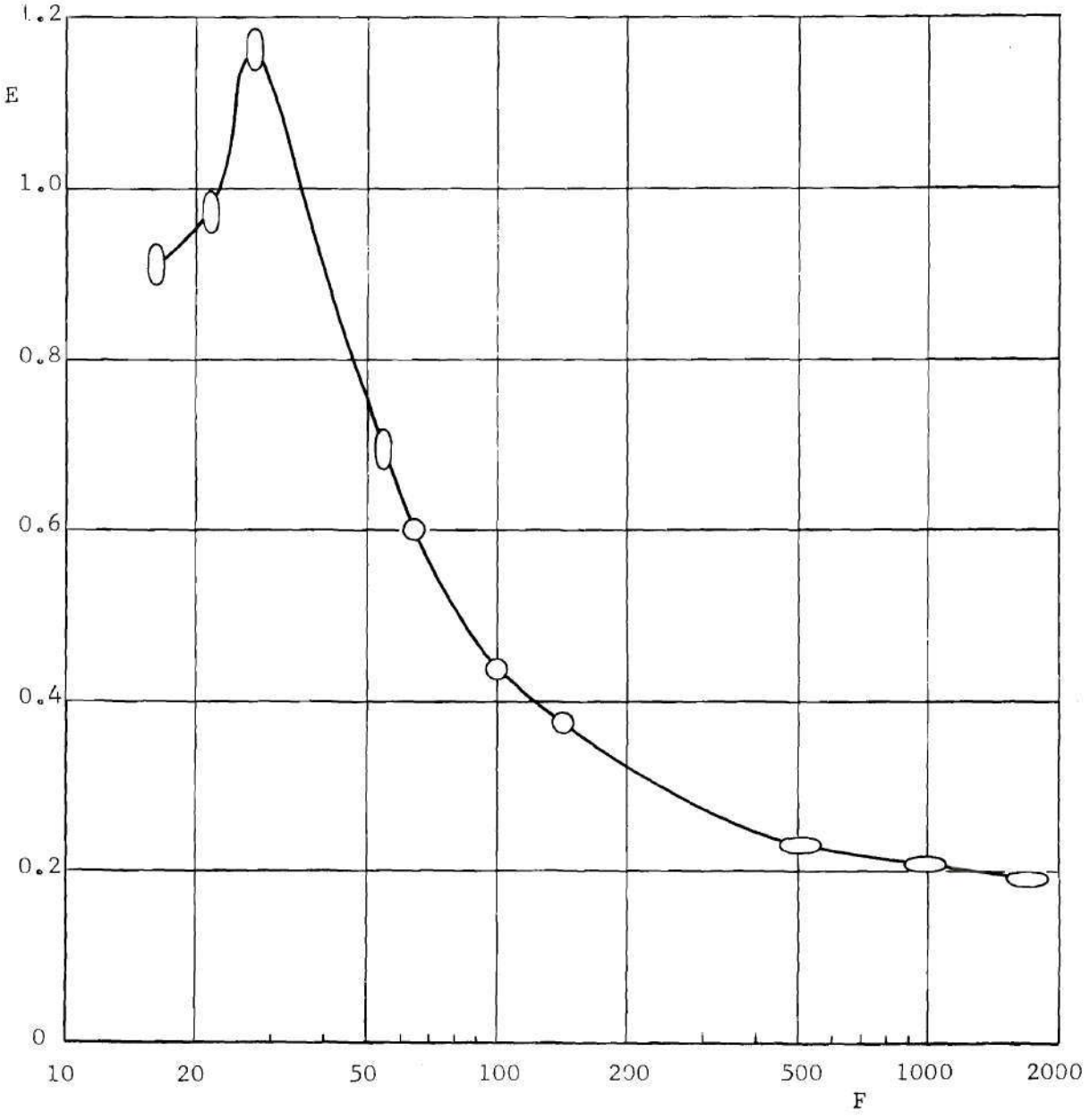

Figure 49. Entrainment Function for Interpolation

CHAPTER III

PARAMETRIC STUDY

Having determined that the blockage-sink models with afterbodies provide reasonably good representation of the plate pressures, it is of interest to examine the effects of varying the afterbody and sink parameters in a controlled quantitative manner to observe their effects. It has already been shown that the parameter ℓ_a, the half-length of the Rankine oval, is unimportant relative to the half-width of the oval, w_a. For a given jet exit configuration the remaining parameters are K, x_s, and β_w.

The values of these parameters resulting in best agreement with the experimental data were determined as discussed in Chapter II. In order to examine the effects of these parameters in a quantitative manner, the "best fit" values for each of the exit configurations at $V_j/V_\infty = 12$ are chosen as reference values, as shown in Table 4. K was varied in increments of 10 percent of K_o over a range of ± 20 percent of K_o for each configuration. The effective sink location was varied over the range $0 \leqq x_s \leqq 4.0$ for the circular and streamwise configurations and over a range $0 \leqq x_s \leqq 7.0$ for the blunt configuration. Plus and minus 10 percent w_{a_o} variations were used for all configurations; and β_w was varied in 10 degree increments to plus and minus 20 degrees from β_{w_o}.

For each jet exit and each set of parameters K, x_s, w_a, and β_w

the plate pressures are calculated and used to find the force distribution coefficient C_F and the integrated interference force coefficient C_s with the upper limits of integration R = 5, 10, and 15, and β_o = 135 degrees (neglecting the wake region). The values of C_s thus obtained are compared to the corresponding values of C_s for the best fit cases and presented in terms of

$$\frac{\Delta C_s}{C_{s_o}} = \frac{|C_s| - |C_{s_o}|}{C_{s_o}} \tag{41}$$

where C_{s_o} is the integrated interference force coefficient calculated with the best fit model. $\Delta C_s / C_{s_o} < 0$ represents a reduction in the suction force.

Table 4. Reference Values of the Parameters

Configuration	K_o	x_{s_o}	w_{a_o}	β_{w_o}	C_{s_o}		
					R = 5	10	15
Streamwise	1.22	2.0	0.20	35°	-15.1	-27.2	-37.7
Circular	1.44	2.0	0.64	73°	-19.6	-36.2	-50.6
Blunt	2.22	5.0	1.05	108°	-22.1	-54.2	-81.1

For the circular jet exit case the effects of entrainment rate and sink position are shown in Figure 50 in terms of the integrated interference force coefficient. Clearly these factors have a very strong influence. Ten percent variations of the dimensionless sink strength K result in approximately 10 percent changes in the suction force, so that as entrainment increases, so does the suction force. Near the jet exit (R = 5) an aftward movement of the sink location from the center of the exit results in first a significant rise in the suction force, a maximum, and then a reduction. However, when the upper limit of integration is R = 10 or 15, increasing suction force with aftward movement of the sink appears to be a general trend. This is because the induced velocities due to a sink are inversely proportional to the distance between the point in the flow field and the sink, while the blockage-induced velocities are inversely proportional to the square of the distance. Thus the sink influences significantly a larger portion of the flow field than the blockage does. As a sink of constant strength is moved aftward, it significantly reduces the plate pressures far from the jet exit and to the side and rear of the exit. Near the exit the coupled effects of the blockage and sink are important, as shown by the force distribution coefficient curves in Figure 51. When a sink of a given strength is at the center of the jet exit, it tends to overpower the blockage effect immediately upstream, greatly reducing the plate pressure. At β = 90 degrees the velocity induced by the sink is normal to that resulting from the blockage in the uniform stream, so that the total velocity is not a great deal larger in

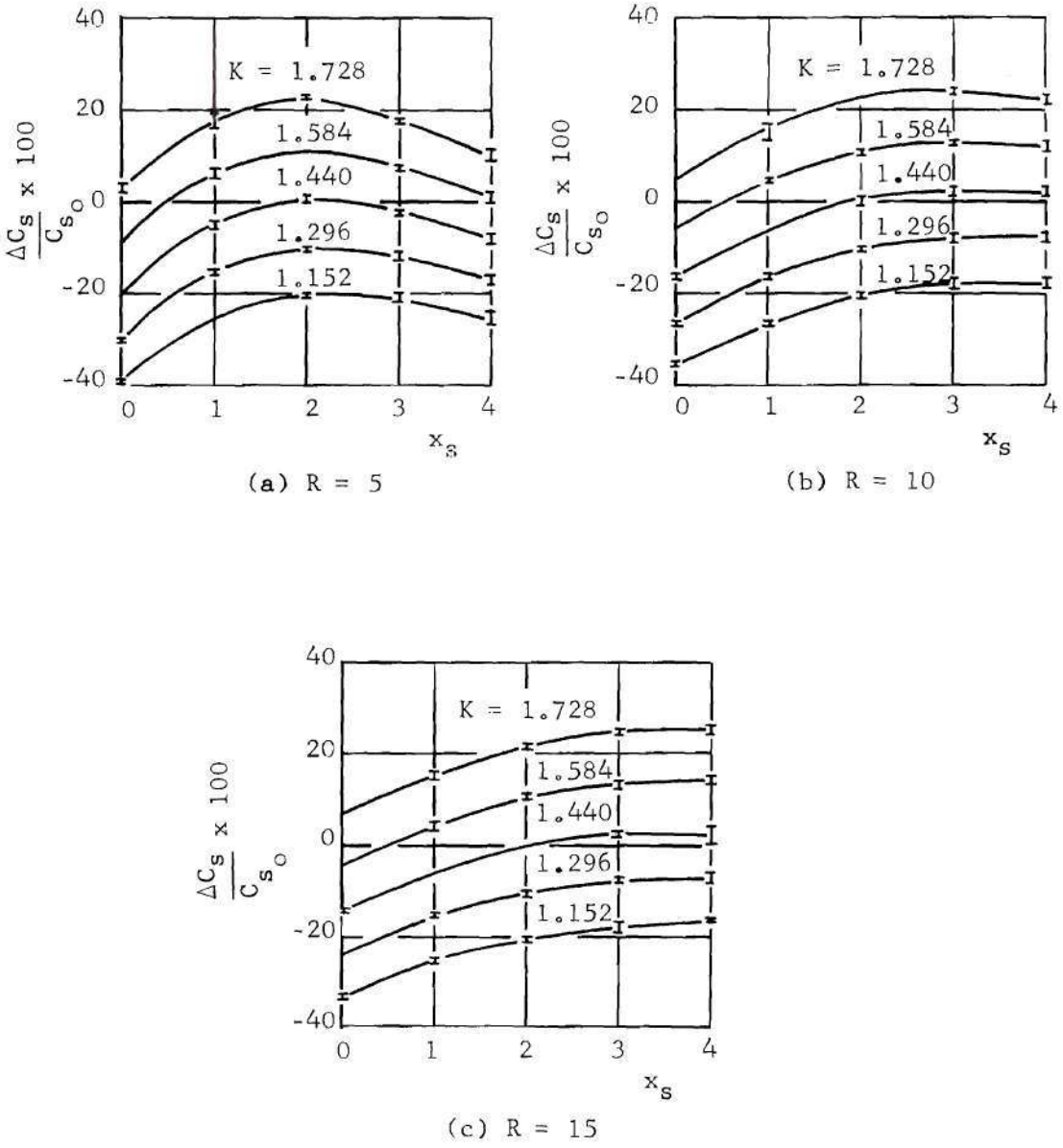

Figure 50. Effect of Sink Strength and Location on C_s when $\beta_o = 135^o$, Circular Exit

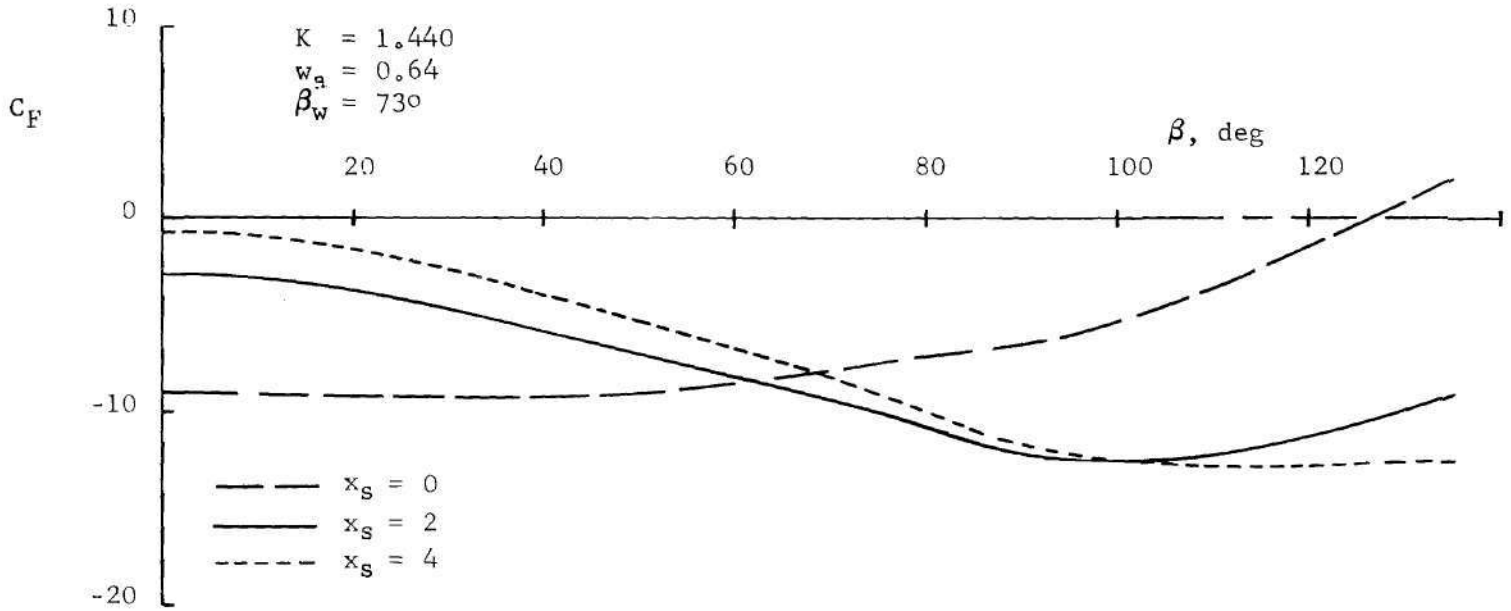

Figure 51. Effect of Sink Position on Force Distribution, R = 5, Circular Exit

magnitude than that due to the blockage and free stream. Aft of the exit ($x > 0$) the sink decelerates the flow, causing a dramatic rise in plate pressure. Hence the suction force, the integral of the force distribution curve, is relative small. When the sink is moved aft to $x_s = 2$ it is relatively far from the region immediately upstream of the exit and its effect is greatly reduced there, although it is still causing a significant reduction of the plate pressure in this region. However, at $\beta = 90$ degrees the velocities due to the blockage and the uniform stream are fairly well aligned with those due to the sink; this causes a significant reduction of the plate pressure. For $0 < x < x_s$ the sink is now accelerating the flow, greatly reducing the pressure. For this case, then, the suction force is quite large. If the sink is moved even further aft, say to $x_s = 4$, the plate pressure distribution is again changed. The effect of the sink is even smaller upstream of the exit. At the side of the exit the induced velocities are even more closely aligned, so that although the velocity induced by the sink is even less, the total velocity is about the same as it was when the sink was at $x_s = 2$. Hence the pressures in this region are about the same. The pressure aft of the exit is somewhat reduced, but the effect on the region considered is fairly small because the sink is within the excluded wake region and relatively far away. The C_s integral in this case is then reduced in magnitude.

The effect of changing the sink strength is more clearly seen in the force distribution curves, Figures 52 and 53. Figure 52 shows that an incremental change in the sink strength when the location is fixed

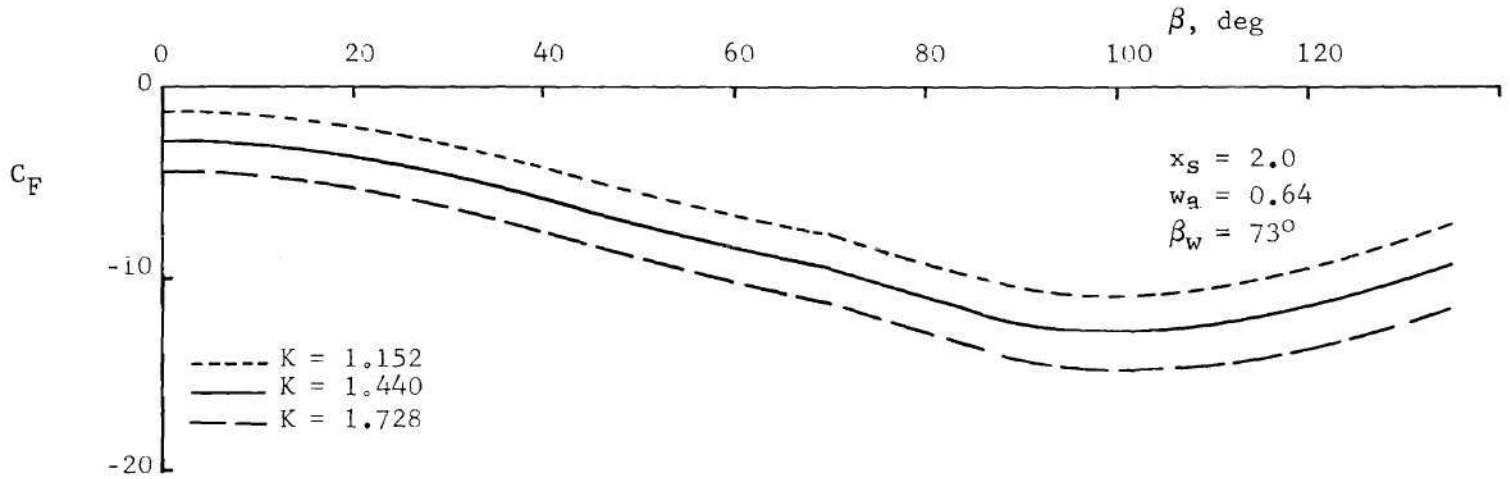

Figure 52. Effect of Sink Strength on Force Distribution, R = 5, Circular Exit

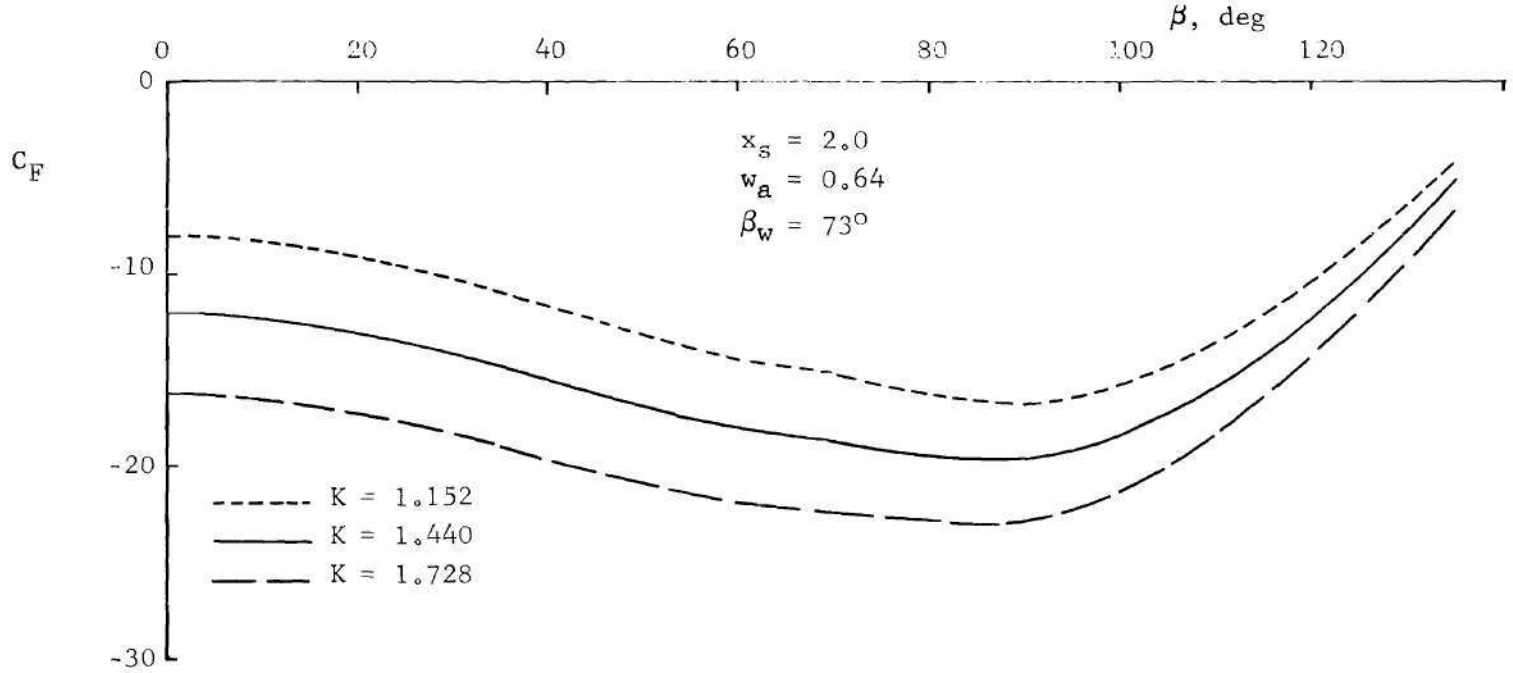

Figure 53. Effect of Sink Strength on Force Distribution, R = 10, Circular Exit

causes an almost constant increment along the distribution curve when R = 5. When R = 10 the change in sink strength has a greater effect upstream of the exit than it does downstream, but it is obvious that the change in the total integral is about constant. The difference between the curves for R = 5 and R = 10 is again a matter of alignment of the induced velocities; at R = 5 the velocities due to the sink and those due to the blockage are rather closely aligned for large β, while at greater distances from the exit the alignment becomes progressively worse.

The effects of varying w_a and β_w were negligibly small on the total integrals. For a given sink strength and position the suction force falls within the bands indicated on Figure 50 for all combinations of w_a and β_w used. Any variations with β_w appeared to be random. There was less than two percent increase in suction force with a 10 percent reduction in Rankine oval width. However, observations made in determining the best fit models indicated that the plate pressure near the jet exit is actually reduced when the afterbody width is increased. The contradiction in these results in terms of the integrals would then appear to be due to the restrictions on the lower limit of integration. In any event, the effect of afterbody width is very small compared to the effects of the sink parameters. Although β_w has no discernable effect on the total integrals, it does have a local effect as shown by Figure 54. Here force distribution curves are plotted for three values of β_w. Clearly there is a slight rise in plate pressure considerably upstream of the intersection point. In the

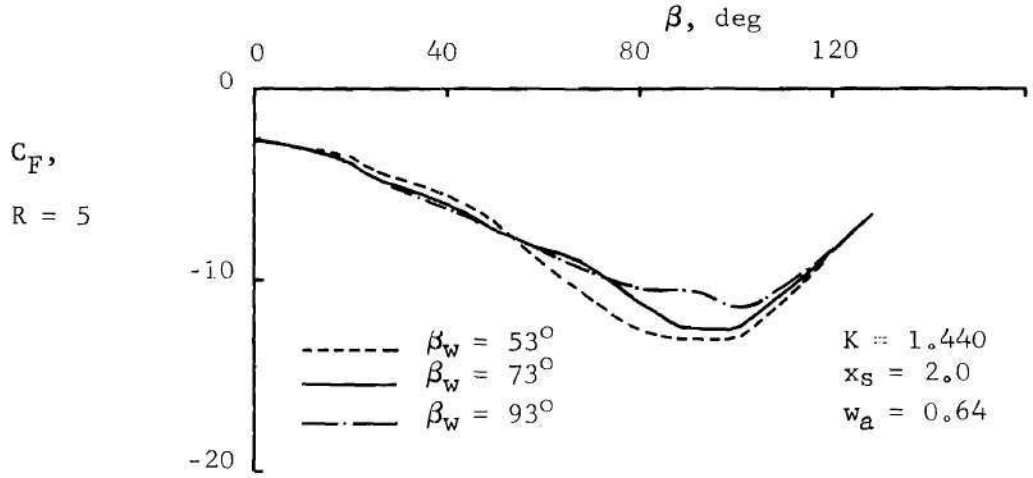

Figure 54. Effect of β_w on Force Distribution, R = 5, Circular Exit

immediate vicinity of the intersection this pressure rise is evident and is seen as a noticeable "bump" in the force distribution curves. Downstream of the intersection there appears to be a reduction of the pressure. When $\beta < 20$ degrees or $\beta > 120$ degrees there is no discernable effect due to β_w. Clearly the integrals of these distribution curves would show a very small effect due to β_w.

The results of the parametric study for the streamwise jet exit were very similar to those for the circular exit. Again the effect of β_w was very small and irregular. Varying w_a produced even smaller changes in the total integrals than it did for the circular case. Again the dominant factors were the sink strength and position. Figure 55 shows that the effects of these factors in the streamwise case is much the same as they were for the circular case. However, in this case, with both a smaller (narrower) blockage and somewhat lower entrainment rates, the variation of suction force with sink position is slightly different. The suction force reaches a maximum when the sink is closer to the jet exit, and it declines more rapidly as the sink moves aft when $R = 5$. This appears to be due to sink dominance, so that as the sink moves aft it has less influence on the region under consideration.

The results obtained with the blunt jet exit were considerably different, as seen in Figure 56. When the sink is at the origin there is a marked increase in suction force. For this case the blockage is very strong; in the region near the jet exit the sink is only dominant when it is very close to the region immediately upstream of the exit. As the sink is moved aft its influence on this region diminishes, and

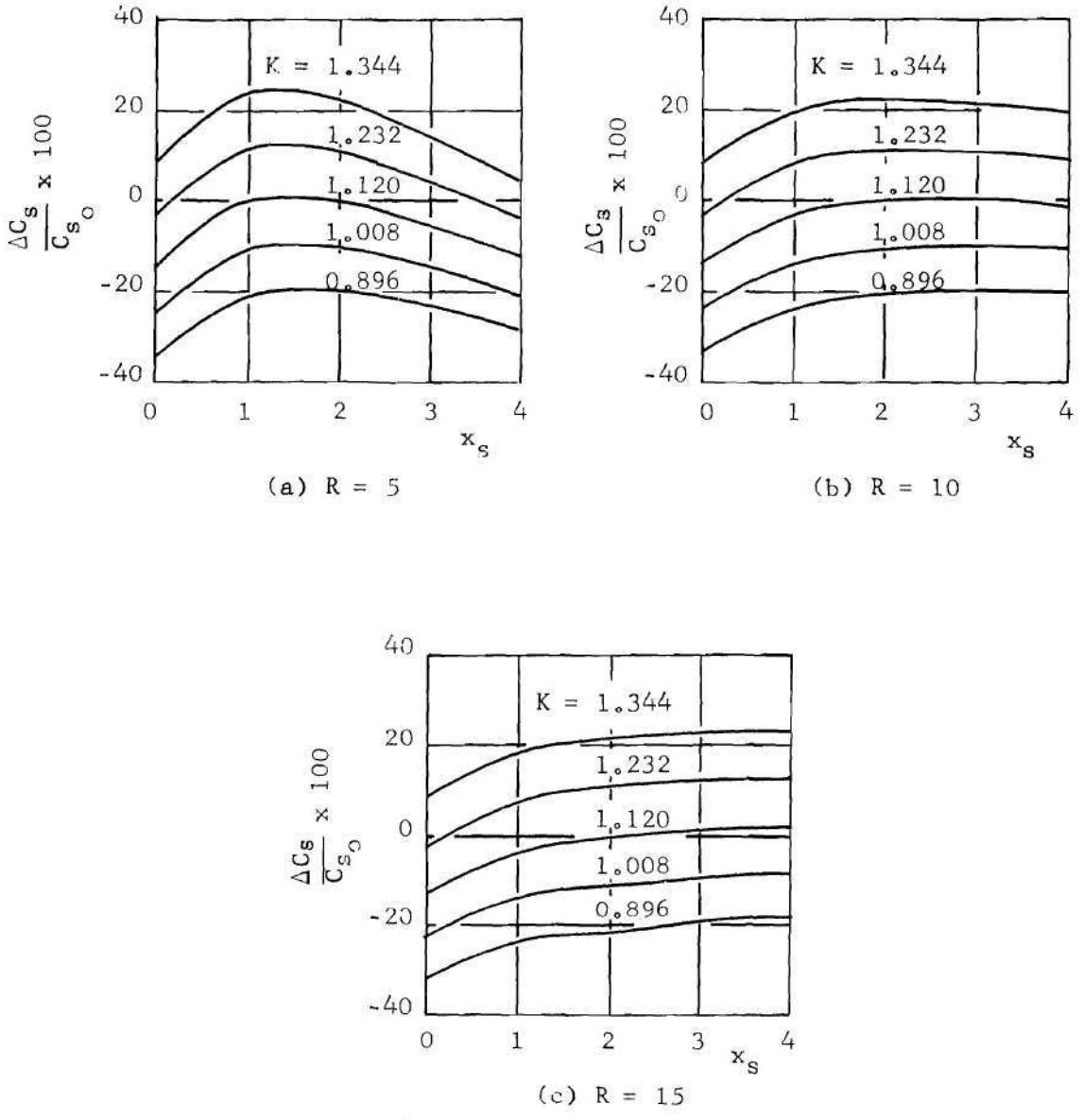

Figure 55. Effect of Sink Strength and Position on C_s for the Streamwise Exit, when $\beta_o = 135^o$, $w_a = 0.20$, and $\beta_w = 108^o$

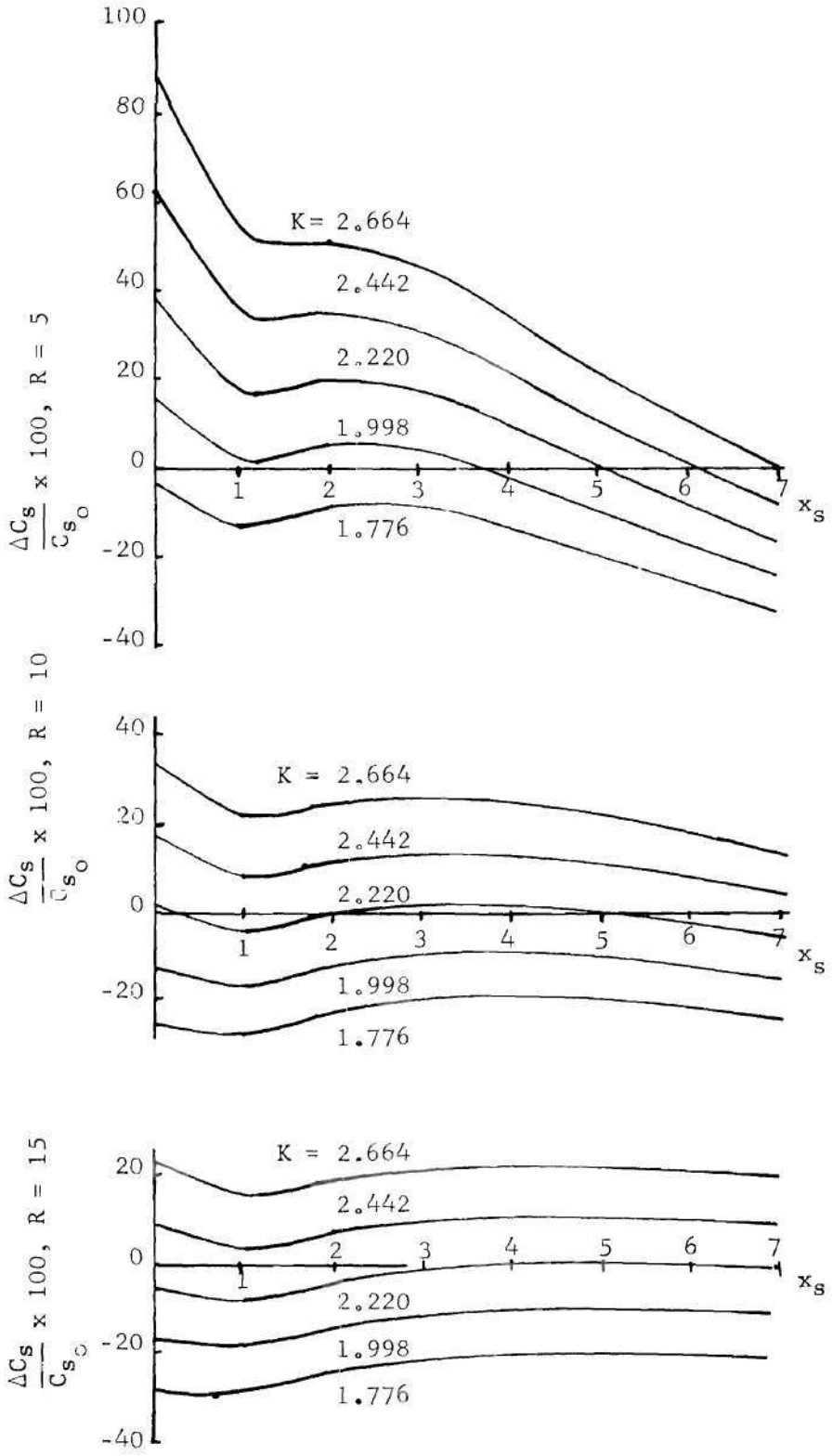

Figure 56. Effect of Sink Strength and Position on C_s for Blunt Jet Exit, $\beta_o = 135^o$, $\beta_w = 108^o$, $w_a = 1.05$

its induced velocity is not well aligned with that due to the blockage to the side and aft of the exit. Hence there is a reduction in the suction force. As the sink moves further aft the velocities become better aligned and the suction force increases slightly. As the sink moves still further aft its influence on the flow field near the exit diminishes and the suction force is consequently reduced.

The results of the parametric study are helpful in determining means of reducing suction force for V/STOL applications. Clearly, excluding the wake region, the sink or entrainment parameters dominate the integrated interference force coefficient for streamwise or circular jet exits. For the circular exit a reduction of the entrainment rate by 20 percent of the reference entrainment rate K_o, coupled with a forward movement of the sink location, can reduce the suction force on the plate excluding the wake region by about 30 percent. Since for this case

$$\frac{\left|C_{s_e}\right| - \left|C_{s_o}\right|}{C_{s_o}} = \begin{cases} 0.229 \text{ at } R = 10 \\ 0.450 \text{ at } R = 15 \end{cases} \qquad (42)$$

where C_{s_e} is the integrated interference force coefficient calculated from the experimental data with $\beta_o = 180$ degrees (including the wake region), a 30 percent reduction in suction force outside the wake region is effectively a 20 percent reduction in the total lift loss, assuming the changes in the entrainment rates and location do not significantly alter the lift loss experienced in the wake region.

This represents a recovery of only about 3 percent of the jet thrust for the case of a jet issuing from a circular exit with $V_j/V_\infty = 12$. For the streamwise exit the same arguments hold, but the recovery of jet thrust due to a 20 percent reduction of the entrainment rate and a forward movement of the effective sink location would be about 4 percent because the lift loss in the wake region is less for this case.

The entrainment parameters are also quite influential in the blunt jet case. However, if a very large region of the plate is considered, say out to R = 10, the force distribution is relatively insensitive to x_s. It would seem reasonable that a reduction of entrainment rate would be coupled with a forward movement of the sink location. It would therefore seem that a 20 percent reduction of entrainment rate could result in about a 20 percent reduction of the suction force. However, for this case about 40 percent of the total suction force occurs in the wake region. Therefore this reduction of the suction force would represent only a very small thrust recovery. At lower speed ratios an even larger portion of the total suction force occurs in the wake region, so that control of the entrainment rate would effect negligible thrust recovery.

Note also that the relative unimportance of the afterbody parameters seen in this study suggests that the presence of an afterbody is important to the predicted plate pressures but the exact shape is insignificant.

CHAPTER IV

CONCLUSIONS AND RECOMMENDATIONS

Conclusions

1. The analysis shows that both entrainment and blockage are significant factors in the jet-in-crosswind interference problem.

2. The basic blockage may be simulated by potential elements representing flow around a cylinder of cross-section similar to the shape of the jet exit.

3. The entrainment may be represented by sinks.

4. The low total pressure wake region has a blockage effect on the crosswind which may be represented by an afterbody attached to the basic blockage element.

5. A steady two-dimensional potential blockage-sink model consisting of a basic blockage element plus an afterbody and a single sink provides a useful means of studying interference effects on the cross-sind in the vicinity of the plate from which the jet issues, provided the jet-to-crosswind speed ratio is sufficiently large and a wake region is excluded.

6. The exclusion of the wake region is not serious, since an analysis of experimental data indicates that the excluded region contributes less than 20 percent of the total suction force on the bounding plate if the jet exit shape is a circle or a round-ended slot aligned with the free stream (streamwise exit).

7. Such a model can be applied successfully to circular and noncircular jet exit cases without undue complexity.

8. Studies with this model show that best agreement with experimental data is obtained when the sink is placed aft of the center of the jet exit, which indicates that there is entrainment into the wake region as well as directly into the jet plume.

9. The entrainment rate and effective location are functions of jet exit geometry and jet-to-crosswind speed ratio.

10. A parametric study undertaken using this model shows that the presence of the afterbody is important, but for predicting the overall plate suction force the exact shape of the afterbody is not very significant.

11. The parametric study also shows that blockage and entrainment effects on the crosswind are coupled so that low plate pressures are produced when the directions of velocities due to these elements are closely aligned.

12. Because of this coupling of blockage and entrainment an upstream shifting of the sink location may reduce the suction force on the plate by 10 percent if the jet exit shape is circular or streamwise.

13. Reduction of the entrainment rate with all other factors held constant reduces the suction force on the plate.

14. A reduction of the entrainment rate by 20 percent coupled with an upstream shifting of the sink location may reduce the total plate suction force by as much as 20 percent.

15. Because of their relatively small wakes and favorable blockage-entrainment coupling, streamwise jet exits appear to be more advantageous in lifting-jet applications than circular or clunt jet exits.

Recommendations

It is suggested that two refinements to the two-dimensional model discussed in this work be considered in order to improve the predicted detailed pressure field. Since the predicted pressures do not agree extremely well with experimentally observed pressures in the immediate vicinity of the afterbody-jet exit intersection, it would seem advisable to smooth the intersection. Therefore it is suggested that afterbodies be generated from bodies that are tapered fore and aft rather than from Rankine ovals. That is, instead of starting with a source-sink pair in a uniform stream one should perhaps begin with a distribution of sources followed by a distribution of sinks in a uniform stream in the ζ'-plane, and then apply the transformation equation (28). Suggested distributions are (1) a uniform source distribution over a distance $\Delta\xi'$ followed by an equivalent strength uniform sink distribution over the same sized $\Delta\xi'$, (2) a linearly increasing source distribution followed by a linearly decreasing sink distribution, and (3) a parabolic source distribution followed by a parabolic sink distribution. Also some attempt should be made to improve the simulation of the non-circular jet exit shapes, particularly on the upstream portion. Perhaps the most simple means of accomplishing this is to forsake the transformations and work directly

in the Z-plane, using sources to form the upstream portion of the blockage and sinks to close the wake portion. For simulating the streamwise exit a single source would probably form the upstream portion and the wake portion could be closed by a uniform sink distribution in the x-direction far downstream. A distribution of sources along the y-axis would perhaps successfully simulate the upstream portion of the blunt exit, and the wake portion could again be closed by a sink distribution in the x-direction.

Since the two-dimensional blockage-sink model has been useful, it is recommended that an attempt be made to extend such a model to three dimensions and investigate the effects of blockage and entrainment for lower speed ratio cases. It is noted, however, that the model cannot be extended directly because the mathematics used in obtaining the afterbodies does not generalize to three dimensions. The wake blockage may be treated in the three-dimensional case by a doublet distribution in the x-direction as well as along the plume centerline. Such a model might also be considered to be an extension of the work of reference [26].

It is also suggested that an attempt be made to simulate the effects of vortex roll-up in the plume, at least for the circular jet exit case, since it is anticipated that for lower speed ratio cases the proximity of the plume to the plate would cause the vorticity effects to have more influence on the plate pressures. The vorticity measurements of reference [34] could be used to estimate the strength of a pair of counter-rotating vortices symmetrically placed beside the

jet centerline as expressed in reference [12].

Because the entrainment parameters appear to be significant in determining the suction force on the bounding plate, it is suggested that experimental investigations of means to reduce entrainment be undertaken. One possible means of reducing entrainment would be a baffle or fence located on the plate immediately downstream of the jet exit. Exploratory tests of baffles of various heights should be performed, and both streamwise and circular jet exits should be considered. Such a baffle should prevent the reversed flow observed experimentally in the near wake from entering the plume, and hence reduce the effective entrainment rate and move the effective sink location upstream. Thus this experiment could provide a check on Conclusion #14.

In a more general vein, considerable effort should be applied to the investigation of the basic mechanism of the wake formation and the interaction of entrainment and wake effects, for these are undoubtedly important physical phenomena in the jet-in-crosswind interference problem and are not understood at present.

APPENDICES

APPENDIX A

DIMENSIONAL ANALYSIS OF INTERFERENCE PRESSURES

Consider a turbulent subsonic jet exhausting normally to a large flat plate into a crossflow. Assuming that the boundary layer on the plate is sufficiently described by its momentum thickness, dimensional analysis of the static pressure p on the plate may be accomplished in the following manner.

Assume

$$p = \text{fcn}\left\{\rho_\infty,\ V_\infty,\ \rho_j,\ V_j,\ \mu,\ \theta,\ w,\ \ell,\ r,\ \beta\right\} \tag{A1}$$

where

ρ_∞ = free stream density, $\left[\frac{M}{L^3}\right]$

V_∞ = free stream velocity, $\left[\frac{L}{T}\right]$

ρ_j = jet density, $\left[\frac{M}{L^3}\right]$

V_j = jet velocity, $\left[\frac{L}{T}\right]$

μ = viscosity of both jet and free stream, $\left[\frac{M}{LT}\right]$

θ = momentum thickness of the plate boundary layer, [L]

w = width of the jet exit, [L]

ℓ = length of the jet exit, [L]

r = radial coordinate of a point on the plate, [L]

β = angular coordinate of a point on the plate, radians

and M, L, T denote units of mass, length, and time, respectively. This is rewritten as

$$g\left\{p,\ \rho_\infty,\ V_\infty,\ \rho_j,\ V_j,\ \mu,\ \theta,\ w,\ \ell,\ r,\ \beta\right\} = 0\ , \tag{A2}$$

for which there are seven dimensionless Π products, since β is dimensionless. Choose ρ_∞, V_∞, and w as the factors common to all products. The first Π product becomes

$$\Pi_1 = f_1\left\{p,\ \rho_\infty,\ V_\infty,\ w\right\} \tag{A3}$$

for which the dimensional equation is

$$(MLT)^0 = (M/LT^2)(M/L^3)^\gamma\ (L/T)^\delta (L)^\epsilon\ . \tag{A4}$$

Solving for γ, δ, and ϵ yields

$$\gamma = -1$$

$$\delta = -2$$

$$\epsilon = 0\ .$$

Hence

$$\Pi_1 = \frac{p}{\rho_\infty V_\infty^{\,2}}\ , \tag{A5}$$

Similarly the other Π products are

$$\Pi_2 = \rho_j/\rho_\infty \quad , \tag{A6}$$

$$\Pi_3 = V_j/V_\infty \quad , \tag{A7}$$

$$\Pi_4 = \frac{\mu}{\rho_\infty V_\infty w} \quad , \tag{A8}$$

$$\Pi_5 = \theta/w \quad , \tag{A9}$$

$$\Pi_6 = \ell/w \quad , \tag{A10}$$

$$\Pi_7 = r/w \quad . \tag{A11}$$

Now Π_6 may be rewritten in the following manner

$$\Pi_6 = \left(\frac{\ell}{w}\right)\left(\frac{w}{w}\right) = \frac{\ell w}{w^2} \quad . \tag{A12}$$

But it is recognized that the product ℓw is an area which may be defined as

$$\ell w = a_e^{\,2} \quad , \tag{A13}$$

so that

$$\Pi_6 = \frac{a_e^{\,2}}{w^2} \quad . \tag{A14}$$

Now some of the Π products may be modified to more convenient forms.

$$\Pi_5' = \Pi_5/\sqrt{\Pi_6} = \theta/a_e \quad , \tag{A15}$$

$$\Pi_7' = \Pi_7/\sqrt{\Pi_6} = r/a_e \quad , \tag{A16}$$

$$\Pi_4' = \frac{\Pi_4}{\Pi_2\Pi_3\sqrt{\Pi_6}} = \frac{\mu}{\rho_j V_j a_e} \quad . \tag{A17}$$

It is noted that Π_4' is the reciprocal of the jet efflux Reynolds number. Furthermore, Π_1 may be modified to

$$\frac{p - p_\infty}{\frac{1}{2}\rho_\infty V_\infty^2} = C_p \quad , \tag{A18}$$

the plate pressure coefficient, without violating the dimensional analysis. Therefore

$$C_p = \text{fcn}\left\{ \frac{\rho_j}{\rho_\infty} , \frac{V_j}{V_\infty} , \frac{\rho_j V_j a_e}{\mu} , \frac{\theta}{a_e} , \frac{r}{a_e} , \frac{\ell}{w} , \beta \right\} \quad . \tag{A19}$$

If constant density is assumed, $\rho_j = \rho_\infty$, and equation (A19) becomes

$$C_p = \text{fcn}\left\{ \frac{V_j}{V_\infty} , \frac{\rho_j V_j a_e}{\mu} , \frac{\theta}{a_e} , \frac{r}{a_e} , \frac{\ell}{w} , \beta \right\} . \qquad \text{(A20)}$$

Now if the jet exit is circular, $\ell/w = 1$ and $a_e = a$ and

$$C_p = \text{fcn}\left\{ \frac{V_j}{V_\infty} , \frac{\rho_j V_j a}{\mu} , \frac{\theta}{a} , \frac{r}{a} , \beta \right\} . \qquad \text{(A21)}$$

APPENDIX B

NUMERICAL CALCULATIONS

All major calculations were carried out numerically on the Univac 1108 digital computer which has the ability to compute complex numbers. Care was taken to insure proper signs since the computer calculates only in the first quadrant of the complex plane.

Afterbody Transformations

All the afterbody transformations were accomplished in the following manner. Approximately 20 points on the generating Rankine oval were calculated on a desk calculator. These points were read into the program as x, y pairs and converted to complex numbers. The parameters A, B, β_w, D, w_a, and ℓ_a were input to the program. The transformation relations (equations (28) and (19)) were programmed directly and the resulting complex numbers were separated into real and imaginary parts and printed out as x, y pairs in the plane of the jet exit.

Pressure Coefficient and Integral Calculations

Plate pressure coefficients were calculated in the following manner. The afterbody parameters and sink parameters and A and B were input. β was varied from 0 degrees to 135 degrees in steps of 5 degrees. The value of β was converted to radians. For each value of β, r was varied from 0.5 to 15.0 in steps of 0.25, with statements

to recycle the calculation if r fell within the boundary of the jet exit. The resulting r, β pairs were converted to x, y Cartesian pairs and the complex number $Z = x + iy$ was defined. If the calculation was for the blunt or streamwise case, this point Z was transformed to the corresponding point ζ' by equation (28). The complex velocity was computed in the ζ-plane and transformed back to the Z-plane, where the real and imaginary parts were separated and defined as real numbers $-u_b$ and v_b, respectively. If the calculation was for the circular jet exit case, the complex velocity was computed directly in the Z-plane and the real and imaginary parts were separated. The velocity components due to the sink were computed directly as real numbers and added to the components due to blockage and the free stream to form total velocity components. The pressure coefficient was then calculated according to equation (12) and stored for one recycle.

A trapezoidal integration scheme was used to obtain the force distribution coefficient C_F.

$$\Delta C_{F_i} = \left(\frac{C_{p_i} + C_{p_{i-1}}}{2} \right) \left(\frac{r_i - r_{i-1}}{2} \right) \left(r_i - r_{i-1} \right) \qquad \text{(B1)}$$

$$C_F = \sum_i \Delta C_{F_i} \quad . \qquad \text{(B2)}$$

The accumulated values of C_F *when i corresponded to* $R = 5$, 10, and 15 were stored. Conditional statements were included to prevent the inclusion of data calculated inside the afterbody in order to avoid proximity to signularities.

A simple step-wise strip integration was used to compute the integrated interference force coefficient C_s.

$$C_s = \sum_j C_{s_j} \Delta\beta_j \quad , \tag{B3}$$

where $\Delta\beta_j$ = 0.0872 radians (5 degrees) except when β = 0 degrees or 135 degrees, when $\Delta\beta_j$ had half that value.

Although this was not a particularly sophisticated program, it ran very rapidly. It was of course possible to print out any important quantity. When the plate coordinates and pressure coefficients were printed out in addition to the integrals, this program ran for a given set of afterbody and sink parameters in an average time of 11.5 seconds. When only the integrals were printed out for the parametric study, the program was much faster and typically calculated 125 cases in 3.5 minutes.

CITED LITERATURE

1. Williams, J., Wood, M. N., "Aerodynamic Interference Effects with Jet-Lift V/STOL Aircraft under Static and Forward-Speed Conditions," British Royal Aircraft Establishment Tech. Rep. No. 66403, December 1966.

2. Skifstad, J. G., "Aerodynamics of Jets Pertinent to VTOL Aircraft, " U. S. Air Force AFAPL-TR-69-28, March 1969.

3. Otis, J. H., Jr., "Induced Interference Effects on a Four-Jet VTOL Configuration with Various Wing Planforms in the Transition Speed Range," NASA TN D-1400, 1962.

4. Vogler, R. D., "Interference Effects of Single and Multiple Round or Slotted Jets on a VTOL Model in Transition," NASA TN D-2380, 1964.

5. Vogler, R. D., Kuhn, R. E., "Longitudinal and Lateral Stability Characteristics of Two Four-Jet VTOL Models in the Transition Speed Range," NASA TM X-1092, 1965.

6. Davenport, E. E., Kuhn, R. E., "Wind Tunnel-Wall Effects and Scale Effects on a VTOL Configuration with a Fan Mounted in the Fuselage," NASA TN D-2560, 1965.

7. Hickey, D. H., Kirk, J. V., Hall, L. P., "Aerodynamic Characteristics of a V/STOL Transport Model with Lift and Lift-Cruise Fan Power Plants," Conference on V/STOL and STOL Aircraft, NASA SP-116, 1966, pp. 81-96.

8. Margason, R. J., "Jet-Induced Effects in Transition Flight," Conference on V/STOL and STOL Aircraft, NASA SP-116, 1966, pp. 177-189.

9. Spreemann, K. P., "Free-Stream Interference Effects on Effectiveness of Control Jets Near the Wing Tip of a VTOL Aircraft Model," NASA TN D-4084, 1967.

10. Margason, R. J., Gentry, C. L., Jr., "Aerodynamic Characteristics of a Five-Jet VTOL Configuration in the Transition Speed Range," NASA TN D-4812, 1968.

11. Carter, A. W., "Effects of Jet-Exhaust Located on the Longitudinal Aerodynamic Characteristics of a Jet V/STOL Model," NASA TN D-5333, 1969.

12. Margason, R. J., "The Path of a Jet Directed at Large Angles to a Subsonic Free Stream," NASA TN D-4919, 1968.

13. Callaghan, E. E., Ruggeri, R. S., "Investigation of the Penetration of an Air Jet Directed Perpendicularly to an Air Stream," NACA TN 1615, 1948.

14. Ruggeri, R. S., Callaghan, E. E., Bowden, D. T., "Penetration of Air Jets Issuing from Circular, Square, and Elliptical Orifices Directed Perpendicularly to an Air Stream," NACA TN 2019, 1950.

15. Jordinson, R., "Flow in a Jet Directed Normal to the Wind," British Aeronautical Research Council R&M. No. 3074, 1958.

16. Keffer, J. F., Baines, W. D., "The Round Turbulent Jet in a Crosswind," Journal of Fluid Mechanics, Vol. 15, Part 4, April 1963, pp. 481-497.

17. Abramovich, G. N., The Theory of Turbulent Jets, M.I.T. Press, Cambridge, Massachusetts, c. 1963, pp. 541-552.

18. Epshtein, A. M., "Shape of Turbulent Jet Axis in an Unbounded Horizontal Cross Flow," Journal of Engineering Physics, Vol. 9, No. 4, October 1965, pp. 303-306.

19. Vogler, R. D., "Surface Pressure Distributions Induced on a Flat Plate by a Cold Air Jet Issuing Perpendicularly from the Plate and Normal to a Low-Speed Free-Stream Flow," NASA TN D-1629, 1963.

20. Bradbury, L. J. S., Wood, M. N., "The Static Pressure Distribution Around a Circular Jet Exhausting Normally from a Plane Wall into an Airstream," British Aeronautical Research Council C. P. No. 822, 1965.

21. Gelb, G. H., Martin, W. A., "An Experimental Investigation of the Flow Field about a Subsonic Jet Exhausting into a Quiescent and a Low Velocity Airstream," Canadian Aeronautics and Space Journal, Vol. 12, No. 8, October 1966, pp. 333-342.

22. Lu, Hsih-Chia, "On the Surface of Discontinuity Between Two Flows Perpendicular to Each Other," National Tsing Hua University Engineering Report 4, October 1948.

23. Fraser, J. P., "Three-Dimensional Study of a Jet Penetrating a Stream at Right Angles," Journal of the Aeronautical Sciences (Readers' Forum), Vol. 21, No. 1, January 1954, pp. 59-61.

24. Gordier, R. L., "Studies on Fluid Jets Discharging Normally into Moving Liquid," St. Anthony Falls Hydraulic Laboratory, University of Minnesota, Tech. Paper No. 28, Ser. B (Contract Nonr 710(26)), August 1959.

25. Monical, R. E., "A Method of Representing Fan-Wing Combinations for Three-Dimensional Potential Flow Solutions," Journal of Aircraft, Vol. 2, No. 6, November-December 1965, pp. 527-530.

26. Wooler, P. T., Burghart, G. H., Gallagher, J. T., "Pressure Distribution on a Rectangular Wing With a Jet Exhausting Normally into an Airstream," Journal of Aircraft, Vol. 4, No. 6, November-December 1967, pp. 537-543.

27. Wooler, P. T., "On the Flow Past a Circular Jet Exhausting at Right Angles from a Flat Plate or Wing," Journal of the Royal Aeronautical Society, Vol. 71, March 1967, pp. 216-218.

28. McAllister, J. D., "A Momentum Theory for the Effects of Cross Flow on Incompressible Turbulent Jets," Ph.D. Thesis, University of Tennessee (Space Institute), August 1968.

29. Soukup, S. M., "Potential Flow Aspects of the Cross-Sectional Deformation of Jet Configurations in Cross Flow," M. S. Thesis, University of Tennessee (Space Institute), December 1968.

30. Wooler, P. T., "Flow of a Circular Jet into a Cross Flow," Journal of Aircraft (Engineering Notes), Vol. 6, No. 3, May-June 1969.

31. Vizel, Ya. M., Mostinskii, I. L., "Deflection of a Jet Injected Into a Stream," Journal of Engineering Physics, Vol. 8, No. 2, February 1965, pp. 160-163.

32. Platten, J. L., Baines, W. D., "Entrainment in Deflected Axisymmetric Jets at Various Angles to the Stream," University of Toronto, UTME-TP 6806, June 1968.

33. Crowe, C. G., Riesebieter, H., "An Analytic and Experimental Study of Jet Deflection in a Cross-Flow," Fluid Dynamics of Rotor and Fan Supported Aircraft at Subsonic Speeds, Paris: Advisory Group for Aerospace Research and Development Preprint, 1967.

34. Margason, R. J., Fearn, R., "Jet-Wake Characteristics and Their Induced Aerodynamic Effects on V/STOL Aircraft in Transition Flight," Analysis of a Jet in a Subsonic Crosswind, NASA SP-218, September 1969, pp. 1-18.

35. Keffer, J. F., "The Physical Nature of the Subsonic Jet in a Cross-Stream," Analysis of a Jet in a Subsonic Crosswind, NASA SP-218, September 1969, pp. 19036.

36. Hackett, J. E., Miller, H. R., "The Aerodynamics of the Lifting Jet in a Cross Flowing Stream," Analysis of a Jet in a Subsonic Crosswind, NASA SP-218, September 1969, pp. 37-48.

37. Wooler, P. T., "Development of an Analytical Model for the Flow of a Jet into a Subsonic Crosswind," Analysis of a Jet in a Subsonic Crosswind, NASA SP-218, September 1969, pp. 101-118.

38. Skifstad, J. G., "Numerical Treatment of Line Singularities for Modeling a Jet in a Low-Speed Cross Flow," Analysis of a Jet in a Subsonice Crosswind, NASA SP-218, September 1969, pp. 119-130.

39. Margason, R. J., "Analytic Description of Jet-Wake Cross Sections for a Jet Normal to a Subsonic Free Stream," Analysis of a Jet in a Subsonic Crosswind, NASA SP-218, September 1969, 131-140.

40. Braun, G. W., McAllister, J. D., "Cross Wind Effects on Trajectory and Cross Sections of Turbulent Jets," Analysis of a Jet in a Subsonic Crosswind, NASA SP-218, September 1969, pp. 141-164.

41. Heltsley, F. L., Kroeger, R. A., "A General Jet Efflux Simulation Model," Analysis of a Jet in a Subsonic Crosswind, NASA SP-218 September 1969, pp. 165-180.

42. Rubbert, P. E., "Calculation of Jet Interference Effects on V/STOL Aircraft by a Nonplanar Potential Flow Method," Analysis of a Jet in a Subsonic Crosswind, NASA SP-218, September 1969, pp. 181-204.

43. Rosen, R., Durando, N. A., Cassel, L. A., "Inviscid Models for the Pressure Induced by a Jet Transverse to a Subsonic Stream," Analysis of a Jet in a Subsonic Crosswind, NASA SP-218, September 1969, pp. 205-230.

44. Werner, J. E., "The Use of Matched Asymptotic Expansions as an Approach to the Problem of the Jet in a Crossflow," Analysis of a Jet in a Subsonic Crosswind, NASA SP-218, September 1969, pp. 231-238.

45. Fearn, R. L., "Mass Entrainment of a Circular Jet in a Cross Flow," Analysis of a Jet in a Subsonic Crosswind, NASA SP-218, September 1969, pp. 239-248.

46. Wu, J. C., McMahon, H. M., Mosher, D. K., Wright, M. A., "Experimental and Analytical Investigations of Jets Exhausting into a Deflecting Stream," Journal of Aircraft, Vol. 7, No. 1, January-February 1970, pp. 44-51.

47. McMahon, H. M., Mosher, D. K., "Experimental Investigation of Pressures Induced on a Flat Plate by a Jet Issuing into a Subsonic Crosswind," Analysis of a Jet in a Subsonic Crosswind, NASA SP-218, September 1969, pp. 49-62.

48. Wu, J. C., Wright, M. A., "A Blockage-Sink Representation of Jet Interference Effects for Noncircular Jet Orifices," Analysis of a Jet in a Subsonic Crosswind, NASA SP-218, September 1969, pp. 85-100.

49. Mosher, D. K., "An Experimental Investigation of a Turbulent Jet in a Cross Flow," Ph.D. Thesis in process, Georgia Institute of Technology.

50. Ricou, F. P., Spalding, D. B., "Measurements of Entrainment by Axisymmetrical Turbulent Jets," Journal of Fluid Mechanics, Vol. 11, Part 1, August 1961, pp. 21-32.

51. Milne-Thomson, L. M., Theoretical Hydrodynamics, The MacMillan Company, New York, 1968, pp. 478-484.

VITA

Mary Anne Jackson Wright was born in Tullahoma, Tennessee, where she attended elementary and high school. She attended David Lipscomb College in Nashville, Tennessee, for one year.

In September 1961 Mrs. Wright entered Georgia Institute of Technology in the School of Aerospace Engineering, where for two years she held the Schroedinger-Ermenzinger Scholarship. She received the Bachelor of Aerospace Engineering Degree in 1964, and entered the Graduate Division in September of that year. The Master's Degree was awarded in 1966. While enrolled in the Graduate School, Mrs. Wright held a National Science Foundation Cooperative Graduate Fellowship, the Zonta International Amelia Earhart Fellowship Award, and an Instructorship and Graduate Research Assistantship in the School of Aerospace Engineering. In December 1966 the former Miss Jackson married Mr. Terry Wright.

Mrs. Wright was employed by ARO, Inc. of Tullahoma, Tennessee, in 1960-61 and the summer of 1962, and by NASA Langley Research Center, Hampton, Virginia, during the summer of 1964. She is presently employed by Allison Division of General Motors Corporation in Indianapolis, Indiana.